Dynamic Spot Diffusing Channel - A Novel Configuration For Indoor Optical Wireless Communications

Dynamic Spot Diffusing Channel - A Novel Configuration For Indoor Optical Wireless Communications

By

FARHAD KHOZEIMEH, B.Sc.

A Thesis

Submitted to the School of Graduate Studies

in Partial Fulfilment of the Requirements

for the Degree

Master of Applied Science

McMaster University

Farhad Khozeimeh. M.A.Sc. thesis.
Dept. of Electrical and Computer Engineering,
McMaster Univ., Hamilton, Canada, 2006.

MASTER OF APPLIED SCIENCE (2006) McMaster University

Hamilton, Ontario

TITLE: Dynamic Spot Diffusing Channel - A Novel Configuration For Indoor Optical Wireless Communications

AUTHOR: Farhad Khozeimeh, B.Sc. (Sharif Univ.of Tech.)

SUPERVISOR: Dr. S. Hranilovic

NUMBER OF PAGES: xvii, 175

In loving memory of my mother, father and grandmother who left this world while I was away from home doing this work,

and to Kamyar, Mahta and Ramin

Farhad Khozeimeh. M.A.Sc. thesis.
Dept. of Electrical and Computer Engineering,
McMaster Univ., Hamilton, Canada, 2006.

Abstract

Indoor optical wireless links can potentially achieve high bitrates because there is a wide and unregulated bandwidth in the optical spectrum. Moreover, optical wireless links can be implemented using simple and inexpensive devices. However, indoor optical wireless links have their own drawbacks such as limited power due to safety issues and incapability of passing thorough opaque objects, which limit their mobility, range and bandwidth and have prevented them from being used widely in commercial systems. Therefore, there has been much effort to find new configurations for indoor optical wireless links which are able to overcome these limitations. In this thesis, a novel configuration for indoor optical wireless communication, termed the *dynamic spot diffusing* (DSD) channel, is proposed. In the DSD system, the transmitter sends optical signals to a small moving area on the ceiling termed a *spot*. The receiver receives reflections of optical signal from the spot when spot is in field of view of the receiver. This configuration is shown to achieve high bitrates and provide a good deal of mobility for users inside the room. In this work, a theoretical model for the DSD channel is proposed and the DSD channel capacity is discussed and computed. Furthermore, the DSD system design is explained and design issues are discussed in order to approach capacity. Finally, using computer simulations, achievable rates inside a room are computed and shown to be close to calculated channel capacity.

Acknowlegements

During my graduate studies at McMaster, I have learned and benefitted from the support, guidance and friendship of many people. I would like to express my deep appreciation to Dr. Hranilovic for his guidance and valuable advice all through this work. Particularly, I am indebted to him for his patience, understanding and support. I would also like to thank Cheryl Gies for her help and support.

I also wish to thank many friends and relatives who were always there for me during very hard moments I had, especially my brother Kamyar, my sister Mahta and her husband Ramin. Finishing this work would not have been possible without their infinite love and support.

My parents provided me with everything I needed, endless love and care throughout my life. I am not able to express my gratitude to them by few words here. Although they are not present anymore, the inspiration and encouragement they gave me will be with me for the rest of my life, and their love and memory will forever remain in the deepest part of my heart.

Contents

Farhad Khozeimeh. M.A.Sc. thesis.
Dept. of Electrical and Computer Engineering,
McMaster Univ., Hamilton, Canada, 2006.

List of Figures

List of Tables

1

Introduction

1.1 Motivation

Computers and electronic devices have become an integral part of our life and are used frequently. Laptops, handheld computers and cellular phones are good examples of such devices which are becoming multi-purpose and complicated tools. These devices depend on high rate wireless communication services to enable connection with infrastructure networks. Hence, there is an especially large and growing demand for new technologies which can provide high processing power, mobility and broad band communications at the same time.

Wireless applications can be categorized into two different groups, *indoor* and *free-space*, according to the environment of the wireless link. Wireless links are called indoor when transmitter and receiver are inside a building, such as the wireless link inside a classroom or conference room. They are typically short range links (few meters). Free-space wireless links are wireless links between a transmitter and the receiver outside a building such as cellular phone links

or satellite links. Thus, these links typically have longer ranges than indoor links because transmitter-receiver distance in these links can be much longer (up to several kilometers).

Particularly, there has been a growing demand for indoor wireless links. These links have some particular limitations such as limited size and power of transceivers. Therefore, a challenging problem, which has been the focus of many researchers recently, is finding an appropriate high-speed, low cost indoor wireless communication solution for mobile devices with power and size limitations.

There have been many radio frequency (RF) wireless solutions developed for indoor and short range communications. For example, IEEE 802.11.g can provide data rates of up to 50 Mbps [12] and Bluetooth standard can provide data rates of at most 3 Mbps [13]. A new indoor RF standard based on Ultra Wide Band (UWB) communication is under development, which is promised to achieve rates of up to 480 Mbps over ranges of less than 10 meters [14]. Current standard based on UWB, 802.11n, provides data rate of up to 100 Mbps [12]. However, indoor RF solutions have a number of problems that make them complex and expensive, and limit their data rates. A serious problem for indoor RF links is *fading*. Fading occurs in RF links when signals from different paths arrive at the receiver. The received signals can have different phases between 0 and 2π depending on the difference of their path lengths. Therefore, these multipath signals, when summed in the receiver, can attenuate and even cancel each other. *Interference*, between different users, is another serious problem of RF links. RF signals can pass through walls and other objects easily. Therefore, any link can detect and receive the signals from other links nearby. As a result, transceivers must be designed to be able

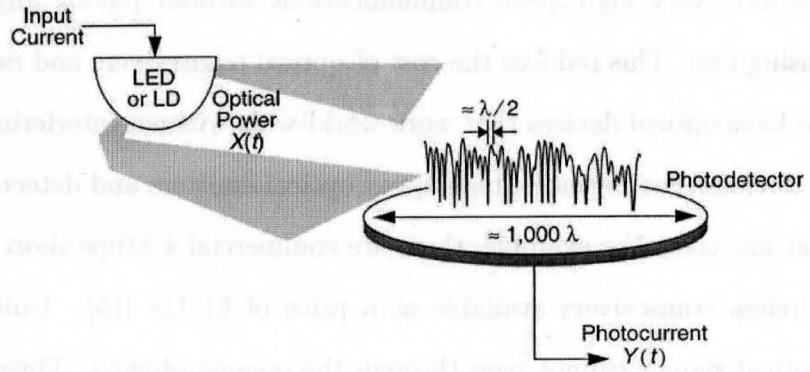

Figure 1.1: An optical wireless link (reproduced from [1, Fig.2])

to distinguish between the desired signal from a background clutter of interference.

Optical wireless links are another solution for indoor wireless communications, which has gained much attention recently. Optical links typically use intensity modulation with direct detection (IM/DD), which results in very simple transceiver circuits and devices. In this technique, as shown in Fig. 1.1, the transmitter, which is usually a light emitting diode (LED) or laser diode (LD), emits an optical signal, $X(t)$, whose power is proportional to the input electrical current signal. Data is modulated in the instantaneous power of infrared signal. In the receiver, a detector, which is typically a photodetector, transforms the received optical power to an electrical photocurrent signal, $Y(t)$.

Optical links have several advantages for indoor usage over RF links, which make them attractive for these applications. In the optical band, there is a wealth of bandwidth that is unregulated world-wide, making it theoretically

possible to have very high-speed communications without paying any spectrum licensing fees. This reduces the cost of optical transceivers and makes it possible to have optical devices that work world-wide without interfering with any other devices. Furthermore, high-speed optical emitters and detectors are available at low cost. For example, there are commercial 4 Mbps short range, optical wireless transceivers available at a price of $1 US [15]. Unlike RF signals, optical signals cannot pass through the opaque objects. Thus, every optical link is limited to inside a room as optical radiation is confined by the walls, ceiling and floor, which avoids interference with similar links in other rooms. Consequently, optical links are more secure than RF links since it is easier to restrict transmitted signals. Hence, optical wireless links are ideal choices for applications where RF interference is a serious problem, such as (1) crowded environments with RF congestion, (2) environments where there are sensitive devices such as in aircraft or hospitals and (3) high security applications such as indoor wireless links in military buildings and embassies.

Using IM/DD in optical wireless links, multipath fading does not occur in these links. As shown in Fig. 1.1, the wavelength of optical signal is short compared to detector area which prevents multipath fading. In optical wireless IM/DD links, as shown in Fig. 1.1, the receiver photodiode integrates the received optical waveform over an area of many thousands of square wavelengths. This provides an inherent degree of spatial diversity in such links which mitigates fading. Therefore, optical wireless links can potentially achieve very high bit rates with simple and inexpensive transceivers.

Indoor optical wireless links have their own drawbacks. Although there is no multipath fading in these links, the data rate on optical wireless link is

limited due to *multipath distortion*. Multipath distortion occurs when signals from different paths and therefore with different time delays arrive at a receiver. It has been shown that a linear model for this multipath distortion is good [7, 10]. The impulse response of the multipath limited channel spreads in time domain, and therefore, in frequency domain it would have a low pass shape. Another major problem in optical links is the limited transmitter optical power imposed by eye and skin safety issues. Current indoor optical links typically work in the infrared spectrum region. Unfortunately, infrared signals can be harmful to eye and skin. Therefore, as discussed in Sec. 2.3, in optical links the transmitted signal average power must always be kept in safe level. Blockage which is also called shadowing is another problem faced in optical wireless links. Optical signals can not pass through opaque objects. Therefore, any opaque object can block the link by covering the signal paths at transmitter or receiver. Blockage limits the mobility of optical wireless transceivers since a signal path may be blocked when the position of transceivers changes. There exist many opaque objects such as humans and furniture in an indoor environments, thus, blockage is a challenging problem for indoor environments. Intense ambient light in the room from different sources like sunlight, incandescent lighting and fluorescent lighting causes high intensity shot noise at the receiver. But the transmitter can not emit any arbitrary amount of power due to safety issues. Furthermore, the signal-to-noise ratio (SNR) of a direct detection receiver is proportional to the square of the received average optical power while typically in RF, SNR is proportional to the average power [1]. Therefore, in IM/DD links, one optical dB is equivalent to two electrical dB. Optical wireless links also have larger path loss compared to RF links [7, 10].

In Sec. 2.7, IM/DD SNR is discussed in more detail. These problems makes it difficult to achieve a high coverage range with optical links. Therefore, power limitation due to safety issues are known as one of the main limiting factors in indoor optical wireless links.

1.1.1 Comparison

Optical links and RF links both have advantages and disadvantages, which make each of them suitable for specific applications. Therefore, it is better that they be considered complementary rather than an alternative to each other. Table 1.1 summarizes the important properties of each of these two links. Chapter 2 presents a more detailed model of the indoor optical wireless channel.

Property	**RF link**	**Optical link**
Cost	High	Low
Data Rate	10's Mbps	100's Mbps
Bandwidth Regulated	Yes	No
Transceiver Complexity	High	Low
Security	Low	High
Safety Power limits	High	Low
Blockage Robustness	High	Low
Electromagnetic Interference	High	Low

Table 1.1: RF versus optical links

1.2 Optical Wireless Channel Configurations

Much effort has been expended to develop optimized channel architectures to realize higher data rates and good coverage while keeping the transmitter

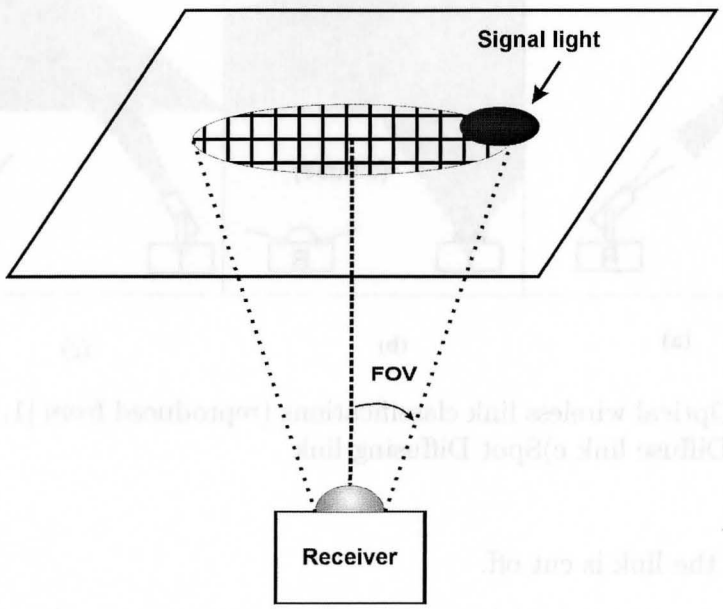

Figure 1.2: Field of View (FOV) for a optical wireless link receiver.

power in the safe level. Before introducing indoor optical wireless configurations, some necessary definitions for understanding these links are proposed.

1.2.1 Definitions

Field of view (FOV), as shown in Fig. 1.2, is maximum angle from which receiver will accept signals. For example, in Fig. 1.2, only signal light from the union surface of black and hashed regions is received in the receiver.

Line of sight (LOS) links are optical links in which signals arrive into receiver directly from the transmitter and without any reflections from the the room surfaces. In non-LOS links, signals arrive into the receiver after at least one reflection from the room surfaces.

Blockage occurs in optical wireless links when an opaque object is placed among the the signal path. In this case, optical signals can not reach the

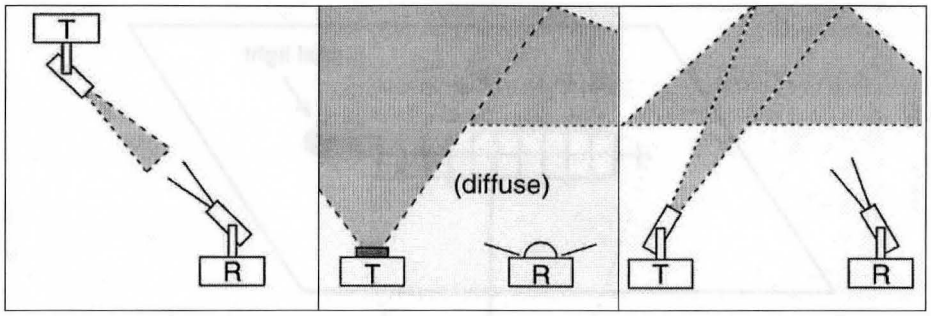

Figure 1.3: Optical wireless link classifications (reproduced from [1, Fig. 1]):a) LOS link b)Diffuse link c)Spot Diffusing link

receiver and the link is cut off.

Current configurations for indoor optical wireless communications are line of sight (LOS), diffuse and spot diffusing. These configurations are shown in Fig. 1.3. In LOS links, as shown in Fig. 1.3 (a), optical intensity signals arrive at the receiver from the transmitter after traveling over a line of sight between them in the air. In non-LOS links, as shown in Fig. 1.3 (b) and (c), the transmitter and receiver do not have a direct LOS between them and the optical signals arrive at receiver after one or more diffuse reflections from room surfaces. In each reflection, a large portion of the signal power is emitted in undesired directions. As a result, non-LOS receivers receive a much smaller portion of the emitted signal than LOS links. LOS links are therefore more power efficient, i.e., they need less power to achieve the desired probability of error for a certain distance between transmitter and receiver. Furthermore, optical signals spread in the room after the reflections in the non-LOS links and are received at the receiver with different time delays. They cause multipath distortion which is modeled as a decrease in channel

bandwidth. Furthermore, mobility is restricted in LOS links and non-LOS links are more robust to blockage. This is due to availability of more than one path from the transmitter to the receiver for signals. Thus, if some paths are blocked, signals can still reach the receiver through the other possible paths.

1.2.2 Line Of Sight Links

In LOS links, as shown in Fig. 1.4, transmitters send data through a very low divergence beam to a receiver having a narrow FOV. These properties result in the reception of much less ambient light and multipath signals at receiver compared to other configurations. Therefore, LOS-directed links have the largest bandwidth and highest power efficiency. They can achieve multi-GHz rates using simple and inexpensive transceivers [16]. Because of the small receiver FOV and low divergence transmitter beam, the transmitter beam must be aligned to the receiver. Thus, if the receiver moves, the transmitter must track it and move the beam accordingly. LOS links which support receiver mobility are termed *tracked architectures* [2, 17–19].

It is possible to provide multiple access for LOS links using *spatial diversity.* This multiple access technique is called space division multiple access (SDMA). In this technique, data for different users is sent to different spatial locations. In order for SDMA systems work, there must be isolation between different channels. In LOS links, the transmitter beam has a low divergence and the receiver has a narrow FOV, therefore, receivers collect a small amount of multipath signals. Thus, LOS optical wireless links can provide good isolation between channels and are a good candidate for SDMA systems. In [20] an optical wireless architecture using SDMA is proposed, which facilitates high

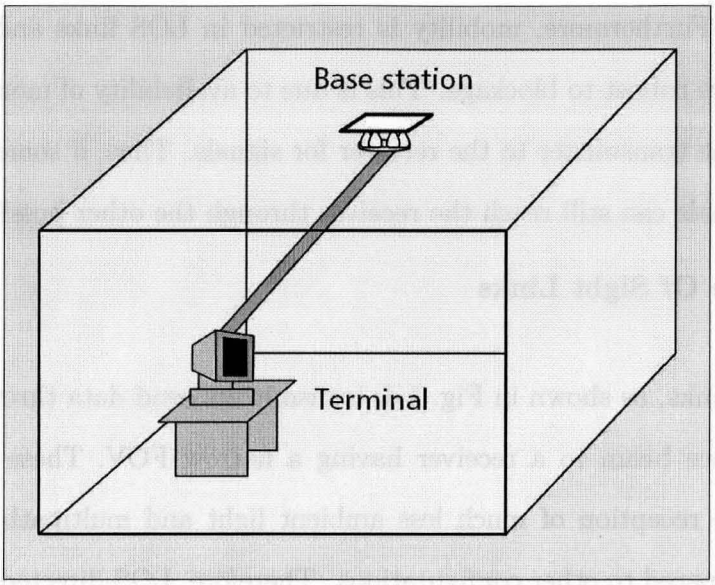

Figure 1.4: LOS Configuration (reproduced from [2, Fig. 2]).

data rates for users (more than 100 Mbps).

Although LOS links can provide the highest bit rates and power efficiency, providing precisely aligned beams for mobile units is a challenging problem, which is difficult and expensive to solve. Also, the transmitter needs to provide a separate beam for each receiver making it impractical to have many receivers in a given room. Finally, in these links, signal reaches the receiver through a very narrow single path, hence, LOS links are not robust against blockage. Although they poses good characteristics, LOS links are difficult to implement in general mobile indoor channels.

Despite all the difficulties, there have been much effort for using LOS links for indoor optical wireless communications. In [17], techniques for operation of indoor infrared wireless networks working at 50 Mbps per user, which employ tracking architecture are considered. Experimental tracked optical wireless

systems having data rates of up to 155 Mbps are reported in [18,19,21] and a 1 Gbps system has been reported in [16]. Recently, a tracking link is reported in [22] working at 155 Mbps, which employs integrated-circuit transceivers.

1.2.3 Diffuse Links

In diffuse links, as shown in Fig 1.5, the transmitter emits radiation over a large solid angle. The receivers, having a wide FOV, collect the reflected signals after one or more reflections from the room surfaces [23]. Due to the divergence of the transmitter, and the receiver's wide FOV, the receiver collects a great amount of ambient light and multipath signals. Therefore, this type of link architecture has significantly less bandwidth than LOS links. For example, the fastest reported diffuse link works at 100 Mbps [24] while LOS links have multi-GHz bandwidth [16]. Furthermore, due to the high divergence of the transmitter beam, a large portion of transmitted power is spread over undesired directions in the room and as a result, diffuse links have low power efficiency. However, it provides the most mobility and robustness against blockage for receivers because signals can reach the receiver through many different paths. These characteristics make diffuse links attractive for mobile indoor optical wireless communications and ad hoc networks. Moreover, diffuse links have the simplest transceiver designs and are the most flexible configurations for indoor optical wireless communications. Gfeller and Bapst were first to introduce diffuse links in 1979 [23]. Experimental diffuse links working at 25 Mbps and 50 Mbps are reported in [25,26] and a 100 Mbps diffuse link is presented in [24]. Standard IrDA advanced infrared (AIr) links support data rates of at most 4 Mbps [27] while IEEE 802.11 diffuse infrared

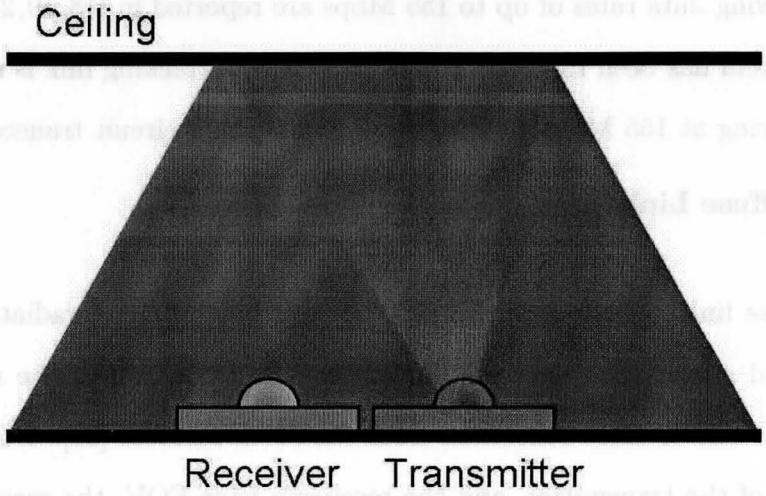

Figure 1.5: Diffuse configuration.

links support maximum rates of 2 Mbps [28].

1.2.4 Spot Diffusing Architecture

The spot diffusing architecture is a relatively new configuration, which is a combination of directed LOS link and diffuse link [3, 29–31]. In spot diffusing links, as shown in Fig. 1.3 (c), the transmitter sends low divergence optical signal to a small area on the ceiling termed *spot*. The receiver images the spot and receives the reflection of the transmitted signal from the ceiling. The idea of spot diffusing channel was introduced by Yun and Kavehrad in [29] where a new architecture termed multi-spot diffusing (MSD) was presented.
In MSD links, as shown in Fig 1.6, the transmitter sends data by modulating several low divergence beams to create an array of spots on the ceiling. Ideally, a receiver images a single spot and decodes the transmitted data. Identical

data is transmitted to all spots in the room and the number and location of the spots are selected so that each receiver has at least one spot in its FOV. Although both diffuse and MSD links depend on the reflections from room surfaces to send optical signals to receivers, two major differences,one in the transmitter and one in the receiver, between them gives MSD links much higher bandwidth. The MSD transmitters emit optical signals in low divergence beams toward small spots on the ceiling, while diffuse transmitters emit optical signals over high divergence beams toward all over the room. Thus, there is little power lost from transmitter to ceiling in the MSD systems. Since they have a high divergence, diffuse emitters can emit higher total optical power due to safety issues than the MSD transmitter emitting low divergence optical beams. Consequently, diffuse receivers receive much more multipath signals than the MSD receivers. The second difference between these two links is in the receiver. By providing many spots on the ceiling, MSD receivers can have smaller FOVs, which results in less noise and multipath signal reception and therefore higher bandwidths. In [4, 31] using computer simulations, it is shown that multipath signals have little influence on the MSD channel for frequencies as high as of 2 GHz while diffuse links are limited to less than 100 MHz due to multipath signals. Therefore, while data rates are less than few GHz, MSD channels can be considered practically multipath free. Fig. 1.7 shows the MSD channel impulse response in time and frequency domain. Note that the LOS part in Fig. 1.7 (a) is scaled so that much weaker multipath part is visible in the figure. This spot diffusing channel is a relatively new channel configuration and does not completely confirm to either diffuse or LOS links model. It is based on a line of sight path between receiver and the spot on

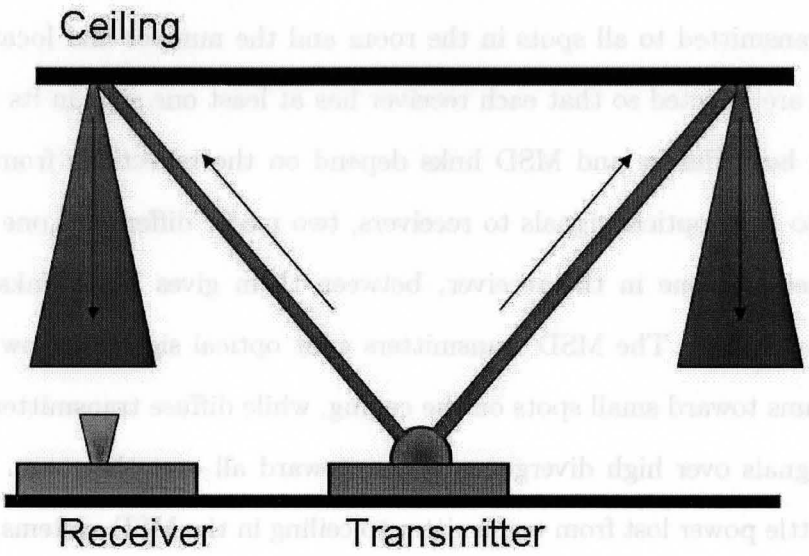

Figure 1.6: MSD configuration.

the ceiling. Therefore, it has some properties of both LOS links and diffuse links. Similar to LOS links, the received multipath signals are weak which results in a high bandwidth and makes it possible to send data at high rates over this channel. However, unlike LOS links, there is no need for precise alignment between transmitter and receiver, consequently, decreasing its design complexity. Spot diffusing channel and its properties are discussed in more detail in Sec.2.9.

Two main challenges in MSD links are creation multiple spots on the ceiling, and the joint optimization of number of spots needed and the receiver FOV. Furthermore, it is difficult to adapt the MSD system to different room sizes. Thus, for any specific room, a MSD system must be designed separately.

The simplest manner to make the multiple spots on the ceiling is using multiple emitters aimed in different directions. Using multiple emitters, how-

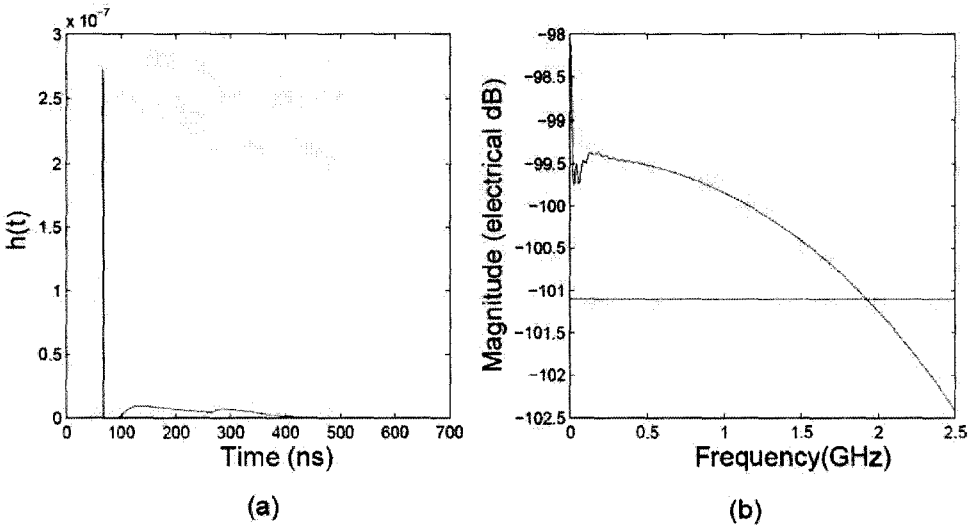

Figure 1.7: (a) MSD channel impulse response $h(t)$ (b) Frequency response of $h(t)$ for a MSD channel with 100 spots, simulated in a $6 \times 6 \times 3$ m room. Receiver is single element with FOV=11.2° and $A_R = 1cm^2$.

ever, is not practical since it makes the transmitter bulky and also, it is not possible to have a large number of spots. Another way to produce multiple spots on the ceiling is using a laser diode and a computer generated hologram (CGH) [3]. Fig. 1.8 shows a CGH which produces 8×8 beams [3]. A CGH is a photo-polymer which is fabricated using computers to produce wavefronts with arbitrary phase and amplitude distribution when is placed over a optical source. In [32], CGH diffusers with six-lobe patterns have been demonstrated which are fabricated in DuPont's holographic recording films HRF 600X001-20. CGHs have been proposed to form arrays of 10×10 spots for this application [33]. However, each CGH is designed for a specific location of the transmitter and room dimensions, and therefore for any specific room

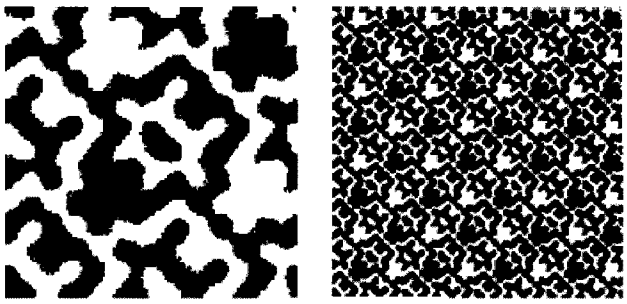

Figure 1.8: Bilevel CGH producing 8×8 beams: (a) elementary cell pattern (b) repeatition of the elementary cell pattern (reproduced from [3, Fig. 2]).

and transmitter location a separate CGH must be designed and fabricated, making such MSD transmitters inflexible and expensive.

The number of diffusing spots and the receiver FOV for MSD channel are discussed in [34]. In MSD design a joint optimization of the receiver FOV and number of the diffusing spots must be done [3]. Increasing the receiver FOV means increasing the amount of received ambient light and multipath signals, which decreases the channel bandwidth and channel quality. On the other hand, the FOV must be large enough so that every receiver in the room can see at least one spot. Let ΔS be the diffusing spot grid spacing and R_{rec} be the radius of the circle area on the ceiling seen by the receiver. In order to ensure that every receiver sees at least one spot, we should have $R \geq \Delta S\sqrt{2}$, as shown in Fig. 1.9.

The MSD configuration provides good mobility and robustness against blockage. In MSD system, many spots are created over the ceiling and the receiver FOVs are chosen large enough so that each receiver in the room has at least one spot in its FOV. Therefore, mobile receivers can receive data with high

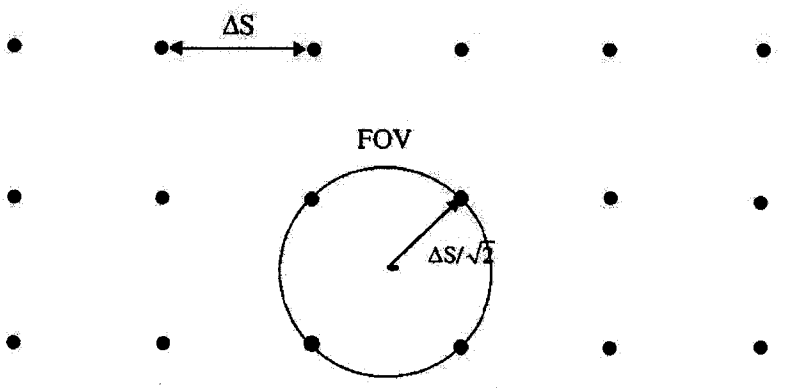

Figure 1.9: The geometry of FOV and MSD spot mesh to have at least one spot in FOV (reproduced from [4, Fig. 4]).

probability. Moreover, in MSD systems signal path is through the ceiling and has less probability of blockage. In [35], it is shown that MSD systems have for the proposed MSD system is robust against shadowing and the probability of blockage is less than 2%.

Recent work considers two other geometries for the multiple spots on the ceiling : line strip and diamond arrangement. These arrangements still offer significant gains (about 4 electrical dB) over diffuse links, with less complex transmitters [36, 37]. In [37], assuming transmitter emits total power of 1 W, SNRs as high as 30 dB are achieved in simulations for line strip arrangement. The design and performance of an experimental prototype MSD system which can maintain 70 Mbps at probability of error, P_e, of 10^{-9} over a 4-m range is discussed in [38]. In [7], the design of a MSD system working at 100 Mbps with P_e of 10^{-9} over 4.5 m ranges is presented.

	LOS	Diffuse	MSD
Channel Bandwidth	High	Low-Moderate	Moderate
Pointing Required	Yes	No	Somewhat
Immunity to Blockage	Low	High	Moderate-High
Mobility	Low	High	Moderate-High
Ambient light Rejection	High	Low	High
Multipath Distortion	None	High	Low
Path Loss	Low	High	Moderate

Table 1.2: LOS, Diffuse and MSD Link Characteristics [10]

Table 1.2 shows the link characteristics for LOS, diffuse and MSD links.

1.3 Contributions of Thesis

The *dynamic spot diffusing* (DSD) architecture proposed here derives many of the advantages of MSD links while reducing the complexity of the transmitter. As shown in Fig. 1.10, the DSD channel configuration consists of a single spot which is translated over the ceiling in a closed path. A multi-element imaging receiver is directed towards the ceiling and performs combining over receiver elements. Data symbols are received whenever the transmitted beam is in the FOV of the receiver. The main difference between the DSD channel and MSD or diffuse channels is that the DSD channel changes with time due to the spot motion while MSD and diffuse channels are considered time constant channels. When a spot is in the FOV of receiver, the DSD channel is identical to an MSD channel since in both channels, the same spot diffusing structure is used to send data from transmitter to receiver. However, in MSD channels, in order to get a good coverage over the room, many spots are created on the ceiling. In the DSD channel only one or a few spots are moving on the ceiling.

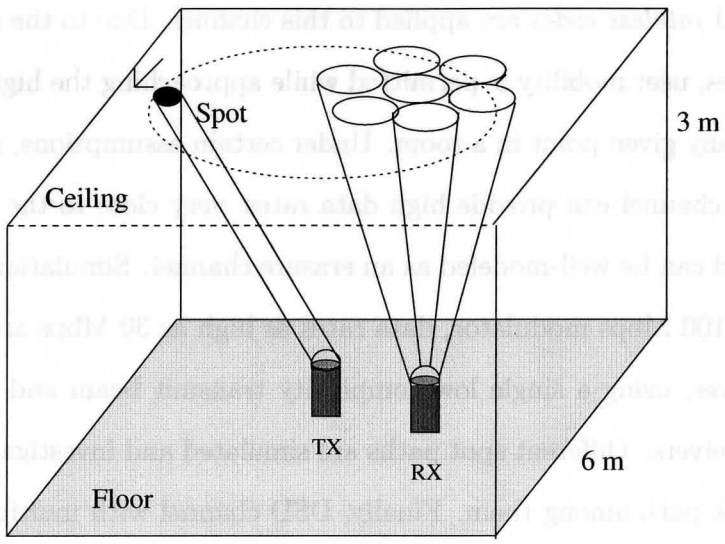

Figure 1.10: The proposed DSD configuration.

Therefore, the DSD channel is an extension of the MSD channel and has the same characteristics as the MSD channel when spot is in the receiver FOV. In the DSD structure, only a single (or few) optical emitters are present in the room which greatly reduces the impact of multipath distortion compared to MSD, allowing for the use of a high speed modulator. Moreover, the movement of the spot relaxes the eye safety power limitation and permits emission of more instantaneous power, which increases the channel quality compared to MSD. Furthermore, the DSD transmitter can be implemented using one or a few number of LDs or VCSELs while the MSD transmitter employs CGHs. Therefore, the DSD transmitter is simpler, more flexible and less expensive than the MSD transmitter. In this work, the channel capacity of the DSD link is discussed and the channel is simulated while it is corrupted with Gaussian noise. In order to realize the channel capacity, a class of erasure correcting

codes termed *rateless codes* are applied to this channel. Due to the robustness of these codes, user mobility is permitted while approaching the highest possible rate for any given point in a room. Under certain assumptions, it is shown that a DSD channel can provide high data rates, very close to the calculated capacity, and can be well-modeled as an erasure channel. Simulations indicate that with a 100 Mbps modulator, data rates as high as 30 Mbps are available at the receiver, using a single low complexity transmit beam and previously reported receivers. Different spot paths are simulated and investigated to find the best spot path among them. Finally, DSD channel with multiple spots is simulated. The results show that employing only few spots (up to 6) the channel capacity is increased and the coverage over the entire room is improved. For example, using two 1 Gbps spots moving in a circle path, rates as high as 440 Mbps are achievable in the proposed room.

This work has been presented at an international conference [39] and a journal paper is currently in preparation.

1.4 Thesis Organization

This thesis is organized as follows: the essential characteristics of indoor infrared wireless channel are reviewed in Chap. 2. These characteristics are different from their RF counterparts so they are reviewed before presenting the DSD channel. In Chap. 3, the DSD channel is introduced. Moreover, the DSD channel capacity and system design issues are discussed in this chapter. Appropriate coding techniques are presented in Chap. 4 to combat the time variant fading of the DSD channel. Code design and optimization issues are

discussed at the end of the same chapter. Chap. 5 shows the simulation results for DSD channel in addition to simulation assumptions and conditions. The thesis is concluded in Chap. 6 with directions for future work.

2

Indoor Optical Wireless Channel Characteristics

The indoor optical wireless channel is fundamentally different from RF channel in many ways. Before introducing the DSD channel, the main characteristics of indoor optical wireless channels are reviewed briefly in this chapter to present the constraints and limitations in this channel. These constraints must be considered in order to design a high-rate and reliable indoor optical wireless link.

The main differences between optical and RF indoor wireless channels can be classified as channel propagation properties, channel modulation and transmitter power limitations issues due to eye and skin safety.

2.1 IM/DD Optical Channel

Nearly all the current optical wireless systems employ intensity modulation and direct detection (IM/DD) technique. A baseband model of an IM/DD link is shown in Fig. 2.1. In indoor optical wireless IM/DD channels, at the

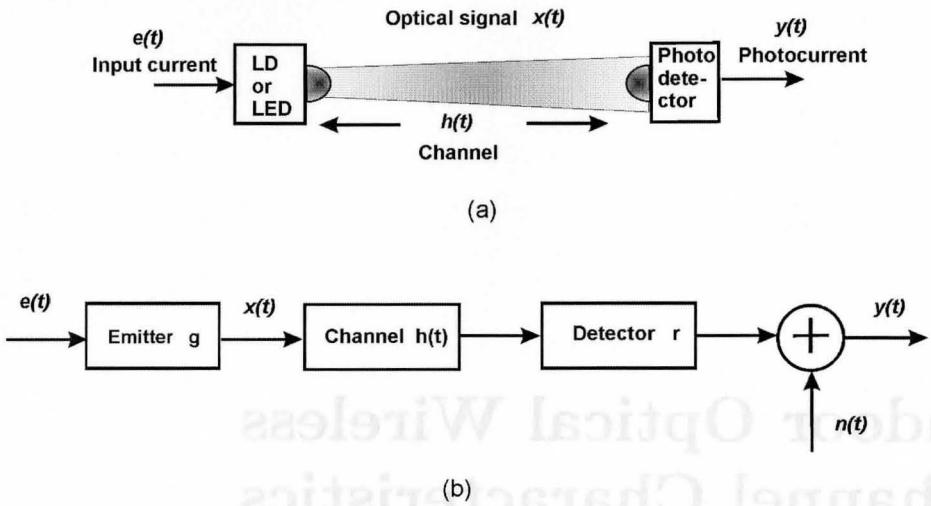

Figure 2.1: (a) Transmission and reception in an optical IM/DD link (b) Infrared IM/DD link model as a linear baseband system.

transmitter the electrical signal, $e(t)$, is converted into an optical intensity signal $x(t)$. This conversion can be modeled as $x(t) = g\ e(t)$ where g is the optical gain of the emitter device in W/A. The optical signal, $x(t)$, is sent over the channel having impulse response $h(t)$. At the receiver, the photodetector performs *direct detection* i.e produces an electrical photocurrent, $y(t)$, proportional to the received optical intensity in addition to noise, $n(t)$. Thus:

$$y(t) = r\ x(t) \otimes h(t) + n(t)$$

where $\otimes$ denotes convolution, r is the photodetector responsivity. The *responsivity* of a photodetector is defined as [10]:

$$r = \frac{I}{P}\ (A/W) \qquad (2.1)$$

where I is the average photocurrent generated and P is the average received optical power.

In this equation, r is a constant, and without loss of generality, it is possible to merge it into $h(t)$. In this manner, the indoor optical wireless IM/DD channel can be well represented as a baseband channel [40] shown in Fig. 2.1 and defined by:

$$y(t) = x(t) \otimes h(t) + n(t) \tag{2.2}$$

We present a formal discussion on IM/DD modulation in Sec. 2.7.

The optical intensity signal, $x(t)$, in IM/DD indoor optical wireless systems must satisfy two constraints. Because it is optical intensity, it can not assume negative amplitudes. Moreover, its average and peak amplitude is limited by eye and skin safety issues. The peak constraint gets important for high data rates where the bit period is short. In this case, the average power of optical signal can be safe while the peak is higher than safe level. However, for current system the main constraint is on average power due to low data rate. These two constraints can be stated as:

$$x(t) \geq 0, \tag{2.3}$$

$$P < P_{safe} \tag{2.4}$$

where P_{safe} is the maximum safe level of optical power and P, the average optical power of $x(t)$, is defined as below:

$$P = \lim_{T \to \infty} \frac{1}{2T} \int_{-T}^{T} x(t)\, dt \tag{2.5}$$

It is assumed that this integral exists in all cases of interest in this thesis. The power limitations due to eye and skin safety issues is the main limiting factor for indoor optical wireless links. These limitations are discussed in greater detail in Sec. 2.3.

In (2.2), $h(t)$ is the channel impulse response from transmitter to receiver. Multipath distortion at the receiver is modeled by $h(t)$ [7,10]. For most indoor optical wireless channels, especially non-LOS links, $h(t)$ is low pass because of the multipath signals which arrive at the receiver with time delay and decaying amplitudes. In indoor optical wireless links, as shown in Sec. 2.6, $h(t)$ depends on transmitter parameters (direction, emission angle, location in the room), receiver parameters (FOV, optical component characteristics, location and direction) and room properties (dimension, material characteristics and shape). The impulse response changes with any variation in these parameters. Therefore, there is not possible to derive an analytic formula for $h(t)$ in general except in a simple case of a LOS links. For non-LOS links, the channel response can be obtained by simulating the channel for each set of specific transmitter, receiver and room parameters [5]. These simulations are expensive in the sense of time and processing power and can not always be used. However, there are approximate models for $h(t)$ which can be used to calculate an approximation for $h(t)$ faster [41–43]. In this work, a simulator based on is implemented based on the well-known Barry and Kahn algorithm [5] which is discussed in more detail in Sec. 2.6.2.

Indoor optical wireless channels are impaired by strong ambient illumination which results in high-intensity shot noise at the output of the photodiode. The noise, $n(t)$, is modeled as white, independent of the transmitted signal

and Gaussian distributed [1,44] as is discussed in Sec. 2.4.

2.2 Optoelectronic Components

Infrared links also differ from RF links in the components used in their transceivers. Optical wireless systems do not employ antennas, instead they use solid-state optical emitters and photodetectors. In this section, essential optoelectronic devices are briefly reviewed to have a better understanding of optical wireless channel.

2.2.1 The Emitting Devices

A major constraint at the transmitter is the average power limitation due to eye safety issues. Most current infrared links work in 800-900 nm wavelength region because photodetectors working in this region are made from silicon and are available at low cost and provide high bandwidth [1,2]. At wavelengths above 1400 nm, the cornea is nearly opaque to optical radiation and eye safety issues permit transmitting more power which makes them more attractive. However, available photodetectors are expensive in this region because they are made from compound semiconductors and have more capacitance per unit area than shorter wavelength devices which decrease their bandwidth [1].
The circuit model for solid-state light emitters is a forward biased diode which produces an optical intensity output approximately linearly related to its drive current, when above the threshold [10]. Light emitting diodes (LED), laser diodes (LD) and Vertical Cavity Surface Emitting Lasers (VCSEL) are the common devices used as emitters in wireless infrared links.

2.2.1.1 Light emitting diodes (LED)

Light emitting diodes (LEDs) are the most commonly used emitters in current infrared systems because of their low price and their large emission area which makes them eye safe without using a diffuser [1]. Typical LEDs have light emission semiangles between $10° - 30°$ [1]. LEDs have poor power conversion efficiency, typically 10-20%, however, new devices have efficiencies of up to 40% [1]. Modulation bandwidths for LEDs are limited to tens of MHz for typical low cost devices. Typically increasing the bandwidth of LED results in a decrease in power conversion efficiency [1]. Moreover, LEDs have wide spectral widths, typically 25-100 nm, which requires employing a wide pass band filter in receiver and consequently receiving more ambient light from the environment [1].

2.2.1.2 Laser diode (LD)

Laser diodes (LDs) are more expensive than LEDs but they have several advantages over them. They provide much more modulation bandwidth, on the order of GHz and they have better power conversion efficiency between 30-70% [1, 10]. Moreover, they have narrow spectral widths which ranges from several nm to less than 1 nm [1]. This narrow spectral width allows using very sharp optical filters at receiver and to reject more ambient light. Moreover, it allows for multiple access using wave division multiplexing (WDM). In this technique, data for each user is sent using a different wavelength optical intensity signal. However, because of their low divergence beam and coherent output, a diffuser such as a thin plate of translucent plastic or a computer

generate hologram should be used to widen the beam and meet the eye safety standards for indoor applications [1]. Another drawback of LDs are changes of their characteristics due to temperature or aging of the device [10].
In this work for the DSD channel, LD must be used because the DSD transmitter must emit the optical signal through a low divergence beam. LED is not appropriate for this application because it emits signal with a wide angle pattern. Furthermore, LED can not operate at GHz rates.

2.2.1.3 Vertical Cavity Surface Emitting Laser (VCSEL)

A Vertical Cavity Surface Emitting Laser (VCSEL) is a solid-state micro laser diode that emits light in a cylindrical narrow divergence beam vertically from the surface of a fabricated wafer. They are available at 1-D and 2-D arrays on a wafer and provide high data rates and low power consumption [31, 45]. Commercial VCSELs working up to 10 Gbps are now available [46]. Moreover, VCSELs can be manufactured using standard microelectronic fabrication process, thus it is possible to integrate VCSELs on-board with other components with makes the transceivers simpler and less expensive [31, 45]. There are several reported experimental works employing VCSELs in transmitters for indoor optical wireless communications [2, 18, 19, 22].

2.2.2 Photodetectors

Photodetectors are the counter part of optical emitters i.e. they are solid state devices that convert the received optical power into an electrical signal. Photodetectors are diodes having reverse bias that convert incident radiant light into an electrical current and are also called *photodiodes* [10]. Photodi-

odes working at 700-1000 nm are made from silicon and are available at low cost and high speed. Photodiodes working at 1400 nm and above are made from compound semiconductors and therefore, are more expensive. Moreover, they have greater capacitance which limits their bandwidth [1, 10].

The *responsivity* of a photodiode as defined in (2.1), is the ratio of the output electrical power to input optical power. Two groups of widely used photodiodes are p-i-n photodiodes and avalanche photodiodes (APDs) [10]. To construct p-i-n photodiodes, relatively large intrinsic semiconducting material are placed between p+ and n+ doped regions. They have responsivities less or equal to unity. The main limiting factor of p-i-n photodiodes is their junction capacitance [10]. This is a more severe problem in optical wireless systems, because in order to collect more optical power, large area photodetectors are used which results in high device capacitance. Typical values for this depletion capacitance varies between 2 pF to 20 pF at a reverse bias of 3.3 V [10]. They have linear behavior over a wide range of input intensities and frequencies (up to 5 GHz) [10].

APDs are p-i-n devices that work at very high reverse bias and have an internal electrical gain [1, 10]. In cases where ambient light level is low, using APD for IM/DD links increases the signal power at receiver because of their higher internal gain and helps overcoming preamplifier thermal noise [1]. Therefore, APD based receivers show impressive performance when environment ambient light level is weak. However, in environments with high levels of ambient light, employing APDs in receivers result in a decrease in SNR because APD's internal gain has a random nature which increases the variance of the shot noise more than the signal power [1]. Therefore, they are typically used in fiber

optical systems. Moreover, APDs are more expensive, require high bias and their gain is dependent on temperature. Typical values for their photocurrent gain is of the order of 10^2 to 10^4 and for their bias voltage range from 30 V for InGaAs APDS to 300 V for silicon APDs. The avalanche gain relation with bias voltage and temperature is strongly nonlinear. Thus, they are well-suited to digital applications.

2.3 Optical Intensity Signalling Constraints

In IM/DD optical links, it is impossible to send data through the phase or frequency of the optical carrier and data is sent through the instantaneous intensity of the optical signal. The intensity of optical signal, $x(t)$ in Fig. 2.1, can not be negative, so the first constraint in IM/DD systems is non-negative amplitude for $x(t)$. The second constraint on $x(t)$ for *indoor* applications, is limited average and peak optical power of $x(t)$. The average of the optical intensity signal $x(t)$ is defined in (2.5).

Optical signals in the infrared band can be harmful to the human eye and skin and their power should be limited to avoid any problem. Power limitations due to safety issues are the main limiting factors for indoor optical wireless systems. Safety issues impose a limitation on both the peak and average optical power of optical intensity signal. However, for current systems the main concern is the average of optical signal because they can not create such narrow pulses that have safe average but harmful peak. Thus, in this thesis safety limitations is only on the average optical power. There are several international references for eye and skin safety standards for LED and laser emissions like

Safety Class	Interpretation
Class 1	Safe under reasonably foreseeable conditions of operation.
Class 2	Eye protection afforded by aversion responses including blink reflex (for visible sources only λ=400-700 nm).
Class 3A	Safe for viewing with unaided eye. Direct intra-beam viewing with optical aids may be hazardous.
Class 3B	Direct intra-beam viewing is always hazardous. Viewing diffuse reflections is normally safe.

Table 2.1: IEC classifications for optical sources [10, 11]

International Electrotechnical Commission (IEC) (IEC60825-1) [11], American National Standards Institute (ANSI) (ANSI Z136.1) [47] and European Committee for Electrotechnical Standardization (CENELEC) [48]. Any optical transmitter must be designed to satisfy an appropriate standard. For example, in the IEC standard which is a widely adopted one, the main exposure limits of optical sources are classified.

Table 2.1 shows the list of the primary IEC classes. It is most desirable that optical wireless systems work at Class 1 operation because in this class, all the emissions are safe. Moreover, there is no need for warning labels and special safety precautions, so they can are convenient to use for indoor applications. The key parameters which determine whether an emitter meets the standard are optical signal's wavelength, transmitter geometry and intensity. Notice that these standards put constraints on both peak and average optical power of the emitter [10]. Table 2.2 shows the limits for the average transmitted optical power for the IEC classes presented in Table 2.1 at four different wavelengths. The sources are assumed to be point emitters for calculation of these allowable average optical powers. In a point emitter optical source, the radiation is emitted from a small aperture and diverges slowly, as is the

Safety Class	650 nm visible	880 nm infrared	1310 nm infrared	1550 nm infrared
Class 1	< 0.2 mW	< 0.5 mW	< 8.8 mW	< 10 mW
Class 2	0.2-1 mW	n/a	n/a	n/a
Class 3A	1-5 mW	0.5-2.5 mW	8.8-45 mW	10-50 mW
Class 3B	5-500 mW	2.5-500 mW	45-500 mW	50-500 mW

Table 2.2: Safety classifications for point sources based on allowable average optical power for 4 different wavelengths [10, 11]

case in laser diodes [10]. The level of the safe average power depends on the wavelength of the signal and the diameter of the optical beam. For example, current indoor optical wireless links typically employ infrared signals having wavelength of 900 nm due to availability of inexpensive and high speed devices for this wavelength. As shown in Table 2.2, using 1500 nm devices, it is possible to send 13 dB more power from the transmitter and achieve higher SNR at the receivers. Sending more power at 1500 nm wave length is possible because optical signal at this wavelength is less harmful to the human eye. However, inexpensive devices working at this region are not available now, and therefore, most of current wireless optical system employ shorter wavelength devices [10].

2.4 Indoor Optical Wireless Channel Noise

Transmitter power in infrared channels is limited due to eye safety issues so it is important to discover the noise sources and minimize the channel noise in order to get a higher SNR. There are two primary sources of noise in optical wireless channels. There exists intense ambient light radiations in indoor environments from sun light, incandescent and fluorescent lamps and other sources [1]. These

ambient radiations induce shot noise in the receiver. The photons arrive in the receiver with a poisson distribution. However, the shot noise induced by a large number of photons tends to a Gaussian distribution with a positive mean and small variance. In this case, shot noise is well modeled as white, signal independent Gaussian noise. The shot noise's variance and one-sided power spectral density (PSD) are approximately given by [49]:

$$S_{shot}(f) = qrP_{bg},$$
$$\sigma^2_{shot} = qrP_{bg}R_b,$$

where q is electronic charge, r is the detector responsivity, P_{bg} is the received background light power, R_b is the bit rate. The PSD is an averaged second order statistic of a random process, and gives an insight on the distribution of power over frequency [10].

The other source of noise is thermal noise produced in the preamplifier of the receiver. This noise is also well modeled as white additive Gaussian noise [1]. The total noise in optical wireless links is sum of these two noises. However, using appropriate preamplifier, the thermal noise level is much lower than ambient light shot noise [3]. Therefore, thermal noise is neglected and ambient light noise is considered as the dominant source of noise in optical wireless links.

2.5 Infrared Propagation Characteristics

Infrared signals do not pass through opaque objects. Thus, infrared links in each room are limited by room walls and can not be detected in other rooms

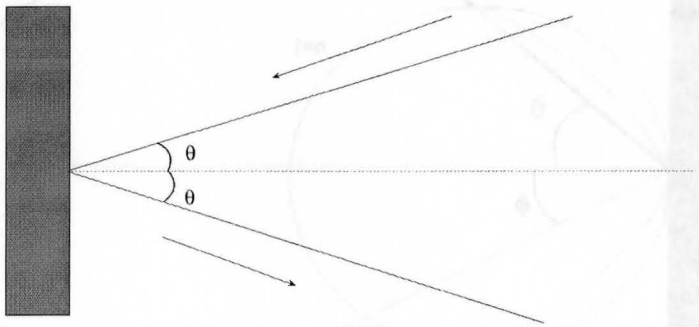

Figure 2.2: Specular reflection.

if the doors are closed and windows are covered by opaque covers. Therefore, it is possible to have simultaneous infrared links in adjacent rooms without any *interference* which is a serious problem in RF links. This makes infrared transceiver design much simpler than their RF counter parts. In addition, this property makes infrared links more secure since it is not possible to eavesdrop on infrared signals outside the room. However, this property has its own drawbacks. Any opaque object (such as a moving human) which covers the receiver or transmitter can block the link. This is termed *shadowing* or *blockage* of the link.

Another different propagation property of indoor optical wireless links is reflection. Infrared signal reflects *specularly* from shiny surfaces and *diffusely* from other surfaces. In specular reflection, as it is shown in Fig. 2.2, the reflection angle depends on the angle of signal arrival with the surface. But in a diffuse reflection, as it is shown in Fig. 2.3, the reflection angle does not depend on the angle of optical signal arrival to the surface. Since indoor surfaces are rarely

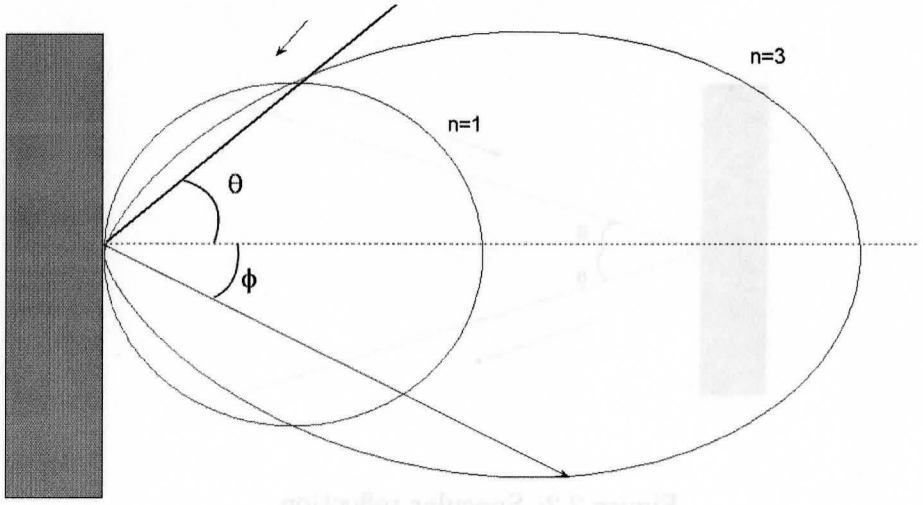

Figure 2.3: Diffuse reflection having Lambertian patterns for $n = 1$ and $n = 3$.

shiny, optical signal reflections are considered to be diffuse for indoor environments. The spatial pattern of reflected optical intensity is modeled using a *Lambertian* radiation pattern. A generalized Lambertian radiation pattern is define as:

$$P(\phi, n) = \frac{n+1}{2\pi} P_{total} \cos^n(\phi) \ \ (W/sr) \tag{2.6}$$

where P_{total} is the total average power of the incident optical signal and n is the *mode number* of the radiation lobe which determines the shape of the radiation pattern. As shown in Fig. 2.3, when n gets bigger, the pattern gets sharper and narrower, i.e. more directive. Note that $\int_c P(\phi, n)\ d\Omega = P_{total}$ where c is a surface of a sphere whose origin is the point of the signal incident on the surface. The units of $P(\phi, n)$ are Watts per steradians where steradians is the unit of solid angle. The solid angle Ω subtended by a surface S is defined as the surface area Ω of a unit sphere covered by the surface projection onto

the sphere. This can be written as:

$$\Omega = \int\int_S \frac{\hat{n}ds}{r^2} \tag{2.7}$$

where $\hat{n}$ is a unit vector from the origin, ds is the differential area of a surface element and r is the distance from the origin to the patch. The solid angle corresponding to all of space being subtended (which is equal to solid angle corresponding to a complete sphere) is 4π steradians.

2.6 Infrared Channel Response

Infrared links are classified as LOS or non-LOS types depending on whether there is line of sight between transmitter and receiver. In general, it is possible to consider the impulse response for indoor optical channels as the sum of two parts, the line of sight (h_{LOS}) and multipath component ($h_{multipath}$):

$$h(t) = h_{LOS}(t) + h_{multipath}(t)$$

The first term models the response for a LOS channel between receiver and transmitter, if it exists, and the second part response models the non-LOS diffuse channel between them. Although, a multipath channel always exists, if there is no line of sight between transmitter and receiver then $h_{LOS}(t) = 0$. Figure 2.4 shows the simulated $h(t)$ for a 10×10 MSD channel in a $6 \times 6 \times 3$ m room. LOS and multipath components are shown in this figure. This simulation is done using the Barry and Kahn [5] algorithm as discussed in

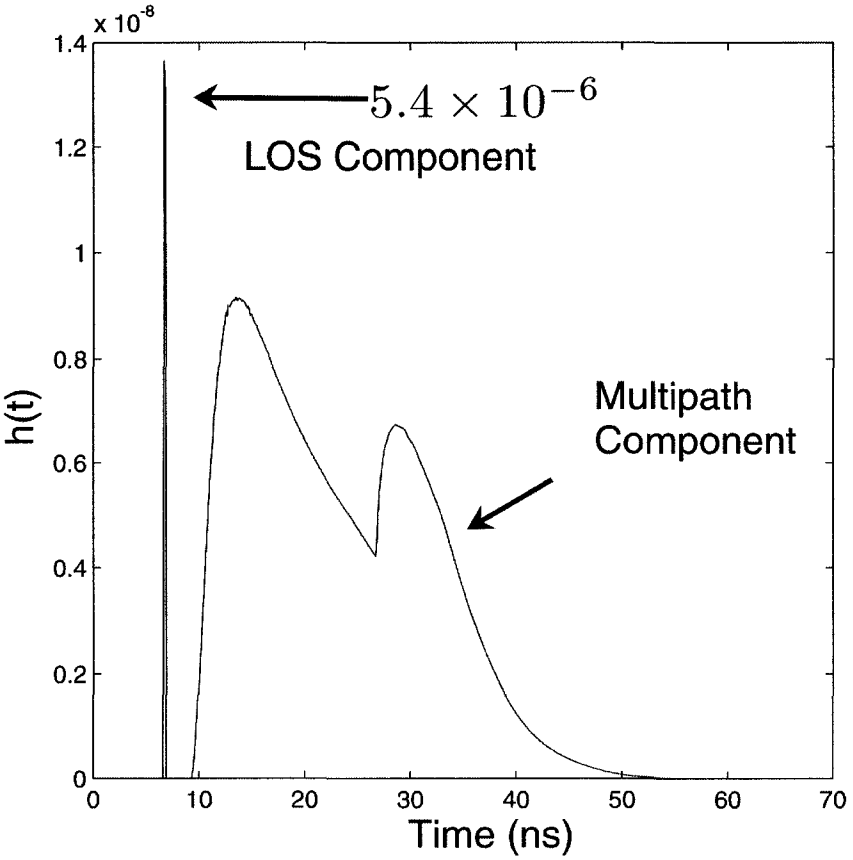

Figure 2.4: LOS and multipath signal for a 10×10 MSD channel.

Sec. 3.1.1.

2.6.1 LOS Component

If there exists a line of sight between transmitter and receiver, then impulse response has a LOS part which is very strong compared to $h_{multipath}(t)$ and $h_{multipath}(t)$ can be neglected in this case. Fig. 2.5 shows the geometry of the transmitter and receiver. Analytical expression for $h_{LOS}(t)$ can be derived

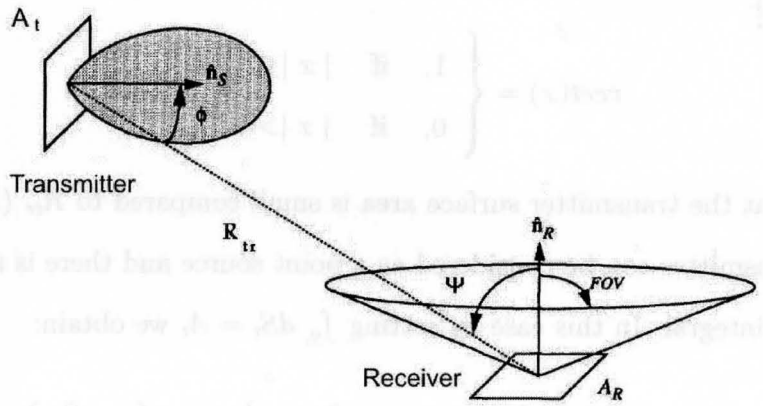

Figure 2.5: Geometry of transmitter and receiver for calculation of h_{LOS} (reproduced from [5, Fig. 2]).

using Lambertian model for transmitter [5]:

$$\begin{aligned} h_{LOS}(t) &= \int_{S_t}\int_{S_R} \frac{n+1}{2\pi}\cos^n(\phi)\mathrm{rect}\left(\frac{\psi}{FOV}\right) d\Omega \, \frac{dS_t}{A_s}\delta\left(t-\frac{R_{tr}}{c}\right) \\ &= G_{LOS}\cdot\delta\left(t-\frac{R_{tr}}{c}\right), \end{aligned} \tag{2.8}$$

where n is the order number of the Lambertian model of the transmitter, ϕ as shown in Fig. 2.5 is the angle between line of sight and transmitter's surface normal, ψ is the angle between line of sight and receiver's surface normal, R_{tr} is the distance between receiver and transmitter and $d\Omega$ is the differential solid angle subtended by the detector surface from transmitter. In this equation, G_{LOS} is the gain of the channel and $\frac{R_{tr}}{c}$ is the time which takes for optical signal to arrive into the receiver. The integral is taken over the all points on the transmitter surface, S_t, and the set of solid angle subtended by the detector surface from transmitter, S_R. The rectangular function, $rect(x)$, is

defined as [5]:

$$rect(x) = \begin{cases} 1, & \text{if} \quad \mid x \mid \leq 1 \\ 0, & \text{if} \quad \mid x \mid > 1 \end{cases}.$$

Provided that the transmitter surface area is small compared to R_{tr} ($R_{tr}^2 >> A_t$), the transmitter can be considered as a point source and there is no need for the first integral. In this case by setting $\int_{S_t} dS_t = A_t$ we obtain:

$$\begin{aligned} h_{LOS}(t) &= \int_{S_d} \frac{n+1}{2\pi} \cos^n(\phi) \text{rect}\left(\frac{\psi}{FOV}\right) d\Omega \, \delta\left(t - \frac{R_{tr}}{c}\right) \\ &= G_{LOS} \cdot \delta\left(t - \frac{R_{tr}}{c}\right), \end{aligned} \tag{2.9}$$

Moreover, if the R_{tr}, is large compared to the detector area A_R ($A_R << R_{tr}^2$), then the received optical irradiance is constant over the detector surface and using (2.7), the solid angle subtended is:

$$\int_{S_d} d\Omega = cos(\psi) \frac{A_R}{R_{tr}^2}.$$

Substituting into (2.9) gives:

$$\begin{aligned} h_{LOS}(t) &= \frac{n+1}{2\pi} cos^n(\phi) \cos(\psi) \frac{A_R}{R_{tr}^2} rect(\frac{\psi}{FOV}) \delta\left(t - \frac{R}{c}\right) \\ &= G_{LOS} \cdot \delta\left(t - \frac{R_{tr}}{c}\right), \end{aligned} \tag{2.10}$$

This equation is the LOS component of channel impulse for the case where R_{tr} is large compared to both receiver detector area, A_R and transmitter surface area, A_t. These conditions are valid typically for indoor optical wireless links where the R_{tr} is in order of meters while A_R and A_t have surface of some mm^2

or less. Therefore, hereafter, (2.10) is used to approximate for LOS component of channel impulse response in this thesis.

2.6.2 Multi Path Component

For multipath channels, receivers collect the transmitted optical intensity after several reflections from room surfaces. Signals arrive at the receiver with different time delays and, moreover, a portion of signal power is lost at each reflection. Thus, $h_{multipath}(t)$ has a decaying shape in time. Unfortunately, it is not possible to derive an exact analytical expression for $h_{multipath}(t)$ since it depends greatly on room conditions, material properties and receiver FOV. Therefore, the exact $h_{multipath}(t)$ should be estimated for each position and orientation of receiver in the room separately using computer simulations. One of the best known simulation algorithms is the method developed by Barry and Kahn [5]. In this algorithm, the room surfaces are divided into many small surface elements and at each step, the received power to every surface element is computed. Then the simulator proceeds recursively considering every surface element as a new transmitter having the received power calculated in previous step. The accuracy of the algorithm depends on the size of the surface elements used to discretize the surfaces. This process can be repeated an arbitrary number of times, but the computational cost increases exponentially with number of considered bounces [5]. Notice that, the amount of received power decreases after each bounce. Therefore, limiting the number of considered bounces to a small number saves time and computations while its influence on results can be shown to be negligible. For example, in MSD links where the multipath portion of impulse response is small due to low divergence

transmitter beam and small receiver FOVs, simulations have shown that more than 96 % of the total power is received after first three bounces [30].

Ray tracing algorithms [50, 51] are another method to simulate the channel response. In this algorithm, at each step, ray directions are chosen randomly according to the radiation pattern of the transmitter. The contribution of each ray from the transmitter to the receiver is computed. The rays not arriving into the receiver, are considered new sources and the process is continued to achieve an arbitrary number of bounces. This algorithm is similar to the Barry and Kahn algorithm, however, instead of discretizing room surfaces, source emissions are discretized at each step. The accuracy of this algorithm depends on the number of rays used in each step for each source.

The room simulator used in this work is based on the Barry and Kahn algorithm [5]. This simulator divides the room surfaces to 5×5 cm patches and calculates the impulse response with time resolution of 100 ps. This simulator is employed to compute the impulse response of the DSD channel in chap 3.

2.6.3 Approximate Models of $h_{multipath}(t)$

Running simulations to find the impulse response for each position is expensive in the sense of time and computation power. In order to facilitate signalling design, several approximate models have been developed to model $h_{multipath}(t)$.

2.6.3.1 Exponential-Decay Model

In this model, multipath reflections which produce multipath dispersion are considered. Reflectivity, σ, is defined as the ratio of the power reflected from

a surface to the incident power. Since room surfaces have reflectivites smaller than one, the power received after $n+1$ bounces is expected to be less than power received after n bounces by a factor of the average reflectivity of the room surfaces. Moreover, the time of arrival of $n+1$ bounces signals is later than n bounces signals arrival time. Therefore, according to this model, the channel impulse response would be a sequence of delta functions having geometrically decaying amplitudes [41]. This geometric series looks like a decaying exponential impulse response as below:

$$h_e(t,\tau) = \frac{1}{\tau}\exp(-t/\tau)u(t)$$

where the step function, u(t), is defined as:

$$u(t) = \begin{cases} 1, & \text{if} \quad t \geq 0 \\ 0, & \text{if} \quad t < 0 \end{cases}.$$

2.6.3.2 Ceiling Bounce Model

In this model the impulse response due to diffuse reflection from a single infinite-plane reflector is used as a approximation for $h(t)$. The reason for choosing infinite Lambertian reflecting plane is that it is a good approximation for a large ceiling [41]. Using this model the impulse response is shown to be as [41]:

$$h_c(t,a) = \frac{6a^6}{(t+a)^7}u(t)$$

where a is a constant which depends on the distance of transmitter with ceiling. This expression is defined as ceiling-bounce model for multipath dispersion

[41]. More details on this model can be found in [41].

2.6.3.3 Statistical Models

In addition to approximate models for $h_{multipath}(t)$, some statistical models have also been developed to show variations of channel DC gain in a room. Several statistical distributions have been considered and investigated to find which is closest to the actual gain distribution in the room for an ensemble of optical wireless channels [42, 43]. The channel DC gain is defined as the ratio of the received power and transmitted power and is defined as below [41]:

$$G_0 = \frac{P_{rx}}{P_{tx}} = \int_{-\infty}^{+\infty} h(t)\, dt$$

where P_{rx} is the average received power and P_{tx} is the average transmitted power. In [42], it is shown that the distribution of the channel gain in dB for only LOS channel case (without accounting for multipath channel) follows a modified gamma distribution defined as [42]:

$$Y = K_{mg} - Z$$

where Z has gamma distribution. The channel gain in dB for LOS links (having both $h_{LOS}(t)$ and $h_{multipath}(t)$), for most transmitter receiver distances, follows a modified Rayleigh distribution defined as [42]:

$$Y = K_{mr} - R$$

where R has Rayleigh distribution. For diffuse channels, it is shown in [43] that shifted lognormal distribution is the best fit for the observed distributions of diffuse channel gains.

2.7 Optical Intensity Modulation

2.7.1 Definitions

Path Loss: Path loss is a measure of the amount of power lost through the channel from transmitter to receiver and is defined as the inverse of the channel DC gain [52].

Bandwidth: The bandwidth occupied by a signal is a measure of the amount of necessary spectral support for the transmission of that signal [10]. There are several different definitions of bandwidth in literature. A widely used one is *-3dB bandwidth* which is the first frequency that the psd is lower from its peak by a factor of 1/2. The *first null bandwidth* is defined as the width of the main lobe of the signal in positive frequencies [10]. In this work, the first null bandwidth of the signal is employed.

Bandwidth Efficiency: The bandwidth efficiency of a modulation scheme is defined as the ratio of the bit rate R_b in bits/second and bandwidth B in Hz [10]. Bandwidth efficiency is used as a figure of merit to compare different modulation schemes.

Optical wireless links use *intensity modulation and direct detection* (IM/DD) with modulation techniques such as on-off keying (OOK) or pulse position modulation (PPM). These techniques are used because there are inexpensive

and simple devices available for implementing these links.

The *power spectrum density* (psd) $S_g(f)$ represents the power distribution of a given function $g(t)$, in frequency domain [53].

SNR: SNR is the ratio of the signal power to the noise power. In this work , similar to [1], SNR is related to the bit error rate (BER) as:

$$BER = Q(\sqrt{SNR}).$$

In these techniques data is modulated onto instantaneous power of the optical signal. At the receivers, a photodetector produces a current proportional to the received optical power. Electrical power is proportional to square of current, thus, the electrical signal power is proportional to the square of optical power. Therefore, in IM/DD systems, SNR is proportional to square of optical power and 1 dB optical power is equivalent to 2 dB electrical SNR which makes IM/DD links sensitive to path loss [1, 10]. As a result, IM/DD links need high transmitter power to cover long ranges. However, transmitter power is limited due to safety issues and power limitation of mobile transmitters. Thus, indoor optical IM/DD links usually can be applied only to short range communications. It is possible to increase the range of IM/DD by using power efficient modulation techniques like PPM which sacrifices bandwidth efficiency to achieve better power efficiency [40] if enough channel bandwidth is available, as will be discussed in Sec. 5.5.

2.7.2 On-Off Keying (OOK)

The most common modulation technique used in optical wireless links is OOK due to its simplicity and the availability of inexpensive devices.

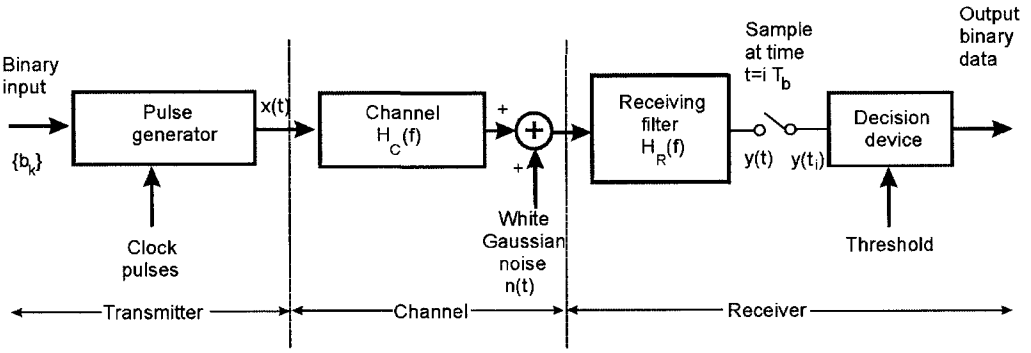

Figure 2.6: Transmission model for base band OOK system (reproduced from [6, Fig. 9.1]).

This modulation is a binary level modulation. A base band transmission model for OOK is shown in Fig. 2.6. In an OOK system, a binary data source, b_k, with period T_b, is the input of the system. The modulator generates pulses, whose amplitudes a_k, depend on b_k as:

$$a_k = \begin{cases} +a & b_k = 1 \\ 0 & b_k = 0 \end{cases}$$

Therefore, the OOK intensity signal $x(t)$ is [6]:

$$x(t) = \sum_{k=-\infty}^{\infty} a_k g(t - kT_b)$$

where $g(t)$ is the normalized shaping pulse i.e $g(0) = 1$.

In this work, only rectangular OOK modulation is considered because of its simplicity. Therefore, $g(t) = Rect\left(\frac{t}{T_b}\right)$. Rectangular OOK shaping pulses are shown in Fig. 2.7.

The OOK signal $x(t)$, after passing through the channel, is modified in a deter-

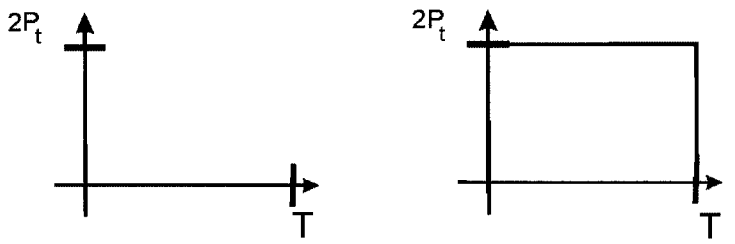

Figure 2.7: Rectangular OOK shaping pulses

ministic fashion according to channel transfer function $H_c(f)$. Moreover, the channel adds noise $n(t)$ to the signal at the receiver input. The noisy signal is passed through a *receiver filter* with transfer function $H_R(f)$. The output of this filter is sampled *synchronously* with the transmitter. The sampling instants is determined by a clock or timing signal which is usually extracted from the receiving filter output. At the end, the original data sequence is reconstructed from the sequence of obtained samples using a *decision device.* In the decision device, the amplitude of each sample is compared with a threshold. If the sample exceeds the threshold it is reconstructed as a '1' else it is reconstructed as a '0' [6]. The optimum receiving filter for this system in sense of minimizing the probability of error in receiver is a matched filter [53].

Matched Filter: A matched filter with transfer function $H_{opt}(f)$ is a filter whose transfer function is proportional to Fourier transform of pulse shape $G(f)$ and inversely proportional to additive noise power spectral density $S_{noise}(f)$, provided that the bandwidth of transmission is within the bandwidth of the channel. Then we have no channel distortion of the transmitted signals. The wide bandwidth of the DSD channel is discussed in Sec. 3.1.1. In this case,

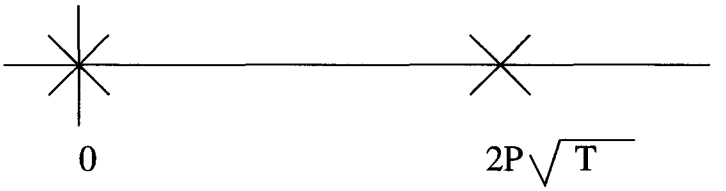

Figure 2.8: Constellation for OOK modulation

the match filter response is [53]:

$$H_{opt}(f) = K\frac{G^*(f)e^{-j2\pi t_d}}{S_{noise}(f)}$$

where t_d is the time delay of the system and K is the total amplification of the system from transmitter to receiver.

Thus, matched filter amplifies frequencies where the signal spectrum if large and attenuates those frequencies where the noise spectrum is large.

2.7.2.1 OOK probability of error

As shown in Fig. 2.7, one of the OOK basis functions has amplitude 0 and the other has amplitude $2P_t$. Using these basis functions, the constellation for this technique is two points in a one dimensional space, shown in Fig. 2.8. Assuming AWGN, matched filtering to the transmitted pulse and channel being flat, the probability of error is obtained as [10]:

$$P_e = Q\left(\frac{rP}{\sqrt{R_b\sigma^2}}\right) = Q(\sqrt{SNR}) \tag{2.11}$$

where $R_b = \frac{1}{T_b}$ is the bit rate and r is defined in (2.1). And:

$$Q(x) = \frac{1}{\sqrt{2\pi}} \int_x^{\infty} e^{-\frac{y^2}{2}} dy$$

Therefore, the SNR for OOK is defined as:

$$SNR_{OOK} = \frac{r^2 P^2}{R_b \sigma^2}, \tag{2.12}$$

OOK has power spectrum density as [10]:

$$S_{OOK}(f) = P^2 \delta(f) + P^2 T sinc^2(\pi f T)$$

where P is the average optical power of OOK signal, and $sinc(x) = \frac{sin(x)}{x}$. Fig. 2.9 shows the spectrum power density for the case $T = 1$ and $P = 1$. As shown in this figure, the first null bandwidth of the OOK modulation is $B = 1/T_b$ Hz which results in a bandwidth efficiency of $R_b/B = 1$ bits/s/Hz.

2.7.3 OOK Channel Capacity

The *channel capacity* of a channel is important because according to the channel coding theorem, it is the maximum achievable rate of data transmission over that channel [54]. Therefore, here the capacity of OOK IM/DD channel is discussed in more detail.

2.7.3.1 Definitions

Mutual Information: The mutual information, $I(X;Y)$, between two random variables X and Y, having joint density function $f(x,y)$ and probability den-

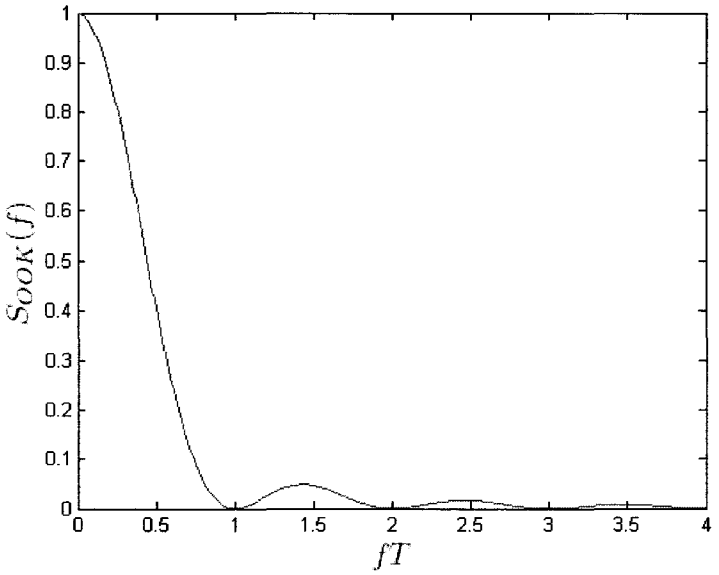

Figure 2.9: OOK PSD for $P = 1$ and $T = 1$

sity functions $f(x)$ and $f(y)$, is defined as:

$$I(X;Y) = \int_{x \in D_X} \int_{y \in D_Y} f(x,y) \log_2 \left(\frac{f(x,y)}{f(x)f(y)} \right) dy\, dx \tag{2.13}$$

where D_X is the domain of x and D_Y is the domain of y.

The optical wireless IM/DD channel, as shown in Sec. 2.1, is modeled as a base band channel with additive white Gaussian noise with average optical power constraint on the channel input due to safety issues.

We limit attention to input distribution, $p(x)$, over a discrete equally likely binary alphabet for practical reasons. The OOK is a binary modulation technique and channel input can be only 0 or 1 i.e $X = 1$ with probability $p(1)$ or $X = 0$ with probability $p(0)$. Therefore, to derive the capacity for OOK, the maximum of $I(X;Y)$ for the this case must be calculated. The constellation of

the OOK modulation is similar to the constellation of 2-pulse amplitude modulation (PAM) technique with a shift, and mutual information is invariant to shift. Therefore, the channel capacity using OOK techniques is equal to the channel capacity using 2-PAM. In order to calculating the channel capacity for OOK modulation, we will follow the procedure in [55] for calculating channel capacity for 2-PAM.

In 2-PAM, a pulse with amplitude $a = a_0$ is sent for 1 with probability $p(1)$ and a pulse with amplitude $a = a_1 = -a_0$ is sent for 0 with probability $p(0)$. Thus, both channels have equal capacity when $a_0 = P\sqrt{T}$. Here we derive the channel capacity for 2-PAM which is also the channel capacity for OOK.

This channel has a discrete input and continuous output. Hence the first integral in (2.13) reduces to a sum over two values of X. Thus:

$$I(X;Y) = \sum_{x\in 0,1} \int_{y\in D_Y} f(x,y) \log_2(\frac{f(x,y)}{p(x)f(y)})dy$$

and assuming independence between noise and signal, we have:

$$f(y) = \sum_{k=0}^{1} f(x=k,y) = \sum_{k=0}^{1} p(k) * f(y|x=k) = \sum_{k=0}^{1} p(k) * f(y|a=a_k)$$

where:

$$f(y|a=a_k) = \frac{e^{\frac{-(|y-a_k|^2)}{2N}}}{\sqrt{2\pi N}}$$

Thus:

$$C = \max \sum_{k=0}^{1} p(k) \int_{-\infty}^{+\infty} f(y|a_k) \log_2 \left(\frac{f(y|a_k)}{\sum_{i=0}^{1} p(i) f(y|a_i)} \right) dy$$

Assuming equiprobable signalling, $p(i) = \frac{1}{2}$, we can omit the max. Inserting the expression for $f(y|a_k)$, the equation above becomes:

$$C = \sum_{k=0}^{1} \frac{1}{2} \left(\int_{-\infty}^{+\infty} f(y|a_k) log_2(2) dy + \int_{-\infty}^{+\infty} f(y|a_k) \log_2 \left(\frac{e^{-\frac{|y-a_k|^2}{2N}}}{\sum_{i=0}^{1} e^{-\frac{|y-a_i|^2}{2N}}} \right) dy \right) =$$

$$\sum_{k=0}^{1} \frac{1}{2} log_2(2) \int_{-\infty}^{+\infty} f(y|a_k) dy - \frac{1}{2} \sum_{k=0}^{1} \int_{-\infty}^{+\infty} f(y|a_k) \log_2 \left(\frac{\sum_{i=0}^{1} e^{-\frac{|y-a_i|^2}{2N}}}{e^{-\frac{|y-a_k|^2}{2N}}} \right) dy =$$

which is:

$$1 - \frac{1}{2} \sum_{k=0}^{1} E \left\{ \log_2 \left(\sum_{i=0}^{1} e^{\frac{-|y-a_i|^2 - |y-a_k|^2}{2N}} \right) \right\}$$

By changing the variable $w = y - a_k$, we'll have:

$$C = 1 - \frac{1}{2} \sum_{k=0}^{1} E \left\{ \log_2 \left(\sum_{i=0}^{1} e^{\frac{-|w+a_k-a_i|^2 - |w|^2}{2N}} \right) \right\}$$

where w has a normal distribution.

The capacity curve versus SNR for OOK would be as Fig 2.10 which is obtained by Mont-Carlo averaging of above equation [10, 55].

2.7.3.2 Pulse Position Modulation (PPM)

In this modulation, the modulator produces a vector with length L in which only one of L elements has unit value and the other $L - 1$ elements have value zero. Thus, the basis vectors are orthogonal to each other and are called symbols. Fig 2.11 shows the 4 basis vectors (symbols) for 4-PPM. L-PPM modulation, can be considered as low rate coded OOK. Input bits a_j first enter a low rate block coder with rate $\frac{log_2(L)}{L}$ and the output of the encoder

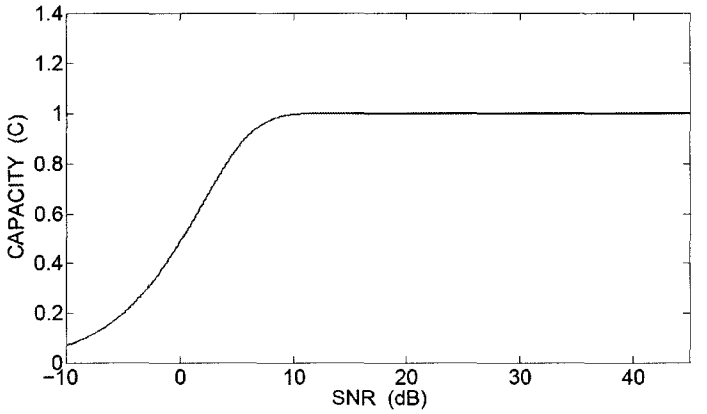

Figure 2.10: Channel capacity for equally likely OOK modulation with SNR defined in (2.12).

is sent over the channel using an OOK modulator. The receiver, based on the position of the one value in the received vector, generates appropriate output. The probability of error for PPM noting that constellation points are orthogonal to each other and have equal distance from each other, is shown to be [10]:

$$P_{esym} \approx (L-1) \cdot Q\left(rP\sqrt{\frac{L}{2R_s\sigma^2}}\right) = (L-1) \cdot Q\left(\sqrt{SNR}\right)$$

where $R_s = 1/T$ is the symbol rate. Therefore, SNR for L-PPM is defined as:

$$SNR_{L-PPM} = \frac{(rP)^2 L}{2R_s\sigma^2} \tag{2.14}$$

Setting $R_b = \log_2(L).R_s$ and comparing (2.14) with (2.12), we observe that using L-PPM, results in $-5\log_{10}(\frac{L\log_2(L)}{2})$ dB power gain compared to OOK technique.

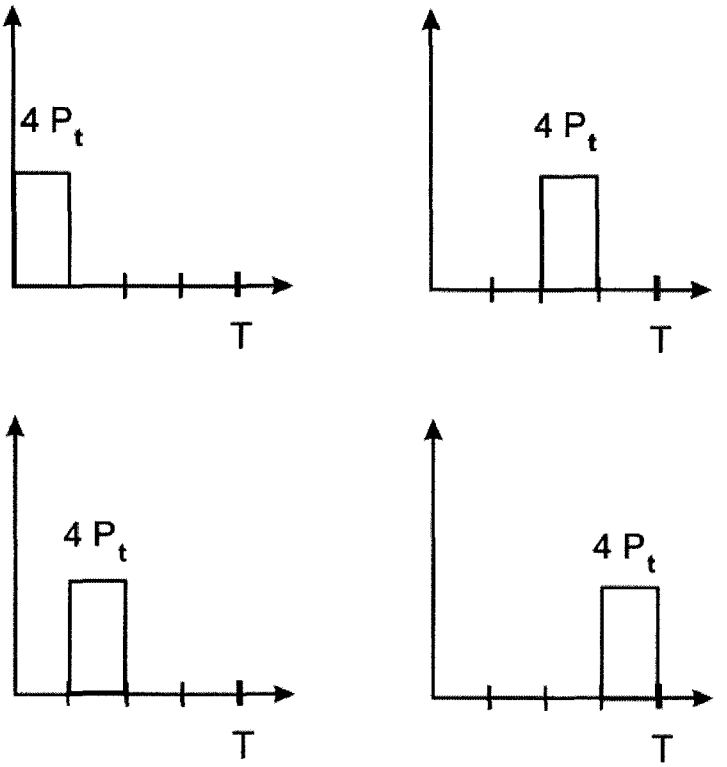

Figure 2.11: Four basis functions of 4-PPM

Assuming orthogonal equiprobable signals, all symbol errors are equiprobable and have probability of [56]:

$$\frac{P_{esym}}{L-1}$$

Moreover, n bits out of k bits can be in error in $\begin{pmatrix} k \\ n \end{pmatrix}$. Therefore, the average number of bit errors per symbol having k bits is [56]:

$$\sum_{n=1}^{k} n \begin{pmatrix} k \\ n \end{pmatrix} \frac{P_{esym}}{L-1} = k \frac{L/2}{L-1} P_{esym}$$

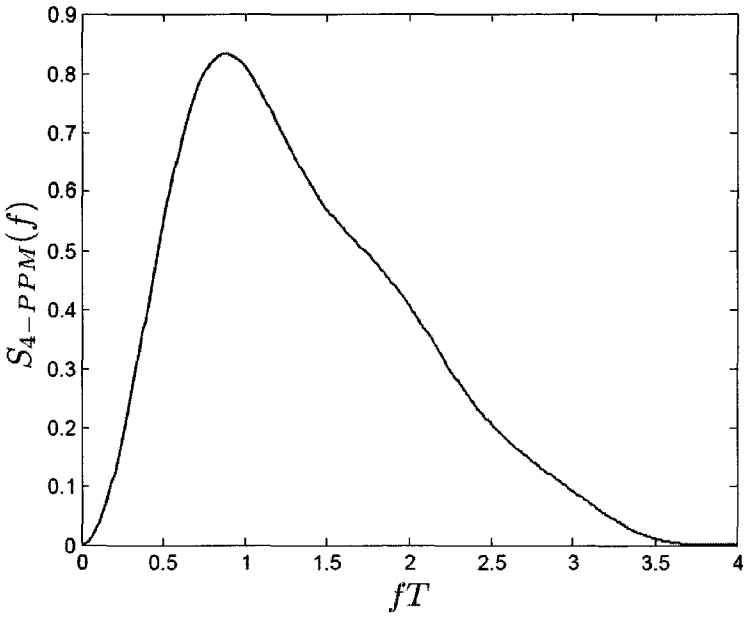

Figure 2.12: 4-PPM PSD for $P = 1$ and $T = 1$

Hence, the average probability of bit error is obtained by dividing the above expression by k, length of symbol bits, and is equal to:

$$P_e \approx \frac{L}{2} \cdot Q\left(rP\sqrt{\frac{L\log_2(L)}{2R_b\sigma^2}}\right) \tag{2.15}$$

where $R_b = R_s \log_2(L)$ is the bit rate.

The power spectrum density for L-PPM is [10]:

$$S_{PPM}(f) = P^2\delta(f)+P^2T\text{sinc}^2(\frac{\pi fT}{L})\left[1-\frac{1}{L^2}\left(L+2\sum_{i=1}^{L-1}(L-i)\cos\left(\frac{2\pi fT}{L}i\right)\right)\right]$$

Fig. 2.12 shows the PSD of 4-PPM when $P = 1$ and $T = 1$. As shown in this figure, the first-null bandwidth of 4-PPM is $B = 4/T_b$ Hz. Therefore,

Modulation Scheme	Normalized Average Power Requirement (Optical dB)	Normalized Bandwidth Requirement
OOK	0	1
L-PPM	$-5\log_{10}(\frac{L\log_2(L)}{2})$	$\frac{L}{\log_2(L)}$

Table 2.3: Normalized average power and normalized bandwidth requirements for OOK and L-PPM modulations on ideal distortion less channel with AWGN. The OOK modulation has power and bandwidth requirement of 0 dB and unity [1]

the bandwidth efficiency of this technique is $R_b/B = \log_2(L).R_s/B = 2/4 = 0.5$ bit/s/Hz. Comparing this value with bandwidth efficiency of the OOK technique, we see that 4-PPM requires 2 times more bandwidth than OOK. In general, the bandwidth efficiency of L-PPM is $\log_2(L)/L$ [1, 10]. Table 2.3 shows the power and bandwidth difference between OOK and L-PPM. The powers and bandwidths are normalized to the values for OOK [1].

In Fig. 2.13, normalized power and normalized bandwidth efficiency required to achieve bit error rate (BER) of 10^{-6} are plotted for OOK and L-PPM. Although L-PPM offers better power efficiency, non-LOS links, such as diffuse, typically use OOK modulation scheme because they suffer from multipath distortion which limits their channel bandwidths. Moreover, OOK transceivers are simpler and less expensive.

The SNR in (2.12) for IM/DD shows that the SNR is proportional to inverse of the root of bit rate. Therefore, by increasing the bit rate and not changing the power, the probability of error increases. For indoor optical wireless systems average optical power is limited by safety issues and can not be increased. One of the ways to increase the bit rate and keep the probability of error at the same level without increasing the transmitter power is using more power efficient

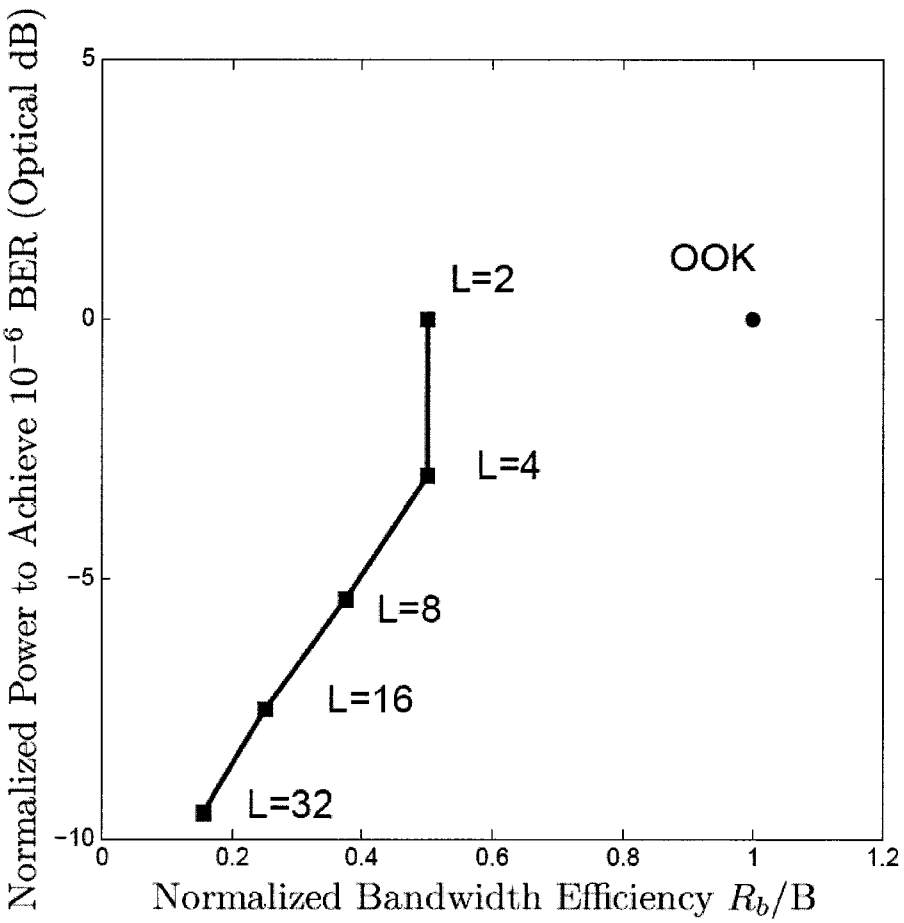

Figure 2.13: Comparison of average power efficiency and bandwidth efficiency of OOK and L-PPM modulation schemes on channels with IM/DD and AWGN

modulation schemes such as L-PPM when enough bandwidth is available. The DSD channel is constrained by power and not bandwidth because, as discussed in Sec. 3.1.2, it has a wide bandwidth. Therefore, L-PPM modulations can be employed to achieve higher rates. In Chap. 5, L-PPM technique is employed to compensate the SNR decrease due to bitrate increase.

2.8 Receiver Architectures

There are two types of receivers, single element and multi element receivers, used in optical wireless links. Single element receivers, shown in Fig. 2.14 (a), are the simplest type which use a single photodetector as the receiver. In this type, receivers collect all the ambient light and multipath signals received in its FOV in addition to the data signal. Therefore, as the FOV increases receiver collects more noise and multipath signal. Single element receivers are the least expensive group but they can not reject any of their received ambient light.

Multi element receivers, shown in Fig. 2.14 (b) and (c), are more complicated and expensive. However, they are able to reject a portion of received ambient light and improve SNR compared to single element receivers. Multi element receivers are essentially several detectors whose outputs are combined together in an appropriate way. Based on their implementation, multi element receivers are categorized to *angle diversity* and *imaging* receivers. Angle diversity receivers, as shown in Fig. 2.14 (b), are composed of several single element receivers while imaging receivers, as shown in Fig. 2.14 (c), employ arrays of integrated photodetectors instead of separate receivers.

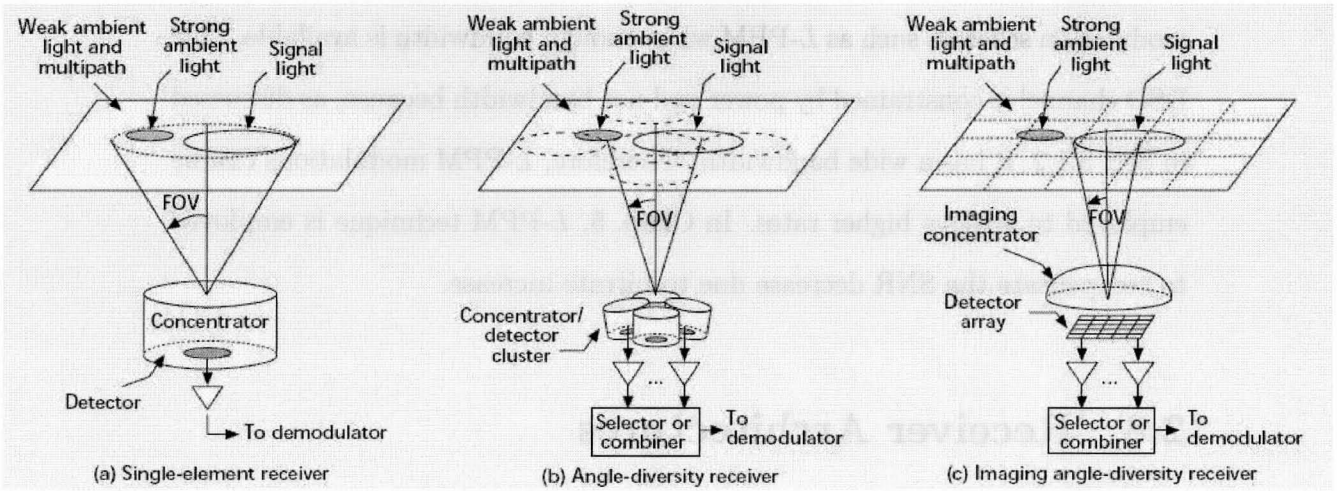

Figure 2.14: Different types of optical receivers: a)Single element receiver b)Angel diversity receiver c)Imaging receiver (reproduced from [7, Fig. 1]).

Multi element receivers are composed of several separated detectors whose outputs are combined using an appropriate combining technique. *Select Best* (SB) and *Maximal-ratio Combining* (MRC) are the two widely used combining techniques.

In SB, the receiver branch which has the highest SNR is selected and its signal is passed as the receiver output. The SNR using SB for a multi element receiver having J single elements is [57]:

$$SNR_{Multi,SB} = \max_i \left(SNR_i\right), 1 \leq i \leq J.$$

where $SNR_{Multi,SB}$ is the SNR of multi element receiver using SB technique and SNR_i is the SNR of the i element. Assuming OOK modulation technique, replacing SNR_i with (2.12), we obtain:

$$SNR_{Multi,SB} = \max_i \left(\frac{r_i^2 P_i^2}{\sigma_{tot,i}^2} \right), 1 \leq i \leq J.$$

where P_i is the received average optical power in ith element, $\sigma_{tot,i}$ is the noise variance in ith element and r_i is the responsivity of ith element.

In MRC, signals from J elements are combined using appropriate weights $w_i, 1 \leq i \leq J$. To maximize the SNR of the weighted sum, w_i must be equal to $r_i P_i / \sigma_{tot,i}^2$ [57]. In order to estimate these gains, a power detector must be employed at the output of each element to estimate its SNR. Using these weights, MRC combiner performs matched filtering which maximizes the SNR. The obtained SNR using MRC and these weights for OOK modulation is [57]:

$$SNR_{Multi,MRC} = \frac{\left(\sum_{i=1}^{J} r_i P_i \frac{r_i P_i}{\sigma_{tot,i}^2} \right)^2}{\sum_{i=1}^{J} \left(\frac{r_i P_i}{\sigma_{tot,i}^2} \right)^2 \sigma_{tot,i}^2} = \sum_{i=1}^{J} \frac{r_i^2 P_i^2}{\sigma_{tot,i}^2}.$$

where $SNR_{Multi,MRC}$ is the SNR when employing MRC.

Although angle diversity receivers can provide higher SNR at the same FOV of single element receivers, they are not very practical because each element needs a complete set of optical equipments which makes them bulky and expensive. Imaging receivers employ the same concept as angle diversity receivers but arrays of integrated photodetectors instead of separate receivers. Therefore, they require a single set of optical elements and have small size and low cost.

The SNR in this case is the same as angle diversity receivers based on the combining technique used, however branch signal power and noise power must be replaced by pixel signal power and noise power in formulas.

Although imaging and angle diversity receivers have improvement even for diffuse links, they show a significant improvement when signal power is received in one or few pixels or receiver branches as the case in LOS or MSD links. Kahn *et al* have investigated these three types of receivers in [7] for diffuse, LOS and MSD links. The results show that using imaging receiver provides 3.7 to 13 dB decrease in power requirement for LOS link when for fixed FOV=45°, the number of detector elements changes from 7 to 1000. The power reduction for diffuse link is 1-7 dB and for MSD link is 7-13 dB. Moreover, the results show that MRC can provide up to 2 dB decrease in power requirements over SB combining. Furthermore, in [7] it is shown that SB and MRC have similar performance for small number of receiver elements (< 20), but MRC has a gain of approximately 2 dB when number of receiver elements increases to over 1000.

2.9 Diffusing Spot Channel Analysis

The DSD configuration proposed in this work is based on the spot diffusing channel. In this section, the spot diffusing channel in which the transmitter sends data into a spot on the ceiling is discussed. This channel is first introduced in [29] and has been under research in much other work [4, 7, 34]. The spot diffusing channel does not completely belong to either diffuse and LOS channels, instead it is based on a light of sight path between the spot

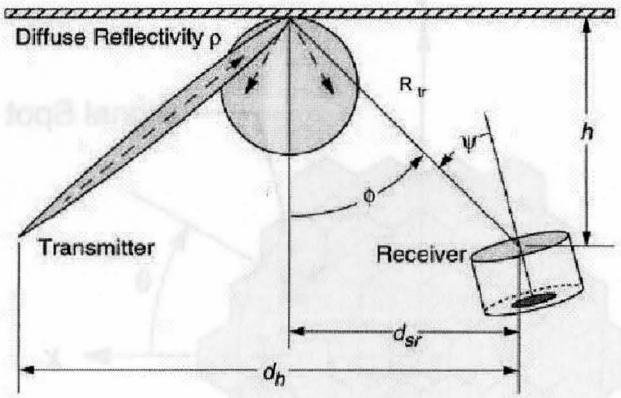

Figure 2.15: Spot Diffusing Configuration (reproduced from [1, Fig. 6]).

on the ceiling and the receiver as shown in Fig. 2.15. Therefore, it is a combination of both LOS and diffuse channels and has some properties of both of them. The spot diffusing channel, like LOS channel, is shown to have high bandwidth. For example, the MSD bandwidth is shown to be up to 2 GHz for the proposed system [4, 31]. Since the spot diffusing channel is based on the LOS channel from spot on the ceiling to the receiver, as it is shown for MSD configuration [35], it is more robust against blockage and does not need precise alignment between transmitter and receiver. This allows for greater mobility for units and makes it more flexible and practical than LOS links.

In a spot diffusing channel, signal power is concentrated on a small area on the ceiling. Therefore, using multi-element receivers, it is possible to reject significant ambient light and multipath signal. As shown in [7], imaging receivers are the best type of receivers for spot diffusing channel. For example, if the signal power is received in three of 37 receiver's pixels as shown in Fig. 2.16, then by considering only those three pixels, receiver collects nearly

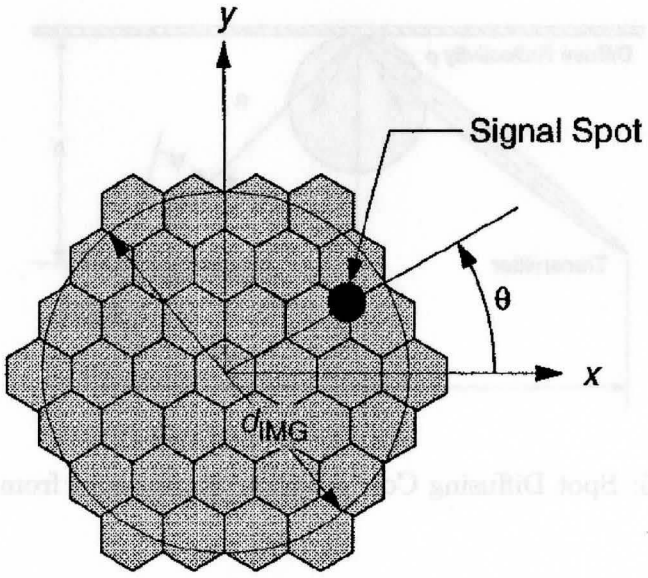

Figure 2.16: 37 hexagonal photodetector array (reproduced from [7, Fig. 2]).

3/37 ambient light and multipath signal compared to a single element receiver with equal FOV. Previous works have shown that employing multi-element receivers increases the SNR [7, 57]. In [7, 57], it is shown that using imaging receiver with 37 pixels for spot diffusing channel results in at least 7 dB less over single element receiver for the proposed receiver with FOV=45°. In Fig. 2.17, the required power to achieve probability of error of 10^{-9} for single element and multi-element receivers with FOV=45° for both case of SB and MRC techniques are shown.

In order to calculate the channel response for spot diffusing channel, it is possible to consider the spot on the ceiling as a transmitter with Lambertian emission pattern [57]. Then the spot diffusing channel is a LOS channel between this transmitter on the ceiling and the receiver. Thus, it is possible to

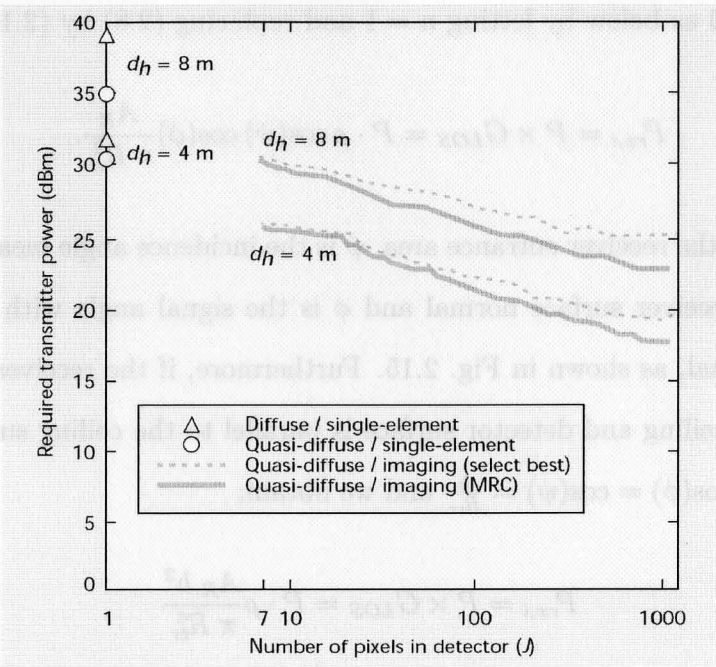

Figure 2.17: Required power to achieve probability of error of 10^{-9} for single element and multi-element receivers with FOV=45° (reproduced from [7, Fig. 3]).

use LOS channel formulas from Sec. 2.6.1 to compute this channel response. In Fig. 2.15, the receiver and the spot are shown graphically. The received power in ith pixel is obtained by multiplying P by LOS channel response, computed from (2.8):

$$P_{rx,i} = P \times G_{LOS} = \frac{P}{S_s} \cdot \rho \int_{S_s} \int_{S_d} \frac{1+n}{2\pi} \cos^n(\phi) d\Omega \, dS_s,$$

Provided that the spot area is small compared to R_{tr}^2, the transmitter receiver distance, the spot can be considered as a point Lambertian source of order one [5,30] for the receiver. In this case, the received power for ith element can

be calculated as below by letting $n = 1$ and replacing (2.8) by (2.10):

$$P_{rx,i} = P \times G_{LOS} = P \cdot \rho \cos(\psi) \cos(\phi) \frac{A_R}{\pi R_{tr}^2}. \tag{2.16}$$

where A_R is the receiver entrance area, ψ is the incidence angle measured with respect to receiver surface normal and ϕ is the signal angle with respect to surface normal, as shown in Fig. 2.15. Furthermore, if the receiver is aligned toward the ceiling and detector surface is parallel to the ceiling surface, then $\psi = \phi$ and $\cos(\phi) = \cos(\psi) = \frac{h}{R_{tr}}$ and we obtain:

$$P_{rx,i} = P \times G_{LOS} = P \cdot \rho \frac{A_R \, h^2}{\pi R_{tr}^4} \tag{2.17}$$

where $R_{tr} = \sqrt{h^2 + d_{sr}^2}$.

2.10 Conclusion

In this chapter, the main characteristics of the indoor optical wireless channel are presented and discussed. The major differences between optical wireless links and RF links are propagation characteristics, modulation techniques and components used in transceivers. Optical signal propagation characteristics are different from RF signal in two aspects. Optical signals are reflected from surfaces diffusely while RF signals are reflected specularly. Moreover, optical signals are not present outside the link room. This avoids interference with similar links in nearby rooms and makes optical wireless links simple to imple-

ment. In addition, it makes optical wireless links much more secure than RF links and there is no need to add complicated encryption schemes to secure the links. Almost all current optical wireless links employ IM/DD modulation technique due to their simple design and availability of inexpensive devices. In this technique, data is modulated in the intensity of the optical signal. An IM/DD system is shown to be well represented as a base band system corrupted by additive white Gaussian noise produced from environment ambient light and preamplifier thermal noise. Two widely used modulation schemes for optical wireless links, OOK and L-PPM, are presented and explained. OOK is shown to have better bandwidth efficiency while L-PPM provides better power efficiency. Optical wireless systems employ photo emitters such as LED, LD or VCSEL and photodetectors such as photo diodes or APDs instead of antennas. Three different types of receivers used in optical wireless links are presented and compared.

Using IM/DD technique imposes a non-negativity constraint on electrical signals and safety issues impose a limit on both peak and average optical power of the signals which is the main limiting factor in optical wireless systems.

Channel impulse response for optical wireless systems has two parts. One part due to LOS path between transmitter and receiver called $h_{LOS}(t)$. This part can be calculated using analytical expressions. The other part called $h_{multipath}(t)$ is due to multipath signals reaching receiver after one or more bounces from the room surfaces. This part can not be calculated exactly by mathematical expressions but by simulating the channel. However, there are several models that obtain a approximate value for $h_{multipath}(t)$.

Finally, the spot diffusing channel is explained and discussed in more detail.

This channel is based on a line of sight path between a spot on the ceiling and receiver. It has shown to a much higher bandwidth than diffuse channel and is more flexible and robust against blockage than LOS links. Previous works has shown that using imaging receivers results in a significant power gain for this channel.

In the next chapter, we introduce a novel channel architecture, the dynamic spot diffusing (DSD) channel, which is based on spot diffusing channel. It retains the advantages of spot diffusing channels while allows mobility.

3

The Dynamic Spot Diffusing Channel

In this chapter the dynamic spot diffusing (DSD) architecture is proposed. An appropriate channel model for this link is discussed. Furthermore, the capacity of the DSD channel is discussed and calculated. Moreover, DSD system design is explained and its effect on channel capacity is discussed.

The *dynamic* spot diffusing architecture proposed here derives many of the advantages of MSD links while reducing the complexity of the transmitter. The DSD channel configuration consists of a collection of moving spots which are translated over the ceiling in closed paths. A receiver is directed towards the ceiling and data symbols are received whenever one of the transmitted spots is in the FOV of the receiver. Since spots are moving on the ceiling, the number of necessary spots to provide coverage for the room is much less than MSD links. Therefore, the DSD transmitter is simpler, more flexible and less expensive than the MSD transmitter using computer generated holograms (CGH). Moreover, the impact of multipath distortion is greatly reduced in DSD versus MSD architectures, allowing for the use of a higher speed modulators.

However, the DSD transmitter requires mechanical motion of the beams which may not be easy to implement for any arbitrary spot path. This can accomplished with a rotating mirror or commercial scanner assembly [58].
The channel capacity of the DSD link is estimated and it is shown that the DSD channel is well-modeled as an erasure channel. Moreover, due to the motion of the spot, a human eye is not always exposed to the transmitter beam. This allows allows for the emission of more optical power at the transmitter than stationary MSD links while maintaining eyesafety. This power gain results in an increase in the SNR at the receiver and makes it possible achieving higher rates and longer ranges. However, the motion of spot has its own drawbacks. This motion adds a random fading to the channel which results in a increase in receiver complexity compared to the MSD systems. The DSD system must employ appropriate coding techniques to combat this random fading, as it will be discussed in Chap. 4.

3.1 DSD Architecture and Channel Model

3.1.1 Architecture

In the DSD link, one or a few spots move on the ceiling and are modulated with high bit rate data. It is not practical to consider random motion of spot, thus, the spot is considered to move on a specific closed path such as a circle or a line on the ceiling in a periodic manner with period T_s.
As shown in Fig. 3.1, the receiver is oriented toward the ceiling. Each receiver receives data in addition to ambient light whenever the spot is in its field of

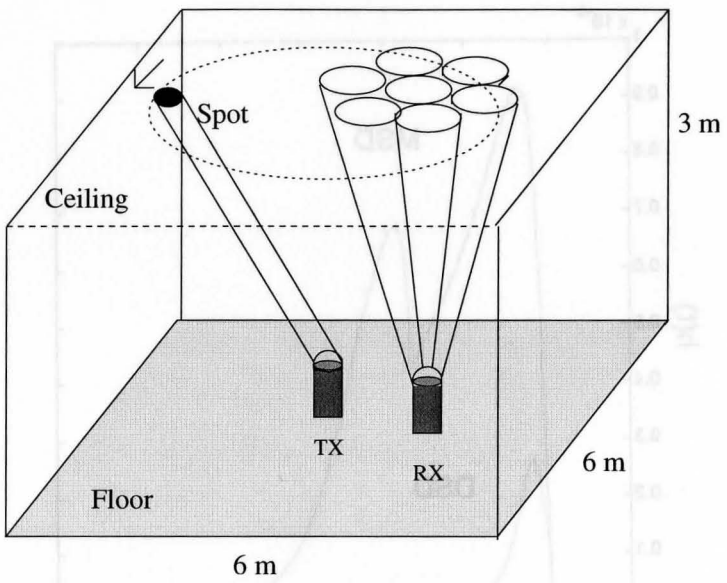

Figure 3.1: The proposed DSD configuration

view and receives only ambient light when the spot is not in its field of view. This architecture, like the MSD architecture, employs the spot diffusing channel discussed in Sec. 2.9. Spot diffusing channels, as discussed in Sec. 2.9, are based on a line of sight path between a spot on the ceiling and the receiver. Thus, this channel is present only when at least one spot is in the FOV of the receiver. In the MSD configuration, multiple spots are created over the ceiling to make sure each receiver in the room has at least one spot in its FOV. However, in a DSD link, one or a few spots are created and moved on the ceiling to achieve a good coverage. Thus, the number of required spots to achieve the coverage is significantly reduced in the DSD system. For example, a previously proposed MSD system requires 100 spots to cover all the room while the DSD system, as will be shown in Sec. 3.4, using circular path can provide full coverage in the same room with 2 spots.

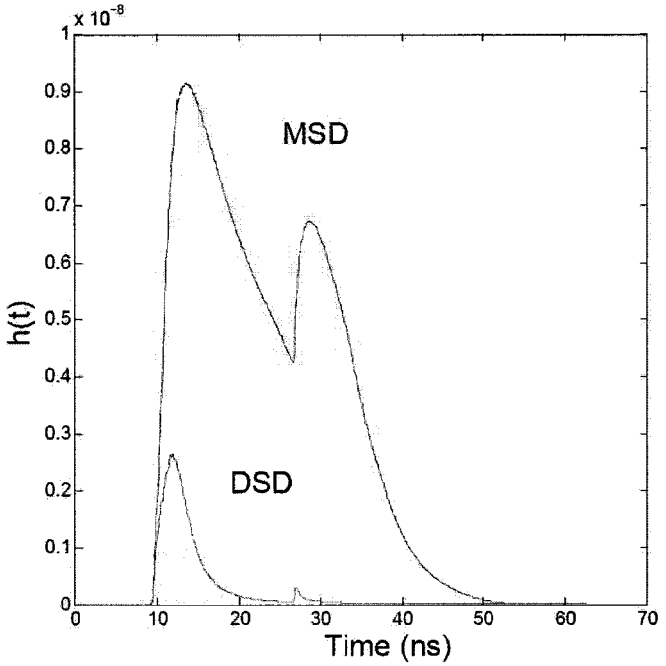

Figure 3.2: Received multipath signals for DSD and MSD channel

3.1.2 DSD Channel Bandwidth

The DSD channel is based on a spot diffusing channel which, as discussed in Sec. 2.9, has high bandwidth compared to diffuse channel. The previous works have shown that the MSD channel has bandwidth in excess of 2 GHz [4, 31]. The DSD system also has reduced multipath signal compared to the MSD channel since less spots are employed. Thus, the DSD channel data rate is not limited by multipath distortion but by device speed and average optical power limit. For example, a DSD channel and a MSD channel similar to the one proposed in [4] with 100 spots are simulated in a $6 \times 6 \times 3$ m room. The receiver was placed at a height of 1 m from the floor. A 10×10 array of equal power spots was used for the MSD channel, as in [4]. The DSD channel

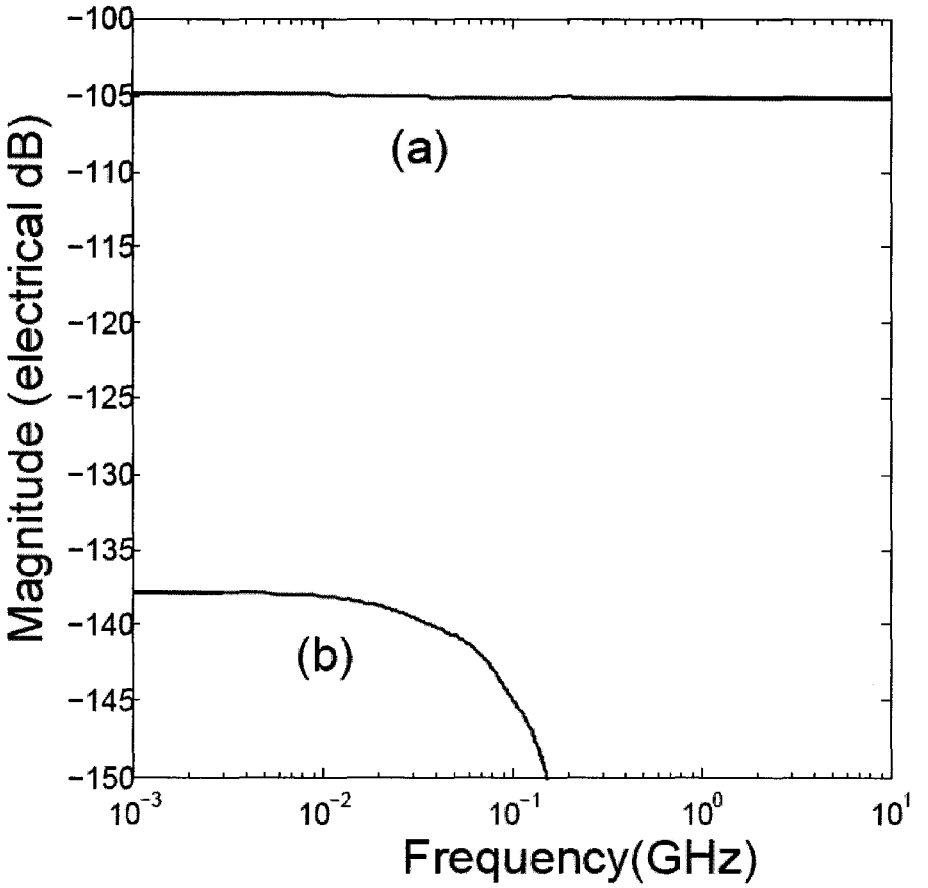

Figure 3.3: DSD channel gain (a) when spot is in FOV (b) when spot is out of FOV

was simulated for a single spot centered in the receiver FOV with power equal to a single MSD spot. For a fair comparison, in both cases, a single element receiver with FOV=11.2° and $A_R = 1\text{cm}^2$, like the one used in [4], is employed. The simulator is based on the Barry and Kahn algorithm [5] described in Sec. 2.6.2. Fig. 3.2 shows the received multipath signals for the DSD and the MSD channels. The results confirm that the DSD channel receiving much

less multipath signals than the MSD. Therefore, the DSD channel can be considered flat for even higher frequencies than MSD channel. For example, the simulated DSD channel in a similar room, shown in Fig. 3.3, is flat up to 10 GHz when spot in FOV of the receiver. For this simulation, the receiver is a single element receiver with $A_R = 1cm^2$, located at (55 cm,75 cm,100 cm) in a $6 \times 6 \times 3$ m room. In the other words, the multipath signals can be neglected and the DSD channel is characterized by only its channel DC gain at each point in the room for up to high frequencies (higher than 10 GHz). Therefore, because of the wide bandwidth of the DSD channel response, the DSD channel can be considered flat and approximated by its DC gain h_t at each time t in the band of interest.

3.1.3 DSD Channel Model

As shown in Sec. 2.1, this channel is well modeled as a base band channel defined in (2.2). As discussed in Sec. 3.1.2, we consider the DSD channel to be flat in the band of interest and replace $h(t)$ with a constant number h_t. Thus, the convolution in (2.2) reduces to a multiplication.
Furthermore, provided that the bit period T_b is much smaller than spot motion period T_s, the channel characteristics can be considered fixed for each bit. Therefore, the DSD channel can be modeled as a discrete time baseband channel with a fixed channel gain h_{kT_b} for each bit period where $h_{kT_b} = h_t$ for $(k+1)\,T_b > t \geq k\,T_b$. Then the DSD channel is modeled as a the discrete time baseband model as:

$$y_k = rx_k \cdot h_{kT_b} + n_k \quad \text{for} \quad T_s >> T_b \qquad (3.1)$$

where y_k is the channel output, x_k is the transmitted optical intensity signal, h_{kT_b} is the channel DC gain and n_k channel additive noise, all at discrete time k. Note that h_t is fixed over each bit period i.e .

Moreover, for a fixed location of the receiver, the h_t is a periodic function of t with period T_s, i.e $h_t = h_{t+T_s}$. Therefore, assuming that the spot and noise powers are constant over the time, the channel statistics are periodic and the DSD channel is a *cyclo-stationary* channel, with period T_s.

Consider the start phase of the transmitter as a random variable chosen uniformly in [0,T_s]. Thus, the average of the ensembles would be equal to the time average and the DSD channel gain is a stationary and *ergodic* random process.

In this work, as explained in Chap. 5, T_b is assumed to be much smaller than T_s. Therefore, the DSD channel is modeled as a discrete-time channel with stationary and ergodic time-varying gain.

3.2 The DSD Channel Capacity

3.2.1 Definitions

Let $\mathcal{T}_s$ denote the set of all discrete times in one spot period $\mathcal{T}_s = [0, T_s)$, $\mathcal{T}_{in}$ denote the set of discrete times when spot is in the FOV in each period and $\mathcal{T}_{out}$ denote the set of discrete times spot is out of the receiver's FOV in each period. Thus, $\mathcal{T}_{in} \cap \mathcal{T}_{out} = \emptyset$ and $\mathcal{T}_{in} \cup \mathcal{T}_{out} = \mathcal{T}_s$. Moreover, K_s is defined as the period of spot in discrete time.

Flat Fading Channel: In a flat fading or frequency-nonselective channel, within

the bandwidth W of the transmitted signal $x(t)$, the time-variant channel response does not change with frequency [59].

Define $\overrightarrow{\rho}$ as a vector denoting a specific receiver configuration with components:

$$\overrightarrow{\rho} = [\text{position, FOV, orientation}]$$

and $\overrightarrow{\tau}$ as a vector denoting a specific transmitter:

$$\overrightarrow{\tau} = [\text{number of spots, spot paths, spot average optical power, spot period}]$$

3.2.2 Capacity

In the DSD channel, there are two states for channel, when spot is in the FOV of the receiver and when it is out of FOV of receiver. The channel gain, h_{kT_b} for $k \in \mathcal{T}_{in}$ is much higher than h_{kT_b} for $k \in \mathcal{T}_{out}$. This difference in channel gain is due to the existence of a LOS path between spot and receiver in the first case while in second case, the channel is a diffuse link between spot and receiver. For example, in Fig. 3.3 the channel gain for the proposed DSD channel for two cases is shown. As shown in figure, the channel gain is 30 dB lower in second case. Note that indoor optical wireless link suffer from power limitations due to safety issues, thus, even when spot is in the FOV, maximum achievable SNR in practical systems is below 15.5 dB [7]. Hence, the SNR when spot is out of FOV is very low, as low as -15 dB in this case, which as shown in Fig. 2.10 for OOK modulation, results in capacity near zero. Therefore, the DSD channel can be considered as a fading channel with two states. Furthermore, as explained in Sec. 3.1.3, the DSD channel is flat at high

frequencies, as high as 10 GHz in the proposed channel. Thus, in this thesis, the DSD channel is considered a *flat fading* channel in the band of interest. The capacity of ergodic fading channels is a well developed topic. A comprehensive review can be found in [59]. Since the channel state varies, the instantaneous channel capacity also is changes in time. The *ergodic capacity* is defined as the maximum long-term achievable rate of channel over all states of the time-varying channel [60].

In the DSD channel, channel information is not available at the transmitter since it cannot determine whether the spot is in the FOV of the receiver or not. However, the channel information is available at the receiver, because it is possible for receiver to determine whether the spot is in the FOV. This can be done for example by using a power detector or coding technique, discussed in Chap. 4. Therefore, the DSD channel is a flat fading ergodic channel in which channel information is available only at the receiver. Thus, the channel state is known to the receiver and the output of the channel is the pair (y_k, h_{kT_b}), where h_{kT_b} has the information about the channel state and y_k has the information about the input of the channel [61]. In this case, the mutual information between input and output is [61]:

$$\begin{aligned} &I(x_k, (y_k, h_{kT_b})) = I(x_k; h_{kT_b}) + I(x_k; y_k|h_{kT_b}) \\ &= I(x_k; y_k|h_{kT_b}) \\ &= E_{h_q}[I(x; y|h_q = h_{kT_b})] \end{aligned}$$

which is the expected value of the mutual information over all channel states. The DSD channel gain is an ergodic and periodic random variable. Thus,

expected value can be replaced by the time average over one period. Furthermore, in this work we only consider binary level modulations for the DSD channel due to their simple implementation. Thus, the channel input has a fixed uniform distribution over 0 and 1 i.e $x \in \{0,1\}$. In the case of fixed input distribution, the channel capacity is the mutual information for that input distribution. Therefore, the DSD channel ergodic capacity, $C_{erg}(h_t)$, for a specific receiver and transmitter configuration $(\overrightarrow{\rho}, \overrightarrow{\tau})$ is,

$$\begin{aligned} &C_{erg}(\overrightarrow{\rho}, \overrightarrow{\tau}) = I(x_k, (y_k, h_{kT_b}(\overrightarrow{\rho}, \overrightarrow{\tau}))) \\ &= E_{h_q}[I(x; y|h_q = h_{kT_b}(\overrightarrow{\rho}, \overrightarrow{\tau}))] \\ &= \tfrac{1}{T_s} \textstyle\sum_{k \in \mathcal{T}_s} I(x_k; y_k|h_{kT_b}(\overrightarrow{\rho}, \overrightarrow{\tau}))) \end{aligned}$$

For the fixed channel input, $I(x_k; y_k|h_{kT_b}(\overrightarrow{\rho}, \overrightarrow{\tau})))$ is the instantaneous capacity $C(\overrightarrow{\rho}, \overrightarrow{\tau}, k)$ at discrete time k for that input distribution. For example, this capacity is shown for OOK modulation in Fig. 2.10. Thus:

$$\begin{aligned} &C_{erg}(\overrightarrow{\rho}, \overrightarrow{\tau}) = \tfrac{1}{K_s} \textstyle\sum_{k \in \mathcal{T}_s} C(\overrightarrow{\rho}, \overrightarrow{\tau}, k) \\ &= \tfrac{1}{K_s} \left(\textstyle\sum_{k \in \mathcal{T}_{in}} C(\overrightarrow{\rho}, \overrightarrow{\tau}, k) + \sum_{k \in \mathcal{T}_{out}} C(\overrightarrow{\rho}, \overrightarrow{\tau}, k) \right) \end{aligned} \tag{3.2}$$

Since the channel gain is much smaller when spot is out of FOV compared to when it is inside FOV, $C(\overrightarrow{\rho}, \overrightarrow{\tau}, k)$ becomes negligible for $k \in \mathcal{T}_{out}$. Therefore:

$$C_{erg}(\overrightarrow{\rho}, \overrightarrow{\tau}) = \frac{1}{K_s} \sum_{k \in \mathcal{T}_{in}} C(\overrightarrow{\rho}, \overrightarrow{\tau}, k)$$

Let $\Delta t(\overrightarrow{\rho}, \overrightarrow{\tau})$ denote the length of time that spot is in the FOV of receiver $\overrightarrow{\rho}$, in one spot period. Thus, $\Delta t(\overrightarrow{\rho}, \overrightarrow{\tau})$ is the length of $\mathcal{T}_{in}$. Define *channel*

duration, C_T, for receiver $\overrightarrow{\rho}$ as the fraction of the spot period which spot is the FOV of the receiver $\overrightarrow{\rho}$:

$$C_T(\overrightarrow{\rho}, \overrightarrow{\tau}) = \frac{\Delta t(\overrightarrow{\rho}, \overrightarrow{\tau})}{K_s}. \tag{3.3}$$

Furthermore, define $C_{in}^{avg}(\overrightarrow{\rho}, \overrightarrow{\tau})$ as the average of instantaneous capacity when $k \in \mathcal{T}_{in}$. Then, the ergodic capacity can be written as:

$$C_{erg}(\overrightarrow{\rho}, \overrightarrow{\tau}) = \underbrace{\frac{\Delta t(\overrightarrow{\rho}, \overrightarrow{\tau})}{K_s}}_{C_T(\overrightarrow{\rho}, \overrightarrow{\tau})} \cdot \underbrace{\frac{1}{\Delta t(\overrightarrow{\rho}, \overrightarrow{\tau})} \sum_{k \in \mathcal{T}_{in}} C(\overrightarrow{\rho}, \overrightarrow{\tau}, k)}_{C_{in}^{avg}(\overrightarrow{\rho}, \overrightarrow{\tau})} \tag{3.4}$$

that is:

$$C_{erg}(\overrightarrow{\rho}, \overrightarrow{\tau}) = C_T(\overrightarrow{\rho}, \overrightarrow{\tau}) \cdot C_{in}^{avg}(\overrightarrow{\rho}, \overrightarrow{\tau}). \tag{3.5}$$

This equation shows that DSD channel capacity is product of C_T and C_{in}^{avg}. Thus, to increase the capacity, these two parameters must be increased.
As Fig. 2.10 shows, the OOK channel capacity gets close to 1 when SNR is large. In the case of high SNR, $C_{in}^{avg} \rightarrow 1$ and: $C_{erg}(h_t) \approx C_T$.

For example, the instantaneous capacity and uncoded probability of error for a DSD system are calculated for different SNR levels of the received signal. As shown in Fig. 3.4, spot moves on a circular path with radius of 120 cm over the ceiling of a $6 \times 6 \times 3$ room. A single element receiver is located at (300 cm,180 cm,100 cm) and has $FOV = 11.2°$. The transmitter is located at the middle of the room. Furthermore, it is assumed that receiver detector area and spot size are much smaller than R_{tr}^2, spot on the ceiling is well-modeled as a Lambertian pattern emitter with n=1 and receiver is aligned toward the

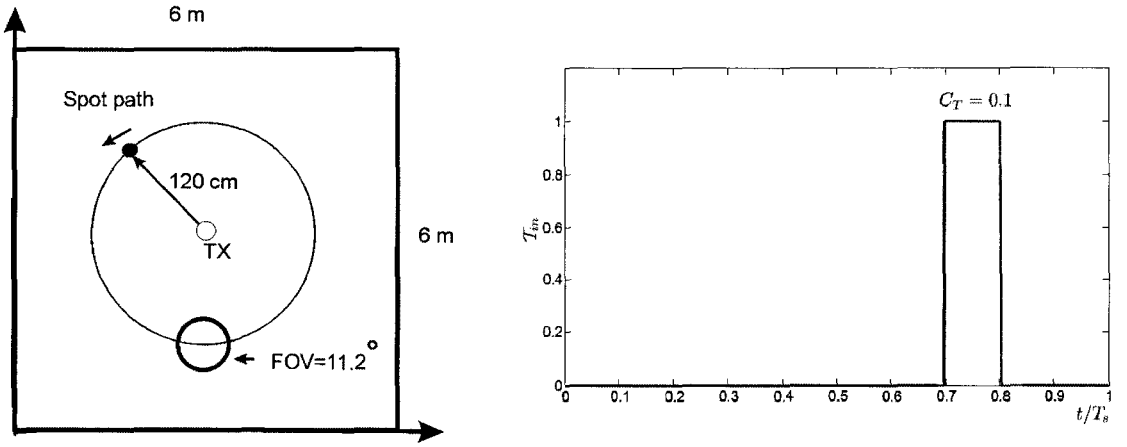

Figure 3.4: (a) The proposed DSD configuration and (b) T_{in} for the receiver in (a)

ceiling. Thus, under these assumptions, as discussed in Sec. 2.9, (2.17) can be employed to calculate the received power. According to (2.17), the received SNR is maximum when spot is exactly above the receiver, i.e $\psi = 0$ or $R_{tr} = h$. Four cases when $SNR_{max} = 5.5\ dB$, $SNR_{max} = 10.5\ dB$, $SNR_{max} = 15.5\ dB$ and $SNR_{max} = 20.5\ dB$ are considered. These values for SNR are chosen to be consistent with reported SNRs for spot diffusing channel [7, 36–38]. The calculated SNR from (2.17) is used to compute the uncoded probability of error using (2.11). Moreover, the instantaneous capacity is calculated from the SNR using Monte-Carlo averaging, as described in Sec. 2.7.3. The results are shown in Figs. 3.5, 3.6, 3.7, 3.8. Table 3.1 shows C_{in}^{avg} for these four cases.

The DSD channel with a good approximation behaves as an *erasure* channel when the SNR is high i.e. when $C_{in}^{avg} \rightarrow 1$. The channel capacity of such

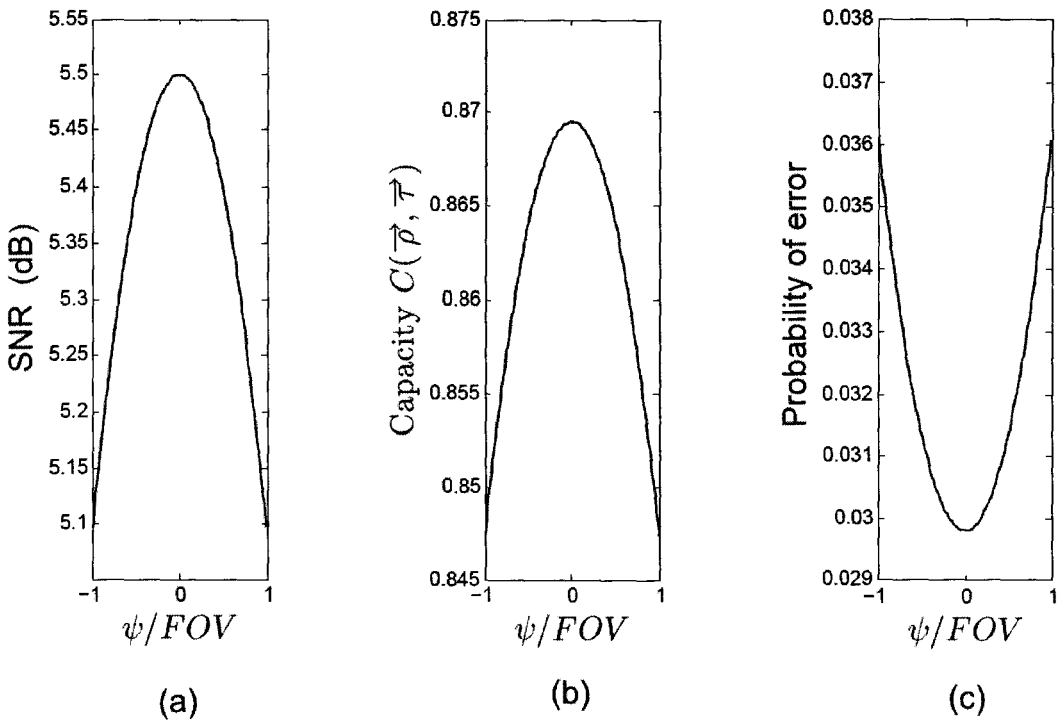

Figure 3.5: (a) SNR (b) Capacity and (c) uncoded probability of error when $SNR_{max} = 5.5$ dB.

an erasure channel with erasure probability $1 - C_T$ is in fact C_T [62]. As Table. 3.1 shows, $C_{in}^{avg}(\rho)$ is very close to one for $SNR \geq 10.5dB$. Thus, for this region, the DSD channel capacity is approximately equal to C_T. Hereafter, we will assume that the DSD system provides at least 10.5 dB for receivers i.e $SNR \geq 10.5dB$. This assumption is made according to works [7,36–38] which have reported 15.5 dB and higher SNRs for spot diffusing channels. Therefore, C_T is used for the DSD channel capacity in this work.

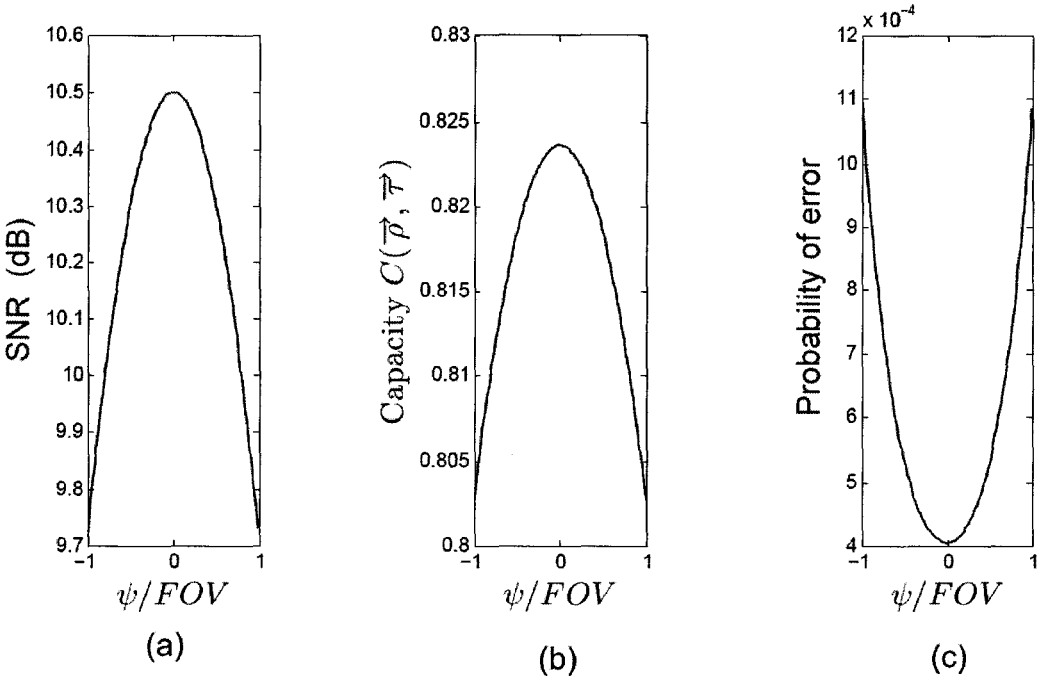

Figure 3.6: (a) SNR (b) Capacity and (c) uncoded probability of error when $SNR_{max} = 10.5$ dB.

3.3 DSD System Design

The DSD channel capacity, as (3.5) shows, depends on C_T and C_{in}^{avg}. Therefore, DSD system must be designed so that provides highest possible C_T and C_{in}^{avg} all over the room. C_{in}^{avg} depends on the spot average optical power, receiver design and modulation technique used. The maximum average optical power of the transmitter is limited by safety issues, therefore, C_{in}^{avg} can be improved only by employing more power efficient modulation techniques and better designed receivers which can reject more noise and provide higher SNR.

C_T depends on the receiver FOV and spot path. Thus, it must be maximized

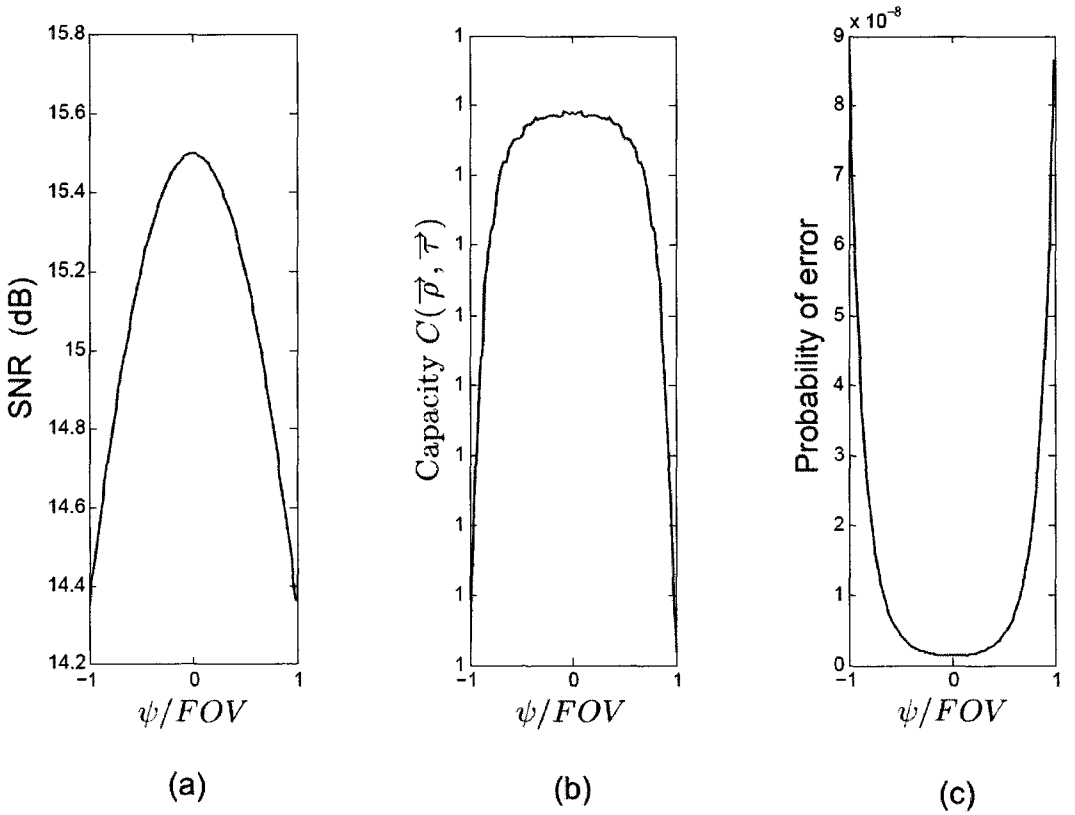

Figure 3.7: (a) SNR (b) Capacity and (c) uncoded probability of error when $SNR_{max} = 15.5$ dB.

by selecting spot paths which provide higher C_T over the room and employing receivers with larger FOV.

Therefore, receiver and transmitter design have significant impacts on the DSD channel capacity.

Define a blind point as a position in the room is where $C_T(\overrightarrow{\rho}, \overrightarrow{\tau})$ is 0 for receiver $\overrightarrow{\rho}$. The receiver must be designed so that it has the highest FOV and highest sensitivity possible at the same time. The spot path must be chosen so that blind points over the room are minimized, C_T is maximized over the

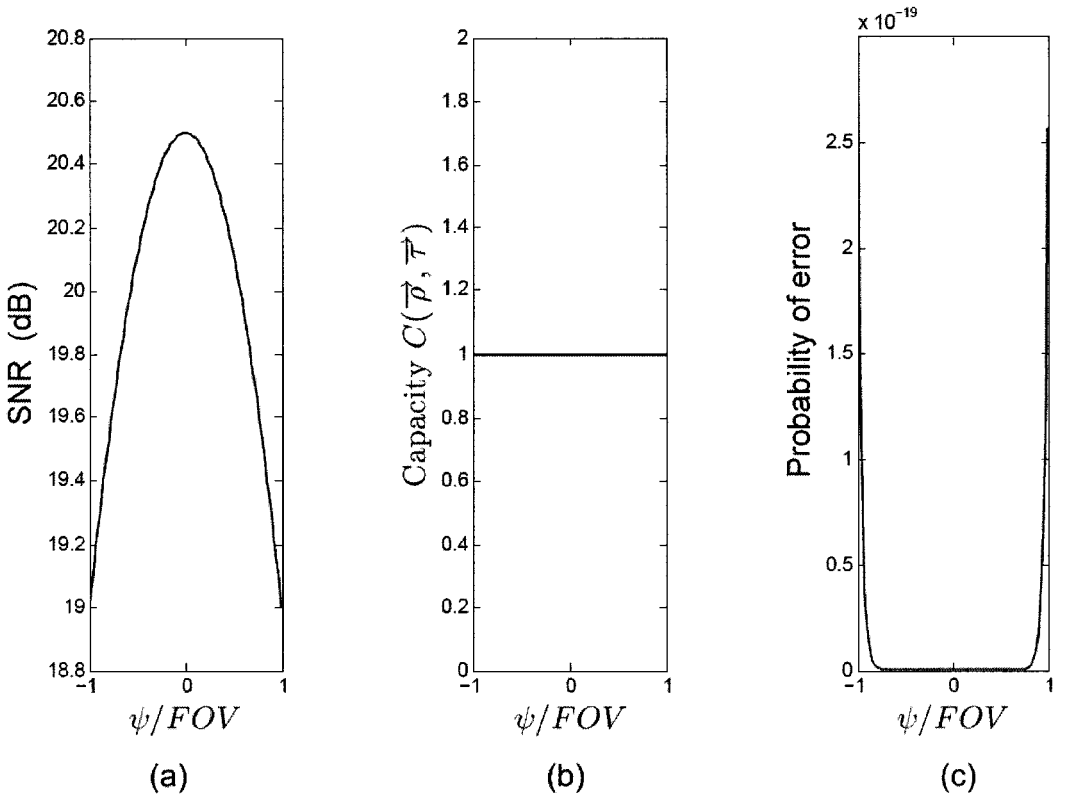

Figure 3.8: (a) SNR (b) Capacity and (c) uncoded probability of error when $SNR_{max} = 20.5$ dB.

Case	1	2	3	4
SNR_{max}	5.5 dB	10.5 dB	15.5 dB	20.5 dB
$C_{in}^{avg}(\rho)$	0.8820	0.9977	$1 - 1.2238 \times 10^{-10}$	≈ 1

Table 3.1: Channel characteristics for four different SNRs

room and the variance of C_T is minimized over the room. In other words, the C_T distribution over the room must have the highest possible mean and lowest possible variance. Moreover, the transmitter must send the highest possible optical power satisfying eye safety requirements as well as using power efficient modulation.

3.3.1 Receiver Design

The design of the receiver has a critical effect on the capacity of the DSD link. As (3.5) shows, the DSD channel capacity depends both on C_T and C_{in}^{avg} and receiver design has impact on both factors. C_T depends on the receiver FOV, receiver location and spot path. To increase the C_T, the FOV must be increased as much as possible. For example, Fig. 3.9 shows the C_T distribution over the prototype room for a circular spot path of radius 2.2 m and two different FOVs. As expected, the maximum capacities occur near the spot path with blind spots far off the path. Table 3.2 presents the key parameters of the DSD channel with 30° and 45° receiver FOVs assuming an imaging receiver with a large number of narrow FOV receive elements. The results indicate that with a FOV of 45° that the average and maximum capacity, C_T, is over three times that of the 30° FOV channel and the proportion of blind points decreases from over 20.13% to 0.02%. On the other hand, $C_{in}^{avg}(\rho)$ depends on the received SNR which depends on receiver type, combining technique used and electrical components characteristics.

Optical wireless links are impaired by ambient light noise and preamplifier circuits thermal noise [1,10]. Using low noise amplifiers and detectors, thermal noise becomes much weaker than ambient light noise and can be neglected in

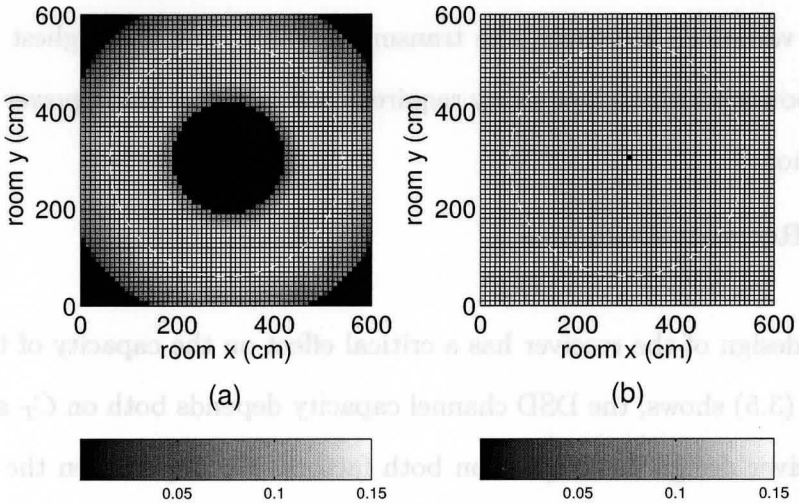

Figure 3.9: C_T distribution over the room for (a) FOV=30° and (b) FOV=45°.

FOV	30°	45°
Average C_T	0.1067	0.3312
Variance	14.02	16.21
Max C_T	0.1697	0.4683
Blind points	20.13 %	0.02 %

Table 3.2: C_T distribution statistics for two FOVs

these links. However, increasing the receiver FOV increases the amount of receiver ambient light.

Kahn and Djahani [7] have investigated single element, angle diversity and imaging receivers for spot diffusing channels. It is shown that imaging receivers provide the highest SNR and single element receivers provide the lowest SNR among these three. Moreover, for a fixed total detector area and receiver FOV, they have shown that SNR increases as the number of pixels increase. As discussed in Sec. 2.8, combining over the received elements is required to

improve the detection fidelity in imaging receivers. Imaging receivers are the best choice for DSD systems because they provide large FOV and high SNR at the same time, and therefore, improve both factors of DSD channel capacity in (3.5). However, the price which must be paid is higher complexity of the receiver.

3.3.2 Transmitter Design

The transmitter in a DSD system must modulate data onto a small area on the ceiling and move it over a closed path. Thus, the transmitter must be able to produce a mobile narrow beam. The diameter of the beam must be large enough to make sure that the beam is safe for human eye and skin for desired average optical power of the beam.

This can be realized using a high-speed laser source such as a LD or an array of VCSELs with a diffuser placed on a controllable mechanical device to move the beam. For example, to provide a circular spot path, this base can be a disk on a rotor. The speed of the spot can be controlled by the speed on the rotor and the radius of the circle path can be controlled by the angle of the beam source on the disk. Several transmitters providing mobile low divergence beam using VCSEL arrays have been previously reported [2, 18, 19, 22]. Furthermore, Micro-Electro-Mechanical Systems (MEMS) are another candidate for implementing a smaller transmitter with higher motion speed [63].

The selection of the spot path is another important issue affecting the capacity of DSD channels. The spot path must provide a C_T distribution over the room with the highest possible mean and lowest possible variance. Note the distribution of C_T depends both on spot path and room dimensions and

shape. Thus, the optimum spot path for different rooms may be different. The distribution of C_T over a $6 \times 6 \times 3$ room is simulated for several candidate paths assuming a receiver with 45° FOV. A valid path for the DSD channel is any closed path on the ceiling. In Fig. 3.10 the C_T distribution over the room is plotted for two simple paths, namely, a line and a circle. The radius of the circle path is set to 220 cm since this radius minimizes the blind points in the proposed room. Another possible family of closed paths are *Lissajou paths*. These paths can be defined as a function of time as

$$\begin{aligned} x &= A(\sin(2\pi\omega_x t/T_s) + 1) \quad [\text{cm}] \\ y &= B(\cos(2\pi\omega_y t/T_s) + 1) \quad [\text{cm}]. \end{aligned}$$

In the case of our prototypical room, we consider the case where $A = B =$ 300 cm, $\omega_x = 1$ with $\omega_y = 4$ or $\omega_y = 5$. Fig. 3.11 presents these paths as well as their C_T distributions.

Table 3.3 compares the DSD channel characteristics of the four different paths. For this square room, the circular path is selected as the best path of the four considered. The length of path, therefore, period of this path is among the smallest reducing the latency of communication and the buffering required for channel coding, discussed in Chap. 4. The average and maximum C_T, over all points in the room is highest for the circular path. The number of blind points is also small for this path. An important feature of the circular path is the low variance in C_T over the room. The goal of path design is to have a "fair" channel which provides high capacities throughout the room. Therefore, circular spot paths have the potential to provide high C_T links at

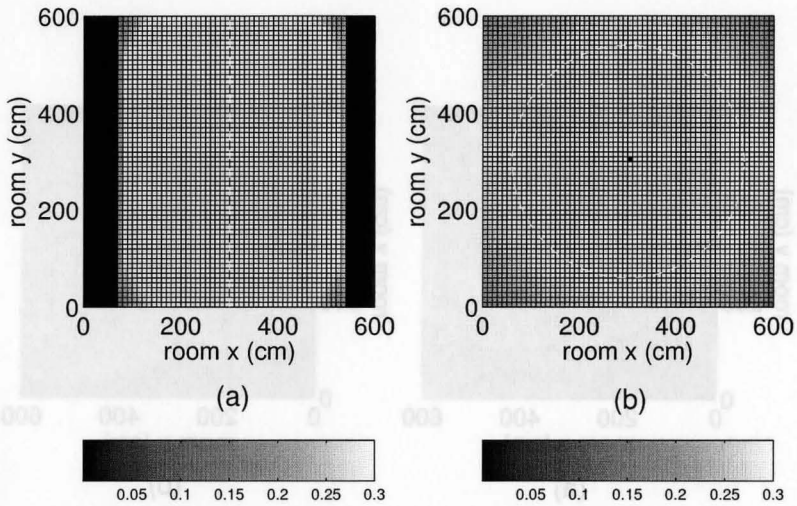

Figure 3.10: Distribution of C_T over the room for (a) line and (b) circle radius=2.2 m paths (paths shown in white dashed line and FOV=45°)

nearly all points in this room. This path is mechanically simple to implement and can be adapted to different sized rooms by altering the radius of the path or its eccentricity creating elliptical path shapes.

The high bandwidth of the DSD links allows employing more power efficient modulation schemes such as L-PPM. As it is shown in Sec. 2.7.3.2, using L-PPM results in a power gain compared to OOK technique. This gain is required especially to achieve higher bit rates. In Sec. 2.7, it is shown that the SNR for optical IM/DD systems in proportional with the square of T_b. Thus, as bit rates increases, SNR decreases. However, it is not possible to increase the transmitted optical power to compensate for this decrease because optical power is limited due to safety issues. Using L-PPM modulation techniques can solve this problem because they provide a gain in SNR while sending the same

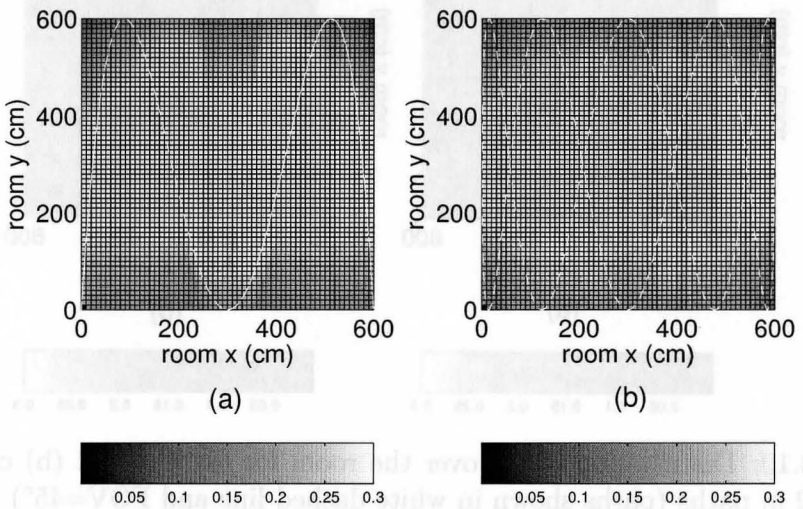

Figure 3.11: Distribution of C_T over the room for Lissajou figures with $\omega_x = 1$ and (a) $\omega_y = 4$, (b) $\omega_y = 5$ paths (paths shown in white dashed line and FOV=45°)

Path	Line	Circle	Lissajou $\frac{\omega_y}{\omega_x} = 4$	Lissajou $\frac{\omega_y}{\omega_x} = 5$
Length (m)	12	15.08	47.6	59
Avg C_T	0.2751	0.3312	0.2153	0.2151
Variance	254.95	16.21	17.25	16.81
Max C_T	0.645	0.4683	0.3009	0.2866
Blind points	36.07 %	0.02 %	0 %	0 %

Table 3.3: Channel characteristics for four different spot paths (FOV=45°)

optical power as OOK. Simulation results using these modulation scheme are presented in Chap. 5.

3.4 DSD Channel With Multiple Spots

It is possible to improve the channel capacity and coverage over the room by using multiple spots. Ideally, having two spots, the C_T over the room should be doubled compared to a single spot, while the complexity of the transmitter is not increased with a considerable amount. However, the relation between C_T over the room and the number of spots is not generally linear because after adding more spots, some receivers may have more than one spot in their FOV at the same time. In this case, C_T is not increased, because C_T is duration of having spot in FOV, thus, having two or more spot at the same time does not increase it.

For example, Table 3.4 shows the results for DSD channel statistics over a room for multiple spots having a circle path with radius of 220 cm. In order to avoid muti-spots in one receiver FOV, spots must have the highest distance from each other possible. Therefore, the n spots in the circle are arranged by a phase shift of $\frac{2\pi}{n}$, as shown in Fig. 3.12. The results show that many of the receivers are saturated after 4 spots i.e., they have always at least one spot in their FOV and the channel statistics have not changed much after that. Moreover, the blind points do not change using multiple spots with equal radii.

In the second considered case, half of the spots have radius of 200 cm and the other half have radius of 300 cm. Using these radii, the variance of the C_T distribution over the room is minimized. In this case, as shown in Fig. 3.13, n

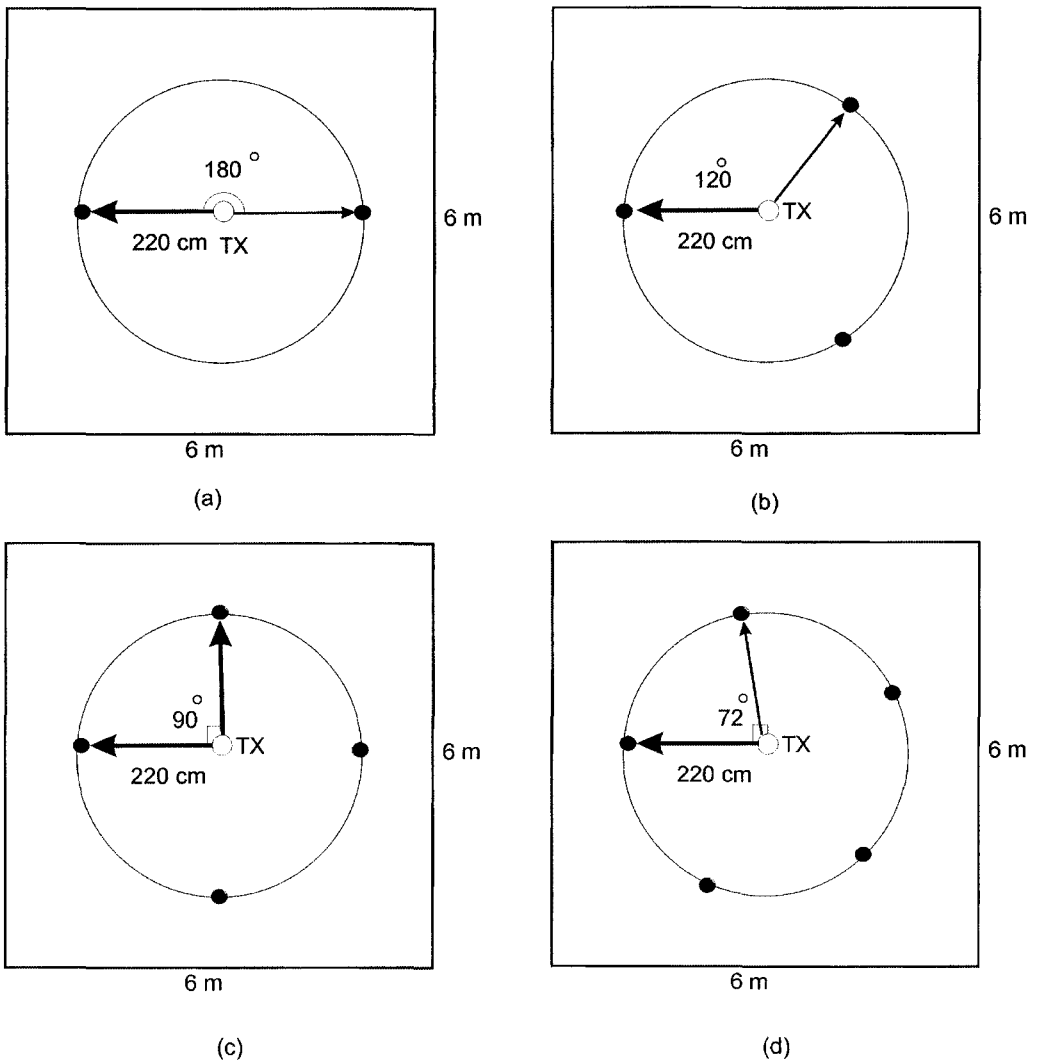

Figure 3.12: Spot arrangement for (a) 2 spots (b) 3 spots (c) 4 spots and (d) 5 spots with radius=220 cm.

Spot Number	1	2	3	4	5
Avg C_T	0.2751	0.5496	0.8120	0.9345	0.9722
Variance	16.76	67	130.48	83	51.85
Max C_T	0.3634	0.7267	1	1	1
Blind points	0.46 %	0.46 %	0.46 %	0.46%	0.46 %

Table 3.4: C_T distribution statistics for different number of spots on a circle path with radius=220 cm

spots have equal phase shift of $\frac{2\pi}{n}$ and consequent spots have different radiuses to avoid multiple-spot in one receiver FOV. Table 3.5 presents the simulation results for this case. The results show that using multiple spots with different radiuses can provide a better coverage over the room i.e less blind points, higher mean and lower variance for C_T distribution. Note that although additional spots are present, the DSD channel still has a wide bandwidth since these few spots do not increase the multipath signal significantly. In the MSD system proposed in Kavehrad *et al.* works [4,31], using 100 spots, the channel is shown the be flat for up to 2.4 GHz. For example, Fig. 3.14 shows the received multipath signal for the receiver located at (55 cm,75 cm,100 cm) in the proposed square room. Receiver FOV is 11.2° and the channel impulse response for 2, 4 and 6 spots having circular path is simulated. However, as shown in [4,31], using multiple spots and single element receiver, the channel bandwidth is limited to multipath signals received from different spots. Thus, for multiple spot system, imaging receiver must be employed which mitigates the multipath signal effect by appropriate combining among elements. Employing single element receiver for this case limits the channel bandwidth to few GHz if more than one spot comes in the FOV at the same time. In this work, we assume employing an imaging receiver which mitigates multi spot reception through appropriate combining techniques. In Fig. 3.15, the channel frequency response for these three cases is plotted and shown to be flat in the band of interest.

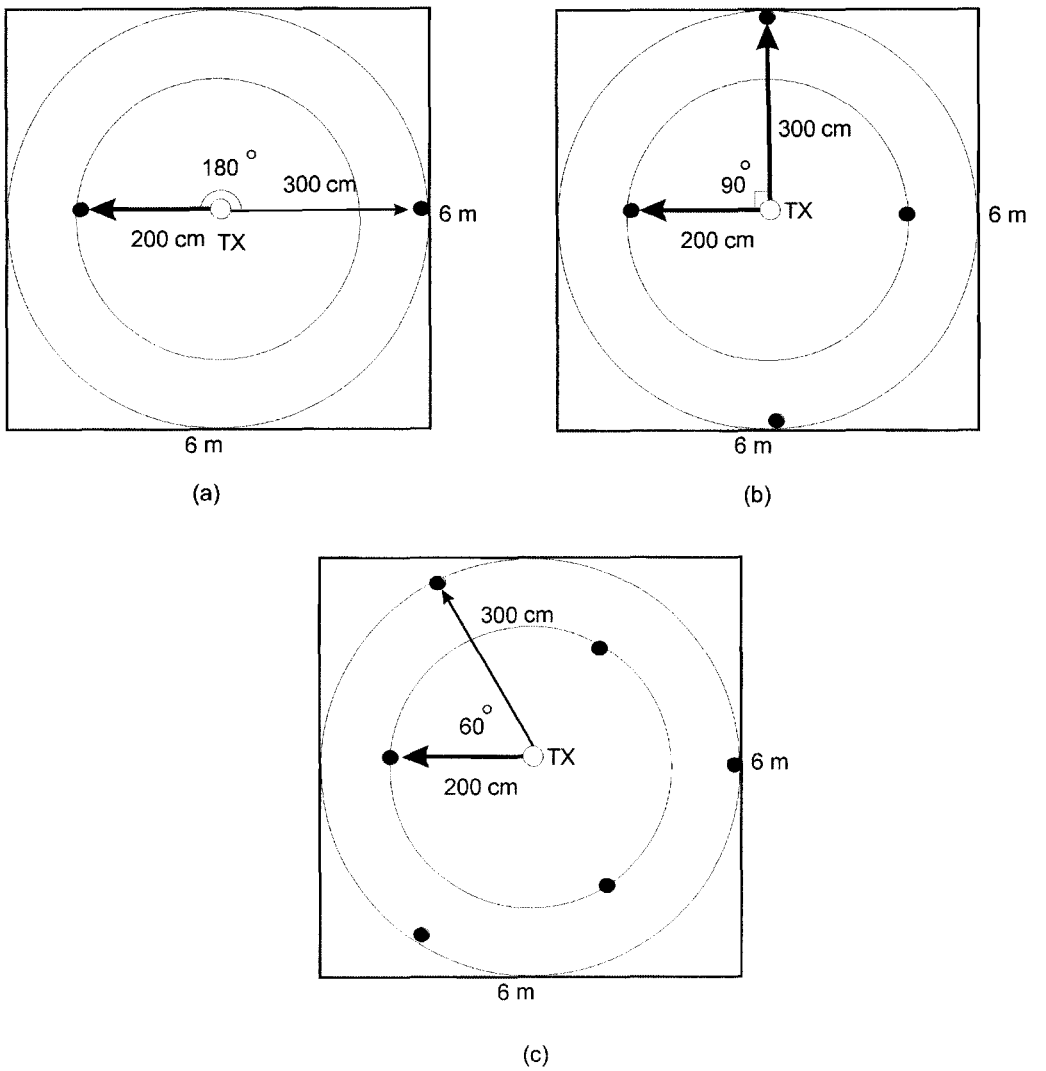

Figure 3.13: Spot arrangement for (a) 2 spots (b) 4 spots (c) 6 spots with two radii.

Spot Number	2	4	6
Avg C_T	0.5072	0.9234	0.9816
Variance	42.5	78	27.1
Max C_T	1	1	1
Min C_T	0.1322	0.2646	0.397
Blind points	0 %	0 %	0%

Table 3.5: C_T distribution statistics for multiple spots on arranged on two circle paths with radius=200 cm and 300 cm

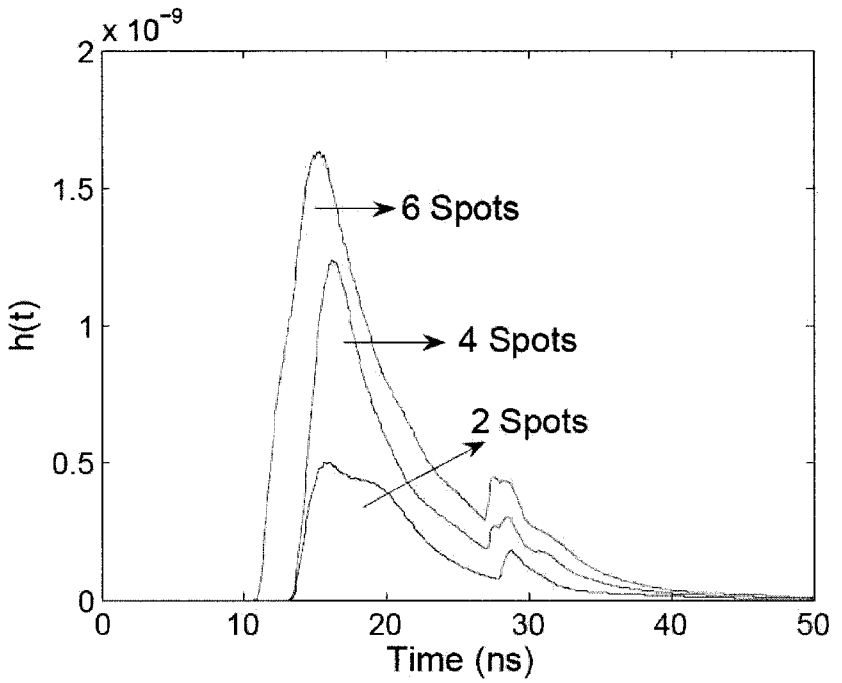

Figure 3.14: Received multipath signals using 2, 4 and 6 spots in a $6 \times 6 \times 3$ m room. Receiver having FOV=11.2° is located at (55 cm,75 cm,100 cm).

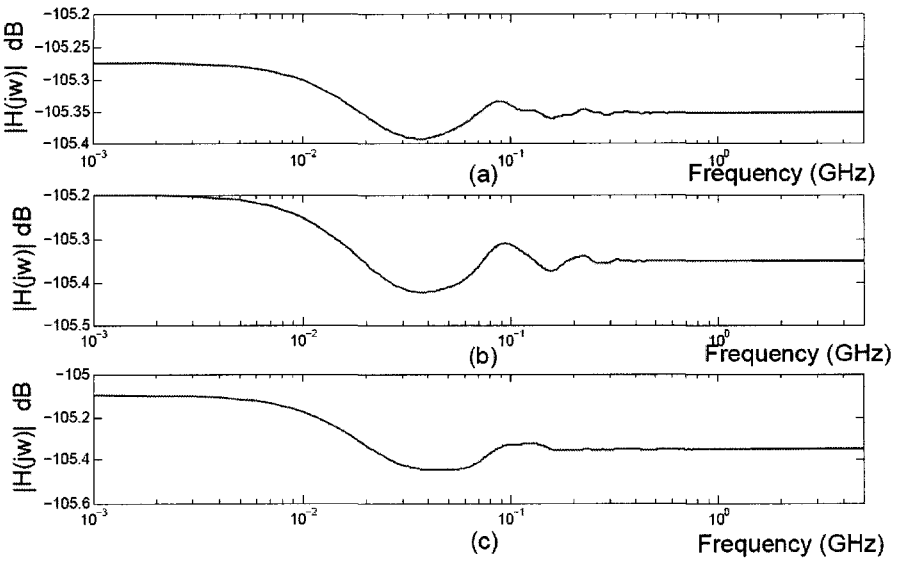

Figure 3.15: DSD channel gain for (a) 2 spots (b) 4 spots and (c) 6 spots over the ceiling.

3.5 DSD Optical Power Gain

The essential difference between the DSD configuration and previous ones is the spot movement on the ceiling. This spot movement results in a significant gain in allowable transmitter average optical power, defined as (2.5), due to eye safety issues. When the spot has a periodic motion and eye is exposed to the beam for a portion of the spot path period. Define $C_{T,eye}$ to denote the portion of each period which beam is subtended by the eye. Notice that the received optical power is zero for $1 - C_{T,eye}$ portion of each period. Thus, the

average optical power received by an eye is:

$$\begin{aligned} P_{eye,avrg} &= \lim_{M\to\infty} \frac{1}{2M} \int_{-M}^{M} x(t) \cdot C_{T,eye}\, dt \\ &= C_{T,eye} \lim_{M\to\infty} \frac{1}{2M} \int_{-M}^{M} x(t)\, dt \\ &= C_{T,eye} P_{avrg} \end{aligned} \tag{3.6}$$

where P_{avrg} is the average optical power of the transmitter beam. Therefore, transmitter can send $1/C_{T,eye}$ times more average power compared to the MSD systems assuming that spot moves fast enough so that a human cannot run after the beam and $C_{T,eye}\ T_s$ is less than 1 second [11] and the peak amplitude of the optical signal is still remains in eye safe level. According to safety regulations, an eye safe optical beam must not be harmful to human eye when it is directed to the eye from distance of 10 cm [11]. Therefore, $C_{T,eye}$ must be calculated for the worst case that the distance between eye and transmitter is 10 cm. For example, the achieved gain using the circular path is calculated. As shown in Fig. 3.16 the transmitter is placed on a table with 1 m height and the spot moves on a circle path with radius of 220 cm. Therefore, $\Psi = 47°$ and $R = 10 \times \sin(\Psi) = 7$ cm. The diameter of pupil is typically near 0.7 cm, then $C_{T,eye} = \frac{0.7}{2\times\pi\times 7} = 0.0152$. Therefore, in this case transmitter can send 66 times more average optical power which is equivalent to 18 dB gain in optical power. Note that the bottleneck in optical wireless systems is transmitter power limitations imposed by safety issues, therefore, this significant gain allows DSD systems to work over larger ranges and at higher rates than MSD systems.

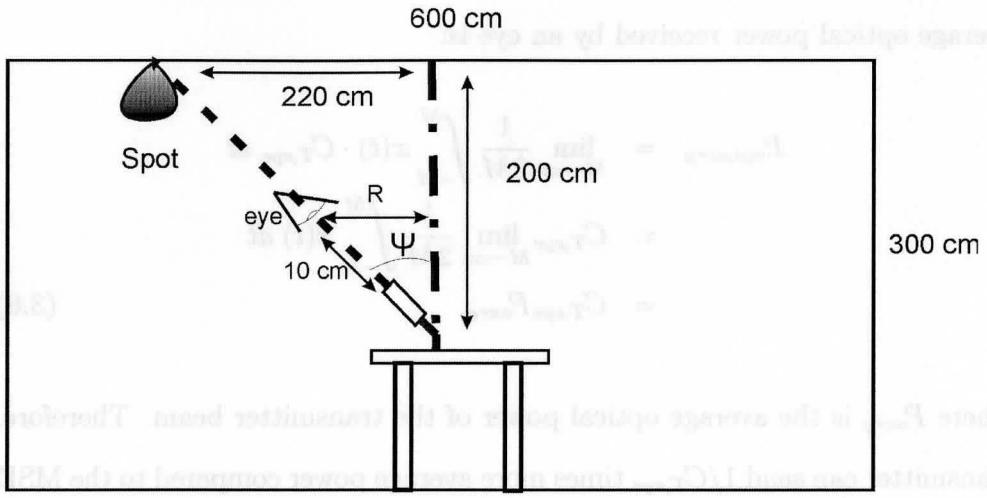

Figure 3.16: Geometry of room and eye for the proposed room

3.6 Conclusion

The DSD configuration is introduced and its architecture is explained in this chapter. Then the DSD channel model is discussed and it is shown that the DSD channel is well-modeled as a erasure channel to a good approximation when receiver SNR is sufficiently high. The capacity of DSD channels is shown to factor into term C_T and C_{in}^{avg}.

The goal of DSD system design is to produce a DSD link with good coverage over the room. Good coverage is defined as high SNR, less blind points, high average and low variance of C_T distribution over the room. The effect of transmitter and receiver design, and also spot path selection on DSD channel capacity and C_T distribution is explained and discussed. Moreover, it is shown that using only few more spots (up to 6) can improve the C_T distribution over the significantly while the complexity of the transmitter is increased modestly. Finally, it is shown that spot motion of DSD systems can result in a optical

gain for transmitter. This optical gain allows DSD links to achieve higher data rates and longer ranges than MSD systems.

The DSD channel is a fading channel and appropriate channel coding must be applied to approach the promised rates. In the next chapter, appropriate coding techniques are presented for DSD channels.

4

Channel Coding

As shown in Sec. 3.1.3, the DSD channel at several SNRs of interest is well approximated as a channel which has two states: one with low capacity (beam out of FOV) and the other with high capacity (beam in FOV). As discussed in Sec. 3.2, this channel is well modeled as an erasure channel with erasure probability $1 - C_T$. In order to approach the channel capacity, erasure coding must be used to combat this erasure and approach to channel capacity for all receivers. Famous fixed rate codes are not suitable for this channel because the probability of erasure is not constant for different receivers in the room and also it is unknown at the transmitter. In this case, it is not possible to employ fixed rate codes efficiently [64]. Therefore, another group of codes called rateless codes are employed for the DSD channel. These codes are shown to work efficiently on erasure channels. In order to make the DSD channel as erasure channel, i.e each packet is either received or lost, a standard error detecting codes termed cyclic-redundancy check codes (CRC) are applied to this channel before the rateless code. Using these two codes, the packet size must be chosen according to channel condition in order to achieve channel capacity.

4.1 Fixed Rate Erasure Correcting Codes

Traditional erasure correcting codes are fixed rate block codes. In these codes, k input symbols are used to generate n encoded symbols. The rate of the code is defined as k/n.

Reed-Solomon (RS) codes are among the most popular erasure correcting codes with a wide range of applications in digital communications and storage. Reed-Solomon codes are block codes constructed over $GF(2^m)$ of length $2^m - 1$ which satisfy the Singleton bound with equality [65]. In other words, for an (n, k) RS code, the minimum distance of the code is $n - k + 1$ and up to t symbol error can be corrected where $2t = n - k$ [65]. For the DSD channel, however, RS codes are not appropriate due to their fixed rate and relatively complex encoding and decoding.

Fixed rates error correcting codes are not appropriate for erasure channels with unknown probability of erasure [64]. In order to design an efficient RS code, the erasure probability of the channel must be estimated accurately at the encoder which is not possible practically for the DSD channel. Furthermore, in the DSD system, different positions in the room may have different capacities, thus, it is not possible to achieve capacity for all of them with one code, and therefore, different RS codes must be be designed for different receivers. Moreover, even if the transmitter has a accurate estimate of probability of erasure, it must employ a code with very long codewords since the bit period, T_b, is orders of magnitude smaller than T_s. Additionally, the number

of operations to encode and decode RS codes is proportional to the data block size. This makes such codes practical for relatively small block sizes such as byte error correcting codes of length 256.

4.2 Rateless Codes

Rateless codes are a relatively new class of erasure correcting codes. The first realization of rateless codes was proposed by Luby in 2002 [66]. The transmitter in this code is often termed a *digital fountain* since it emits "droplets" of *independent* encoded packets continuously from a given message source [67]. The receiver acts as a droplet collector. Once a given receiver has enough packets the entire message can be decoded. It is not important which of the emitted packets are received, rather their number is important.
These codes are termed *rateless* because potentially, an infinite number of independent encoded packets can be generated from a given data block. Digital Fountain Inc. [68] has developed commercial rateless codes for many erasure channels, such as packet networks, digital video distribution, software update protocols, satellite communications and also for file storage.

4.3 LT codes

In this work, a rateless code, called an *LT code* [66], is applied to the DSD channel to approach the capacity of the channel. Originally invented by Luby [66], LT codes can potentially generate an infinite stream of encoded packets from a given data block of k packets. The entire message can be decoded, with

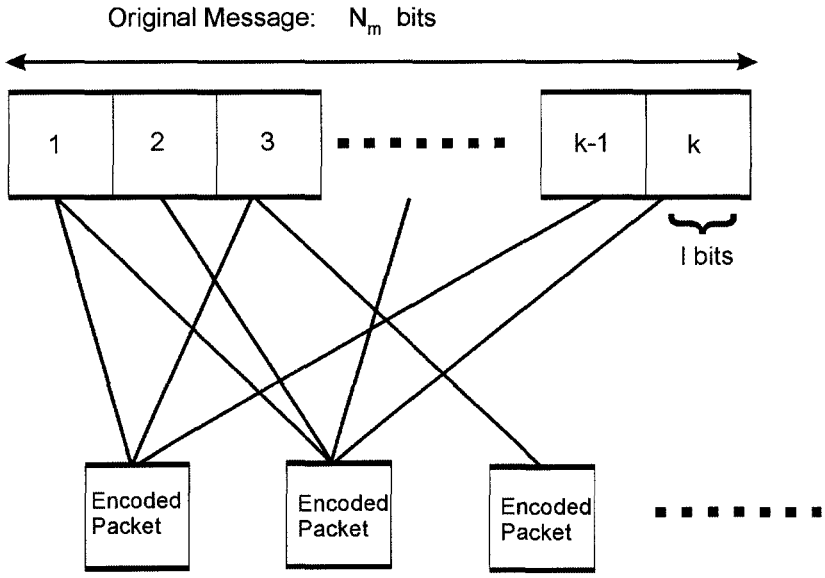

Figure 4.1: The LT code

high probability, when any slightly more that k packets are received [66]. The number of encoded packets necessary to decode the original message is not fixed. Therefore, the achieved rate using these codes is not fixed. However, the average number of necessary encoded packets for decoding is fixed. Hence, in this work the ergodic code rate of LT codes, which is the average of the rate over long time, is used for these codes.

In this section, LT encoder and decoder are presented and discussed. Moreover, the properties of a good degree distribution are explained and a distribution which has these properties is presented. Finally, LT code design is discussed.

4.3.1 LT encoder

In the LT encoder, the data block of length N_m bits is divided into k *input packets* each of them having length of $l = N_m/k$ bits. Then for generating each *encoded packet*, a packet degree d is chose randomly according to degree

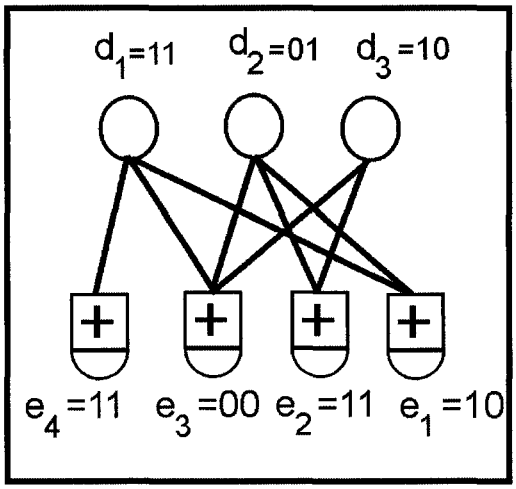

Figure 4.2: Encoding process for a simple LT code with $N_m = 6$, $l = 2$ and $k = 3$.

distribution $\rho(d)$. Next, d distinct data packets are selected uniformly at random from k input packets. The encoded packet is result of bitwise modulo 2 sum (bitwise XOR $\bigoplus$) of these d input packets. The data packets used to create the encoded packet are called *neighbors* of the encoded packet.

For example, Fig. 4.2 shows the encoding process for a very simple case graphically. In this example, the input message is 110110 and has length $N_m = 6$. It is divided to $k = 3$ input packets $d_1 = 11$,$d_2 = 01$ and $d_3 = 10$ each of length $l = 2$ bits. As shown in the figure, four encoded packets e_1,..,e_4 are generated from this input message. Encoded packet e_4 has degree one and its neighbor is only input packet d_1. Thus, $e_4 = d_1 = 11$. Encoded packet e_3 has degree three and has all the input packets as its neighbors. Hence,

$e_3 = d_1 \bigoplus d_2 \bigoplus d_3 = 00$. In the same manner:

$$e_2 = d_2 \bigoplus d_3 = 11$$
$$e_1 = d_2 \bigoplus d_1 = 10$$

Note that using this encoding process it is possible to generate infinite number of encoded packets from the input packets. Moreover, all the encoded packets are generated independently.

4.3.2 LT decoder

The decoder in LT codes performs a simplified belief propagation on the received packets to recover the original message [66, 69]. The encoded packets are generated independently, thus, the order of the received packets are not important. The decoder can decode the original k input packets when it receives slightly more than k encoded packets [66]. In the LT decoding process, erasure condition for channel is assumed, i.e all the encoded packets are assumed to be received without any error or completely lost [66, 69].
Furthermore, the decoder needs to have the degree and neighbors of each encoded packet to perform the decoding. These data can be passed to the decoder either by attaching them as a header to each packet or using similar and synchronized random generators at encoder and decoder. Sending these data through a header is more practical and robust. When sending packet information in a header, this header can decrease the data rate when its size is large compared to packet size. Packet size is discussed in more detail in Sec. 4.5.1.

The set of input packets which are covered by received encoded packets and are not yet recovered is called the *ripple* [66]. When an input packet is recovered it is removed from the ripple. For example, consider the simple LT code shown in Fig. 4.2. When no encoded packet is received the ripple is empty. If e_1 arrives in the decoder, ripple becomes d_1, d_2. Now if e_2 arrives, ripple becomes d_1, d_2, d_3.

The LT decoder works based on the LT recovery rule, namely, if there is an encoded packet with exactly one neighbor, then its neighbor can be recovered immediately since it is equal to the encoded packet. The recovered data packet, η, is exclusive-ored into any remaining received encoded packets which have η as a neighbor and η is removed as a neighbor from each of these encoded packets. The degree of each of these encoded packets is decreased by one because of this removal.

The decoder iteratively applies this rule to the received encoded packets until all the input packets are decoded or there is no more encoded packets to reciever.

LT decoding process is as follows [66, 69]:

1. Receive a new encoded packet and store it in the buffer.

2. Search the buffer to find a recoverable encoded packet i.e a packet with degree one.

3. If found, recover it then remove it from the buffer. Correct the packets in the buffer according to LT recovery rule. Goto step 2.

4. If all the data packets are recovered, decoding process ends successfully.

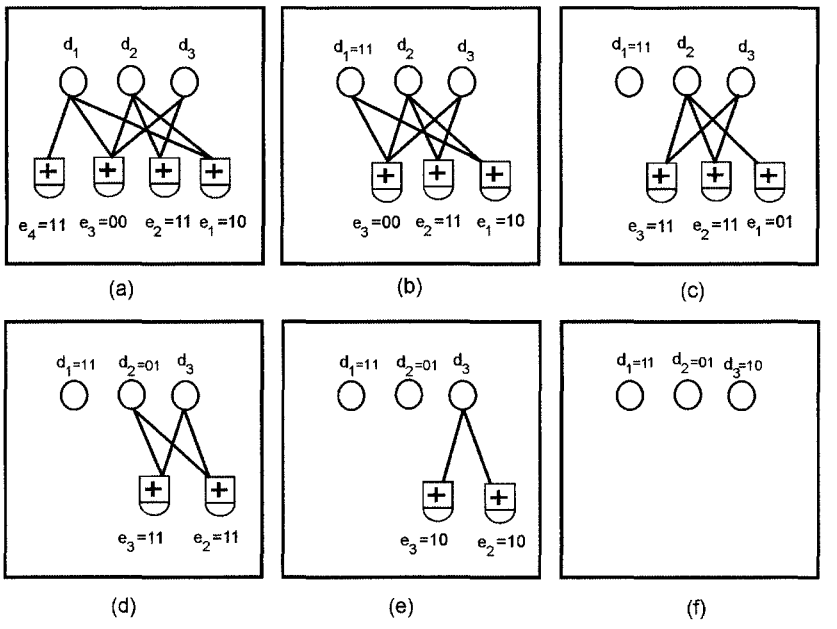

Figure 4.3: Decoding process for a simple LT code with $N_m = 6$, $l = 2$ and $k = 3$.

5. If there is no more encoded packets left to receive, decoding process ends with a failure.

6. Goto step 1.

Fig 4.3 shows the LT decoding process graphically for the simple LT code considered in last section. In this code $N_m = 6$, $l = 2$ and $k = 3$. As explained above, the LT decoding process begins when an encoded packet with degree one is received. Thus, In Fig 4.3 (a), the decoding process does not start until the forth encoded packet, e_4, is received. This process starts with decoding e_4 which has degree one. Thus, $d_1 = e_4 = 11$ (Fig 4.3 (b)). Then d_1 is XORed to e_2 and e_4 which have e_4 as neighbor, then is removed from their neighbors (Fig 4.3 (c)). Now e_1 has degree one and can be decoded. Thus, $d_2 = e_1 = 01$

(Fig 4.3 (d)). Again d_2 is removed from encoded packets which have it as a neighbor, i.e e_2 and e_3 (Fig 4.3 (e)). Finally, d_3 can be recovered from either e_2 or e_3 because it is the only neighbor of these two encoded packets (Fig 4.3 (e)). The decoding process is successfully ended at this stage and all input packets are recovered (Fig 4.3 (f)).

It is possible that this decoding procedure get stuck, i.e. if there is no encoded of degree one. Through the proper design of degree distribution, the probability of decoding failure can be made very small.

4.3.3 LT Code Degree Distribution

The LT code is characterized by k and degree distribution $\rho(d)$. The degree distribution $\rho(d)$ has a critical effect on LT code performance. This degree distribution must be designed so that it results in a low encoding/decoding complexity and a high rate. Among encoded packets, there must be high degree packets to make sure that all the input packets are connected to an encoded packets and no input packet is left without any connection to a encoded packet, after a reasonable number of encoded packets have been generated. On the other hand, many packets must have low degrees so that the decoding can get started and continue without delay. Moreover, having more low degree encoded packets, the average degree of encoded packets, d_{avrg}, decreases. The average number of operation required for encoding/decoding is linearly proportional to d_{avrg}. Therefore, an appropriate degree distribution must have these two properties:

- On average, as few encoded packets as possible must be required to decode the original message to achieve highest possible *average* data

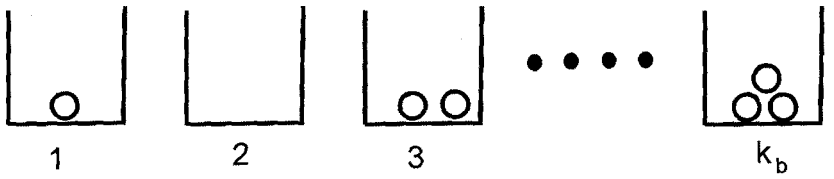

Figure 4.4: Balls and bins problem.

rate.

- The average degree of encoded packets, d_{avrg}, must be as low as possible to decrease the code complexity since number of operations needed for encoding/decoding is proportional to d_{avrg}.

Before finding a appropriate distribution, intuition can be gained by investigating the well-known *balls and bins* problem.

4.3.4 Balls and Bins problem

In the balls and bins problem, as shown in Fig. 4.4, there are k_b empty bins and at each step a ball is thrown to a randomly chosen bin. The question is the expected fraction of empty bins after throwing n_b balls. The analogy between LT codes and this problem can be found by considering the bins as input packets and balls as edges between encoded packets and input packets. In LT codes, we are interested in connecting all the input packets to at least one encoded packet with minimum number of encoded packets and minimum d_{avrg}.

The probability of throwing a ball in a particular bin in each step is $\frac{1}{k_b}$. Thus, $p_{emp,i}(n_b)$, the probability that one particular bin b_i is empty after throwing

n_b balls is:

$$p_{emp,i}(n_b) = \left(1 - \frac{1}{k_b}\right)^{n_b} \simeq e^{-\frac{n_b}{k_b}} \quad \text{for} \quad n_b >> 1$$

So the expected number of empty bins after throwing n_b balls is:

$$k_b e^{-\frac{n_b}{k_b}}.$$

This equation shows that many balls must be thrown to ensure all the bins have a ball with high probability. For example, throwing exactly k_b balls, $n_b = k_b$, the expected fraction of empty bins is $1/e$. If $3k_b$ balls are thrown, the empty fraction of bins reduces to $1/e^3$ which is nearly 5%. Equivalently, after throwing $3k_b$ balls, all the bins have at least one ball with probability 95%.

Define δ as the expected number of empty bins after throwing n_b balls, $\delta = k_b e^{-\frac{n_b}{k_b}}$. As n_b gets larger δ gets smaller exponentially fast. Thus, δ is considered a small number. The probability that all bins have a ball after throwing n_b balls, $p_{ball,all}$ is equal to probability all bins are not empty after throwing n_b. Since balls are thrown independently this probability is equal to:

$$p_{ball,all} = \prod_{i=1}^{k_b} (1 - p_{emp,i}(n_b)) = (1 - p_{emp,i}(n_b))^{k_b} \approx \left(1 - e^{-\frac{n_b}{k_b}}\right)^{k_b}$$

Now expanding this expression and assuming $e^{-\frac{n_b}{k_b}} \ll 1$, we can neglect terms with higher powers of $e^{-\frac{n_b}{k_b}}$. Hence, we would have:

$$p_{ball,all} \approx 1 - k_b e^{-\frac{n_b}{k_b}} = 1 - \delta$$

Thus, $p_{ball,all} = (1 - \delta)$ only if [69]:

$$n_b \geq k_b \log_e(\frac{k_b}{\delta}) \tag{4.1}$$

To link this exercise with LT codes, consider the bins as the input packets and balls as the edges from the encoded packets. In order to have all input packets covered by encoded packets with probability $1 - \delta$, at least $k \log_e(\frac{k}{\delta})$ edges from encoded packets are needed.

4.3.5 Ideal Soliton Distribution

For successful decoding, every input packet must have at least one edge in it. The decoder selects the input packets for connecting edges to, at random, thus, as discussed in Sec. 4.3.4, the number of edges must be at least of order $k \log_e(k)$. At the best case, the k input packets are decoded using k encoded packets. Hence, in this case, the average degree of encoded packets is $\log_e(k)$ and complexity of LT encoding/decoding is at least $o(k \log_e(k))$ [69]. Luby has shown that this bound of complexity is achieved by a degree distribution called *ideal soliton* distribution [66, 69].

In the ideal case, to avoid redundancy, at each iteration of decoding process only one encoded packet must have degree one. When this packet is processed, the degrees of the other encoded packets are reduced so that one new encoded

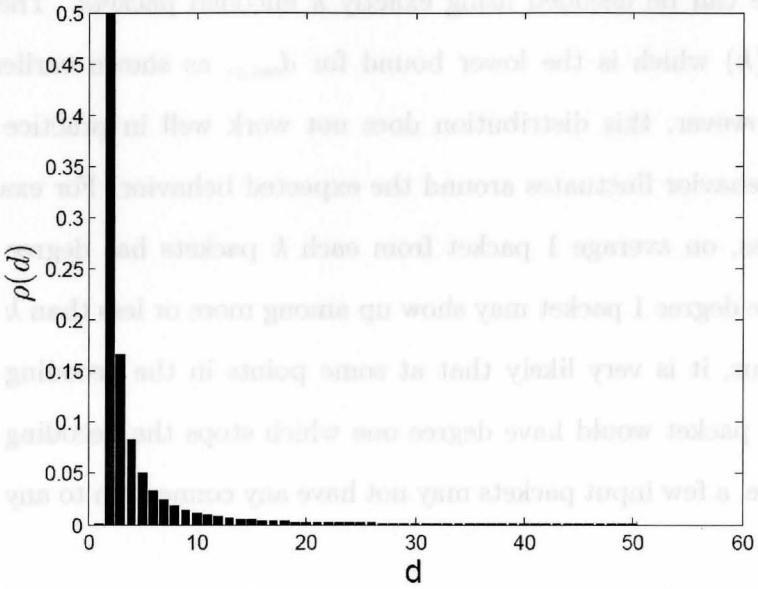

Figure 4.5: Ideal soliton distribution, $\rho_s(d)$ for $k = 1024$.

packet with degree one appears [66, 69]. Ideal soliton distribution defined as below is shown to achieve this behavior [66, 69]:

$$\rho_s(1) = \frac{1}{k}$$
$$\rho_s(d) = \frac{1}{d(d-1)} \quad \text{for} \quad d = 2, 3, ..., k$$

This degree distribution is plotted in Fig. 4.5 for $k = 1024$. The average degree using this distribution is:

$$d_{avrg} = 1/k + \sum_{i=2}^{k} \frac{i}{i.(i-1)} \approx \ln(k) \quad \text{for} \quad k >> 1$$

Ideal soliton distribution theoretically works perfectly if the actual behavior of the decoding process corresponds to the average one. Using this distribution,

the message can be decoded using exactly k encoded packets. The d_{avrg} is of order $\ln(k)$ which is the lower bound for d_{avrg}, as shown earlier in this section. However, this distribution does not work well in practice because its actual behavior fluctuates around the expected behavior. For example, as $\rho_s(d)$ implies, on average 1 packet from each k packets has degree one. In practice, the degree 1 packet may show up among more or less than k encoded packet. Thus, it is very likely that at some points in the decoding process, no encoded packet would have degree one which stops the decoding process. Furthermore, a few input packets may not have any connection to any encoded packet.

Therefore, the ideal soliton distribution requires a small modification to be able to work well in practice. This modified degree distribution is called the *robust soliton* distribution.

4.3.6 Robust Soliton Distribution

The robust soliton distribution has two more parameters, c and δ than ideal soliton distribution. It is designed so that the expected length of ripple during the decoding process is [66]:

$$R_{LT} = c \log_e(\frac{k}{\delta})\sqrt{k}.$$

The intuition for choosing this value is that the probability that a random walk of length k_w deviates from its mean by more than $\ln(k_w/\delta)\sqrt{k_w}$ is at most δ [66]. The parameter δ is a bound for the probability of failure to completely decode all the input packets after processing a certain number of encoded packets. Luby has shown that after receiving $K' = k + 2\ln(\frac{R_{TL}}{\delta})R_{TL}$

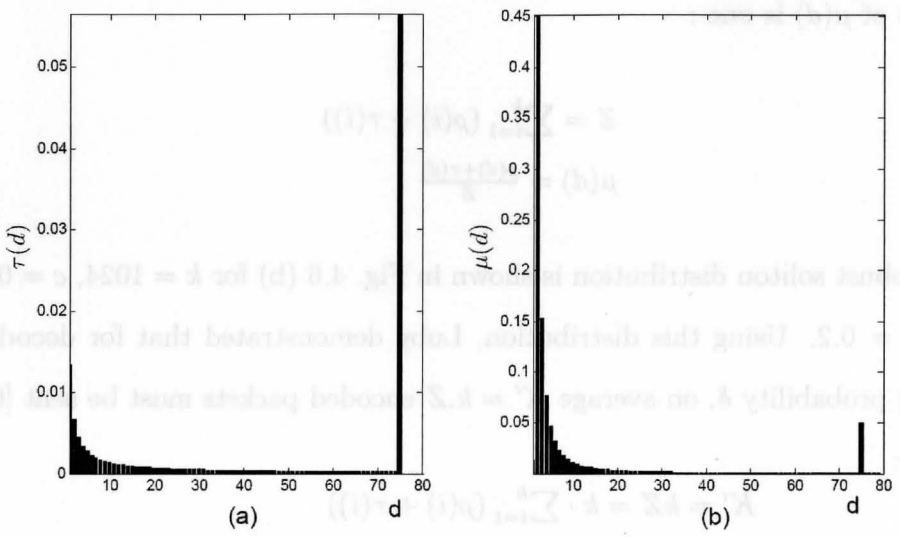

Figure 4.6: (a) $\tau(d)$ (b) Robust soliton degree distribution, $\mu(d)$, for $k = 1024$, $c = 0.05$ and $\delta = 0.2$.

the decoder can decode the whole message with probability $1-\delta$ [66,69]. The parameter c is a constant of order 1. Practically, it can be considered as a free parameter which with values slightly less than 1 gives good results [69].

To obtain the robust soliton distribution, $\mu(d)$, the positive function $\tau(d)$ defined as below, is added to ideal soliton distribution:

$$\tau(d) = \begin{cases} \frac{R_{LT}}{dk} & \text{for} \quad d = 1, .., \frac{k}{R_{LT}} - 1 \\ \frac{R_{LT} \ln(R_{LT}/\delta)}{k} & \text{for} \quad d = \frac{k}{R_{LT}} \\ 0 & \text{for} \quad d = \frac{k}{R_{LT}} + 1, ..., k \end{cases} .$$

This function is plotted in Fig. 4.6 (a) for $k = 1024$, $c = 0.05$ and $\delta = 0.2$. Note that any probability distribution must have total wight of 1. Thus, the result is divided by total weight of these two functions, Z, so that the total

weight of $\mu(d)$ is one :

$$Z = \sum_{i=1}^{k} (\rho(i) + \tau(i))$$
$$\mu(d) = \frac{\rho(d)+\tau(d)}{Z}$$

The robust soliton distribution is shown in Fig. 4.6 (b) for $k = 1024$, $c = 0.05$ and $\delta = 0.2$. Using this distribution, Luby demonstrated that for decoding failure probability δ, on average $K' = k.Z$ encoded packets must be sent [66]. Hence:

$$\begin{aligned} K' = kZ &= k \cdot \sum_{i=1}^{k} (\rho(i) + \tau(i)) \\ &= k + \sum \frac{R_{LT}}{i} + R_{LT} \ln(R_{LT}/\delta) \\ &\leq \quad k + R_{LT}.H_a(k/R_{LT}) + R_{LT} \cdot \ln(R_{LT}/\delta) \end{aligned} \tag{4.2}$$

where $H_a(k) = \sum_{i=1}^{k} \frac{1}{i-1} \approx \ln(k)$ is the harmonic sum up to k [66]. Thus, the number of encoded packets required for successful decoding is $k + O(\sqrt{(}k) \cdot \ln^2(k/\delta))$. A function $f(n)$ is defined to be of order $O(g(n))$ if there is a real constant $c_o > 0$ and an integer $n_0 \geq 1$ such that [70]:

$$g(n) \geq c_o f(n) \quad \text{for} \quad n \geq n_0.$$

Comparing $\rho_s(d)$ with $\mu(d)$, we see that $\mu(d)$ has more packets with degree one than $\rho_s(d)$, which ensures that decoding starts with a reasonable size of ripple and does not got stuck. Furthermore, $\mu(d)$ has a spike at $d = k/R_{LT}$, which ensures that all the input packets would get covered by a reasonable number of encoded packets [69].

The average encoded packet degree d_{avrg} using a robust soliton distribution

can also be bonded by,

$$\begin{aligned} d_{avrg} &= \frac{\sum_i i\cdot(\rho(i)+\tau(i))}{Z} \\ &\leq \sum_i i.(\rho(i)+\tau(i)) \\ &= \sum_{i=2}^{k+1} \frac{1}{i-1} + \sum_{i=1}^{\frac{k}{R_{LT}}-1} \frac{R_{LT}}{k} + \ln(R_{LT}/\delta) \\ &\leq H_a(k) + 1 + \ln(R_{LT}/\delta) \end{aligned} \tag{4.3}$$

Therefore, d_{avrg} is $O(\ln(k/\delta))$ [66].

4.3.7 LT Code Design

The LT code performance depends on three parameters of robust soliton distribution, i.e. k, c and δ. In general, as shown (4.3), the LT encoder and decoder on average requires $O(k\ln(k/\delta))$ operations. Furthermore, the whole message can be decoded from $k + O(\sqrt{(}k) \cdot \ln^2(k/\delta))$ encoded packets with probability $1-\delta$, as in (4.2).

Unlike RS codes, the rate of this code is not deterministic. Thus, LT codes do not have a fixed rate but they have a *ergodic* rate which depend on code parameters k, c and δ.

Define *LT code ergodic rate*, α, as the expected number of required encoded packets to decode k data packets, K', divided by k. Let $\rho_p(K')$ denote the probability distribution of K', number of required encoded packets to decode the message. Then:

$$\alpha = \frac{E[K']}{k} = \frac{\sum_{K'=k}^{\infty} \rho_p(K').K'}{k}. \tag{4.4}$$

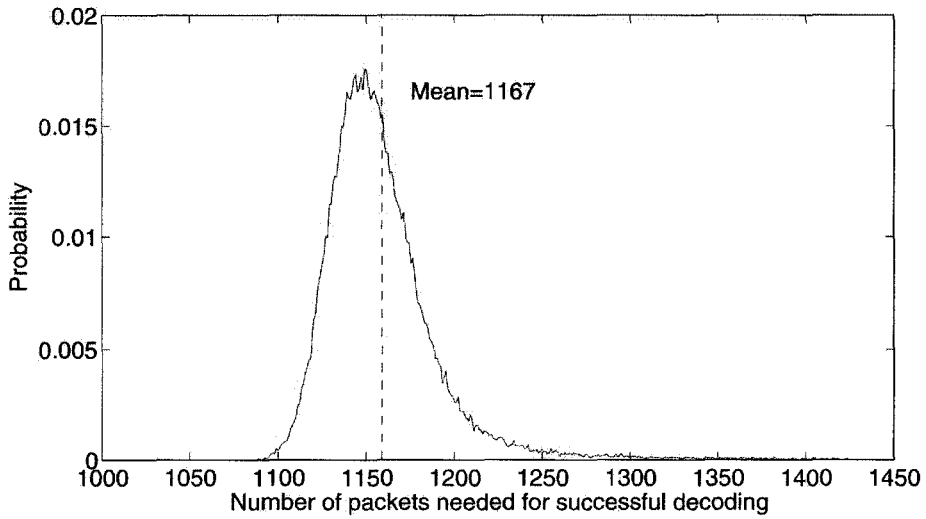

Figure 4.7: Probability distribution of packets required for successful decoding, $\rho_p(K')$, for $k = 1024$, $c = 0.05$, $\delta = 0.2$ over 10000 blocks.

Fig. 4.7 shows the probability distribution of $\rho_p(K')$ for $k = 1024$, $c = 0.05$ and $\delta = 0.2$. As shown in the figure, on average 1167 packets are required to successfully decode the 1024 input data packets. Hence, α for LT code with these parameters is $\frac{1167}{1024} \approx 1.14$.

Thus, the data bitrate on a channel with symbol bitrate R_b using LT code is, is R_b/α because to decode k bits, on average $k\alpha$ bits are required. It is possible to decrease α by changing k, c and δ. However, these changes increase the average operations required for encoding/decoding too. Hence, there is a trade off between rate and required number of operations. Adjusting the parameters to improve one, impairs the other and careful tuning is required. Fig. 4.8 shows d_{avrg} versus c, for 4 different δ and $k = 1024$ and Fig. 4.9 shows α versus c for different δ.

As shown in Fig. 4.8, in order to decrease d_{avrg}, c must be increased and δ

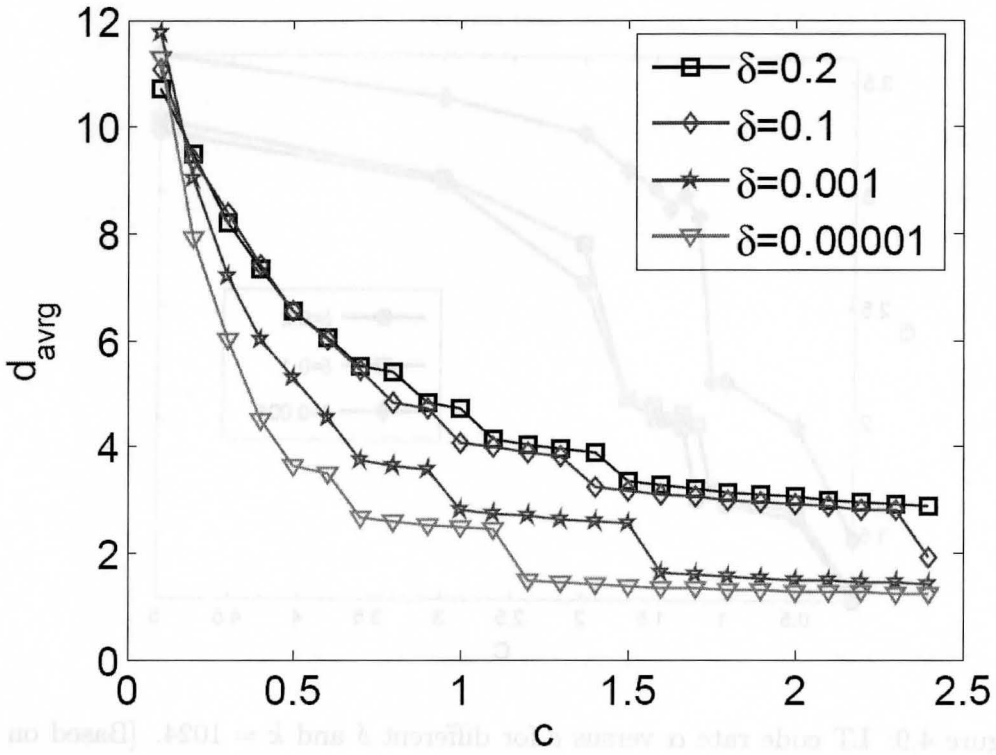

Figure 4.8: Average degree, d_{avrg} for $k = 1024$ versus c for several δ.

must be decreased. However, as shown in Fig. 4.9, increasing c and decreasing δ results in a increase in α. These two figure show the tradeoff between rate and complexity in LT codes. This trade off can be seen by comparison of Fig. 4.9 and Fig. 4.8. For example, consider the LT code with parameters $k = 1024$, $c = 2$ and $\delta = 0.001$ which has $\alpha = 3.27$ and $d_{avrg} = 1.57$. Changing δ to 0.2 results in $\alpha = 2.61$ and $d_{avrg} = 3.055$, i.e. complexity has increased near 100 % while data rate is increased 20 %.

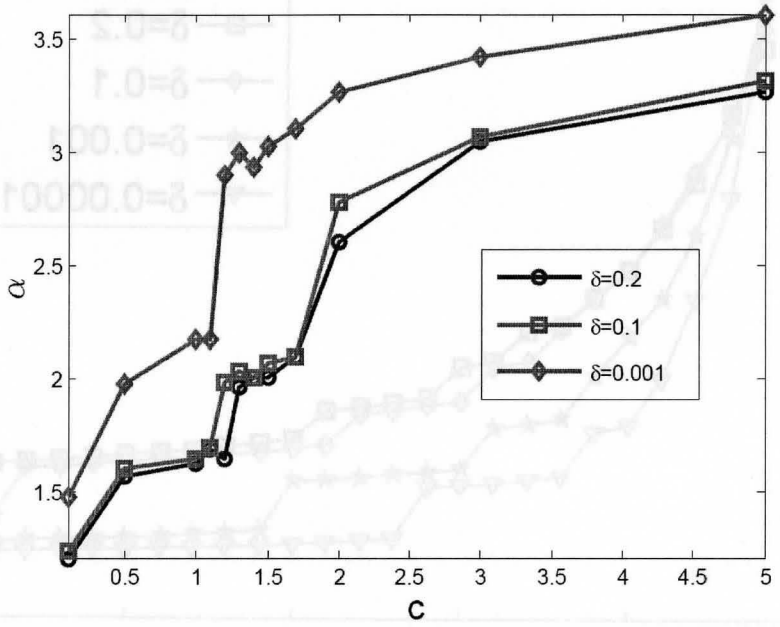

Figure 4.9: LT code rate α versus c for different δ and $k = 1024$. [Based on data from [8]]

4.4 Cyclic-Redundancy Check Codes

Rateless codes are based on the assumption of an erasure channel, i.e. packets are received complete and without any error or are totally lost [66, 69]. Therefore, in order to apply LT codes, two conditions must be met:

1. All channel erasures can be detected.
2. There are no errors in the received packets.

A simple and effective way to detect packet errors is employing cyclic redundancy codes (CRC). These codes are widely used in Internet and data storage purposes as error detectors. For example, are used in IEEE 802.3 standard for

gigabit Ethernet as an error detectors [71]. Furthermore, CRC codes provide strong detection capability and can be implemented using simple and fast shift register circuits. For example, a 10 Gbps CRC design is demonstrated in [72]. The CRC codes are shortened Hamming cyclic codes [65]. The CRC encoder treats data word as a polynomial in GF(2) and performs polynomial division by a generator polynomial, $G(x)$ called the *CRC polynomial.* Parity bits are the reminder of the division. In the CRC encoder, the parity bits of the input data are computed and are attached to the data packet. These parity bits are also called *frame check sequence* (FCS) or *checksum.* In the decoder, the FCS of the received packet is recomputed and compared with the attached FCS. If they are not equal the packet is assumed to be corrupted.

The CRC error detection capability depends on the CRC generator polynomial and packet length. As the packet length gets larger, the error detection capability decreases. There are various well-known CRC generator polynomials, such as CRC-16 or CRC-32. In this work, IEEE 802.3 CRC-32 is used because of better error detection capability. The CRC-32 uses generator polynomial below and generates a 32 bit (4 byte) FCS using:

$$G(x) = x^{32}+x^{26}+x^{23}+x^{22}+x^{16}+x^{12}+x^{11}+x^{10}+x^{8}+x^{7}+x^{5}+x^{4}+x^{2}+x+1.$$

The CRC code is a shortened Hamming cyclic code, thus, its HD is at least 3 and is able to detect all 1 bit errors in the packet. The HD of the CRC codes depend on the data length. As the data length gets larger, the HD of the code decreases. For example, Fig. 4.10 shows the HD for the CRC-32 versus packet size.

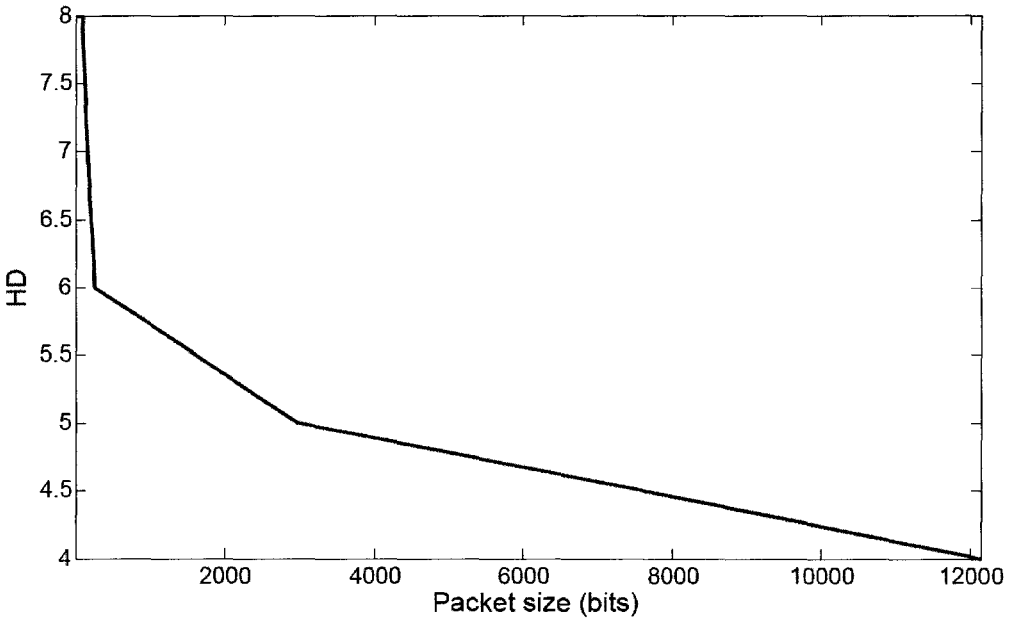

Figure 4.10: Hamming distance (HD) versus packet size N, for CRC-32 (based on data from [9]).

The packets length for IEEE 802.3 standard must be a multiple of 8 and less than 12144 [71]. The HD for this packet size, as shown in Fig. 4.10, is at least 4. Therefore, the CRC-32 is able to detect all 1, 2 and 3 error patterns in the packet.

Undetectable error: Undetectable error for a CRC code is a error pattern in the packet which results in the same FCS as the original data.

The undetectable errors for CRC-32 and packet lengths less than 12144 bits occur with 4 or more bit error patterns. Let $A_{n,i}$ be the number of code words with weight i in code with length n. The probability of undetectable error when C_n is used for a binary symmetric channel (BSC) with bit error rate p,

can be expressed as below [73]:

$$P_e(C_n, p) = \sum_{i=1}^{n} A_{n,i} p^i (1-p)^{n-i}$$

The $A_{n,i}$ are tabulated for CRC-32 in [73]. Moreover, $P_e(C_n, p)$ is computed and shown to be smaller than 10^{-9} for $10^{-5} < p < 0.5$ and $12144 \geq n \geq 512$. For $p < 10^{-5}$, $P_e(C_n, p)$ is less than 10^{-15}. Therefore, using CRC-32 and packet sizes smaller than 12144 bits, the probability of undetected error is very small and can be ignored. Therefore, in this work, it is assumed that using CRC-32 code all corrupted packets are detected by CRC-32 and erasure condition is valid for LT code. Furthermore, CRC can be used to detect the channel erasure. When spot is out of FOV, as discussed in Sec. 3.1.2, the channel gain is very low. Therefore, receiver receives the all zero packet plus noise in this case. Note that all zero packet is a valid packet for CRC code but it is not a valid packet for LT code. Therefore, when spot is out of FOV, receiver can detect erasure since it receives only all zero packets.

4.5 DSD Channel Coding

In the DSD channel, LT codes are used to combat the random fading of the channel. Moreover, an IEEE standard CRC-32 is employed to detect corrupted packets and provide the LT code with erasure channel condition. The encoder module of the DSD system in shown in Fig. 4.11 (a). At transmitter, data first enters the LT encoder and LT encoder starts producing encoded packets from data. Next, the encoded packets created in LT encoder enter the CRC

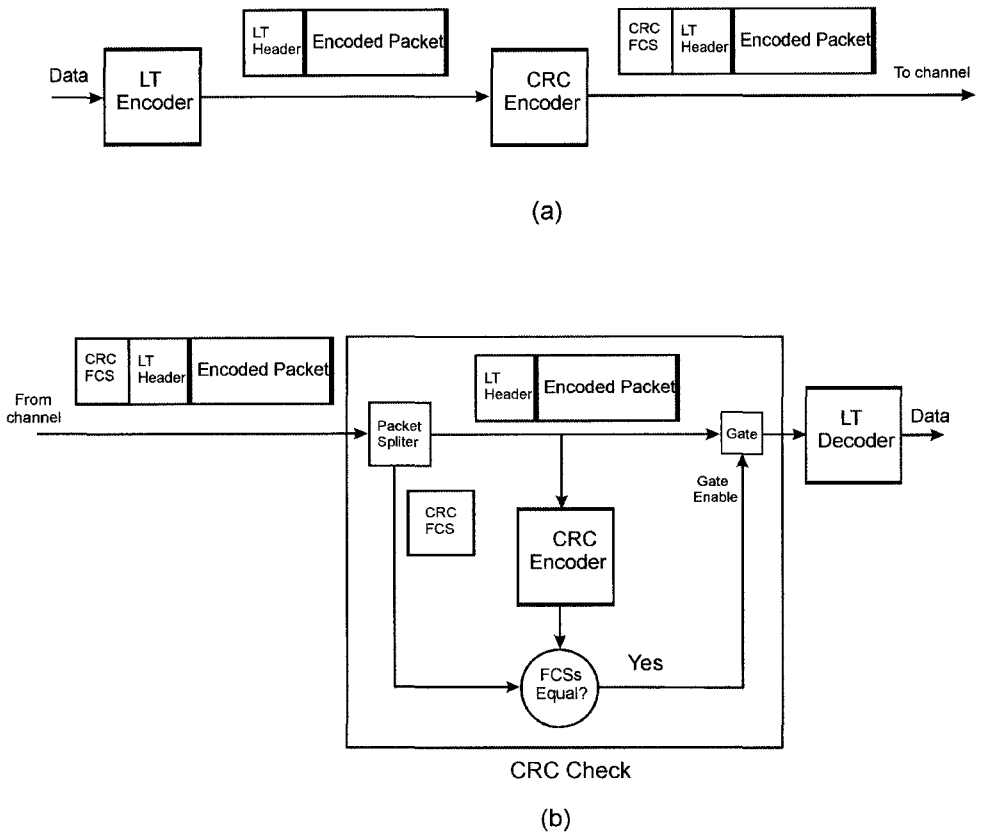

Figure 4.11: Encoder diagram of the DSD system.

encoder. The CRC encoder, calculates the FCS of the packet and attaches it to the packet. Next, the packet is sent over the channel.

The decoder module of DSD system is shown in Fig. 4.11 (b). At the receiver, first the received packet enters the CRC decoder. The CRC decoder takes out the FCS and recomputes the FCS for the encoded packet. If the computed FCS is equal to received FCS, the encoded packet is passed to LT decoder. Otherwise, the packet is assumed to be corrupted i.e erased by the channel and is dropped out.

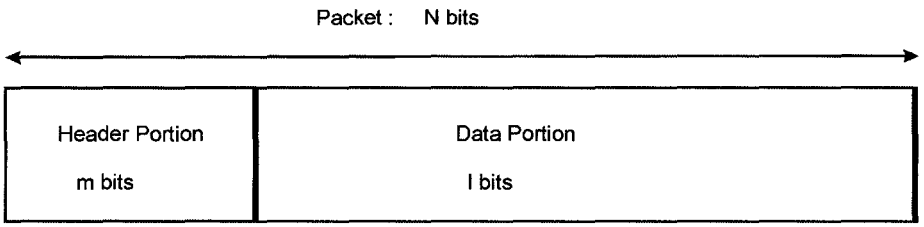

Figure 4.12: Two portions of the packets.

4.5.1 Packet Size

Employing both CRC-32 and LT code in the DSD system, every packet of length N, as shown in Fig. 4.12, is composed of a header portion of length m and and a data portion of length $l = N - m$. The length of header part m is fixed because it contains coding information such as LT packet degree and neighbors, and CRC-32 FCS. This header consists of the packet degree, which has length $\log_2(k)$ bits, the neighbors of the packet, which on average have length of $d_{avrg} \cdot \log_2(k)$ bits and CRC FCS, which has length of 32 bits. Therefore, the average length of m is:

$$\overline{m} = \log_2(k) + d_{avrg} \cdot \log_2(k) + 32 \tag{4.5}$$

However, it is possible to set l to any arbitrary number by adjusting the packet size of the LT code.

In order to increase the data bitrate, the ratio $\frac{l}{N}$ must be increased. For example, using an LT code with $d_{avrg} = 12$ and $k = 1024$ the average header length is $\overline{m} = 10 + 120 + 32 = 162$ bits or 20.25 bytes. Setting $l = 20$ bytes, only half of each packet is data and half of channel bit rate is wasted by packet headers. Setting $l = 1000$ bytes, $\frac{1000}{1020.25} = 0.98$ of each packet is data and data

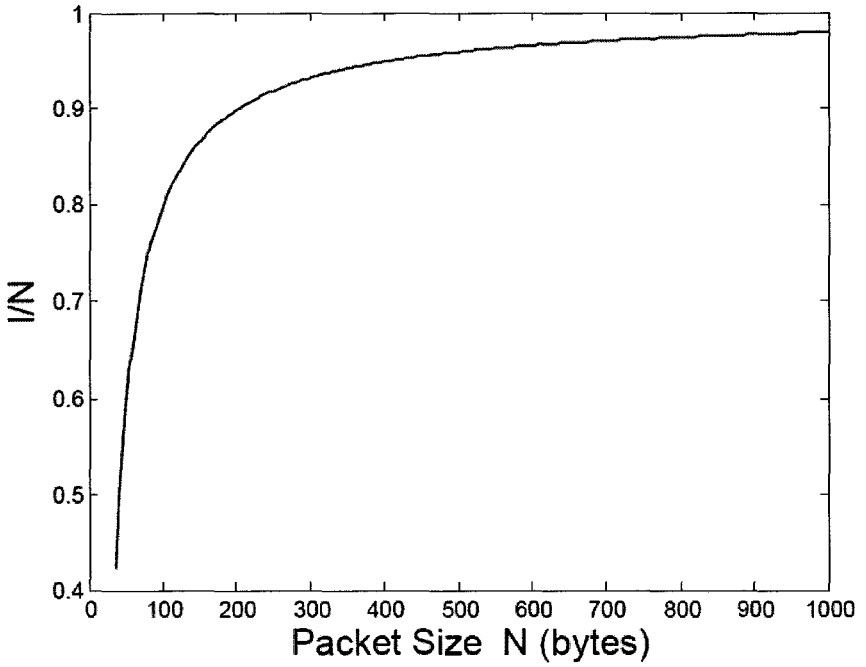

Figure 4.13: Data rate vs packets size, N, for header size $\overline{m} = 20.25$ bytes.

rate gets closer to channel bit rate. Fig. 4.13 shows how the data rate changes versus packet size for $\overline{m}$=20.25 bytes.

However as packet size gets bigger, by increasing l, the probability of error occurring in the packets $P_{packet-error}$ gets higher. The probability of packet error $P_{packet-error}$ is:

$$P_{packet-error} = P_1 + P_2 + P_3 + ... = \sum_{i=1}^{N} P_i$$

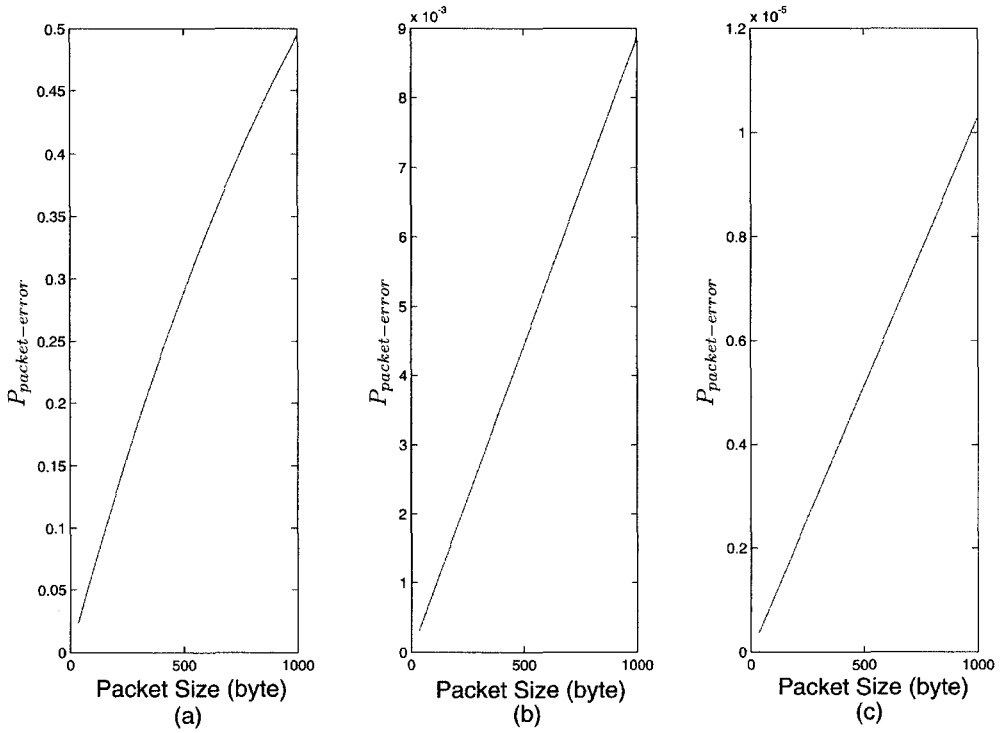

Figure 4.14: $P_{packet-error}$ for (a) $p = 8.5 \times 10^{-5}$ (SNR=11.5 dB) (b) $p = 10^{-6}$ (SNR=13.5 dB) (c) $p = 10^{-9}$ (SNR=15.5 dB) versus packet size N.

which is sum of probability of exactly i bit errors in the packet, P_i. The probability of exactly i bit errors in the packet can be expressed as:

$$P_i = \frac{N!}{i!(N-i)!} \cdot p^i \cdot (1-p)^{N-i}.$$

Fig. 4.15 shows $P_{packet-error}$ for three values of p as a function of N. Note that p is calculated from the receiver SNR, using (2.12) or (2.14), as discussed in Sec. 2.7.

The CRC-32 detects all the corrupted packets and drops them out, i.e. on average $(1 - P_{packet-error})$ portion of received packets are not dropped by CRC-

32 and can enter the LT decoder. Therefore, increasing l results in increasing $P_{packet-error}$ and dropping out more received packets which decreases the data rate of the channel.

Considering extreme limits for l, we can see that data rate becomes zero as $l \rightarrow 0$ and $l \rightarrow \infty$. When $l \rightarrow 0$, no data is sent over the channel and when l gets very large, all the packets are corrupted and dropped by the CRC-32. Therefore, there is a optimum value of data portion l which maximizes the data rate. This optimum value depends on channel probability of error p.

LT decoder needs on average $\alpha \cdot k$ packets to decode k data packets and from every encoded packet, $\frac{l}{m+l}$ portion is data. Also, $(1 - P_{packet-error})$ portion of packets are not dropped out by CRC-32 and enter the LT decoder. Therefore, the average data rate using CRC-32 and LT code would be,

$$R_{coded} = \frac{(1 - P_{packet-error})l}{\alpha(\overline{m} + l)} R_b \tag{4.6}$$

Therefore, the effect of the CRC-32 on the DSD channel is decreasing the probability of error, at the expense of decreasing the data rate by a factor of $(1 - P_{packet-error})$. For example, using an LT code with parameters: $k = 1024$, $c = 0.05$ and $\delta = 0.2$, then $\alpha = 1.14$ and average degree of the packets would be 12. So on average, using (4.5), $\overline{m} = 162$ bits or 20.25 bytes are required for coding header. Fig 4.15 shows the data rate versus packet size for three different values of p for this code.

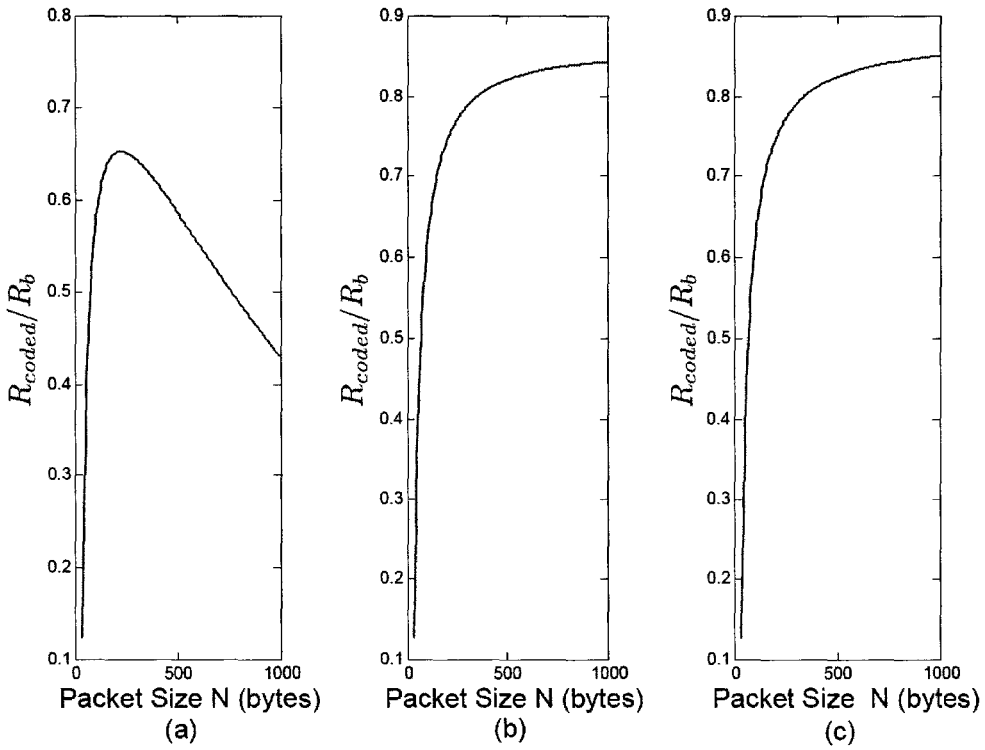

Figure 4.15: Data rate vs packets size for $\overline{m} = 20.25$ bytes, and (a) $p = 8.5 \times 10^{-5}$ (SNR=11.5 dB) (b) $p = 10^{-6}$ (SNR=13.5 dB) (c) $p = 10^{-9}$ (SNR=15.5 dB).

4.5.2 Border Effect in The DSD Channel

Packet size has an effect on the data rate in another way. When the spot crosses the FOV borders, two packets, one when spot is entering the FOV and another one when spot is leaving the FOV, may be received incomplete, and are dropped out by CRC-32 check. Thus, if the packet size is so large that these two dropped packets are not negligible compared to the total number of received packets, the data rate can be decreased. We term this rate decrease as a *border effect*. Define, $I_{in,i}$ as the duration from when spot enters the FOV

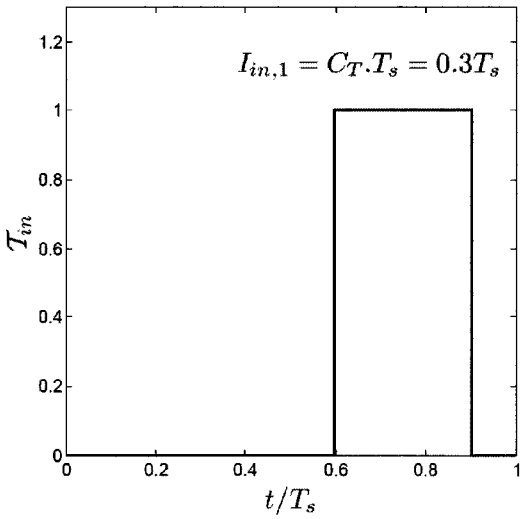

Figure 4.16: I_{in} for the case that spot enters the FOV only once in one spot period.

till it leaves it for the ith time in one spot period. Therefore,

$$\sum_i I_{in,i} = C_T.T_s$$

Consider the case when in each spot period the spot enters the FOV only once, as shown in Fig. 4.16. In this case, $I_{in,1} = C_T.T_s$. This figure shows T_{in} for a receiver with FOV=45° located at (300 cm,200 cm,100 cm) in a $6 \times 6 \times 3$ m room. The spot path is a circle with radius of 220 cm.

In this case, if the packet size is a a large portion of C_T, then large portion of the channel rate is wasted due to 2 incomplete received packets on the borders. Define s as the number of packets in I_{in}. Then,

$$s = \left[\frac{I_{in} \cdot R_b}{N} \right], \tag{4.7}$$

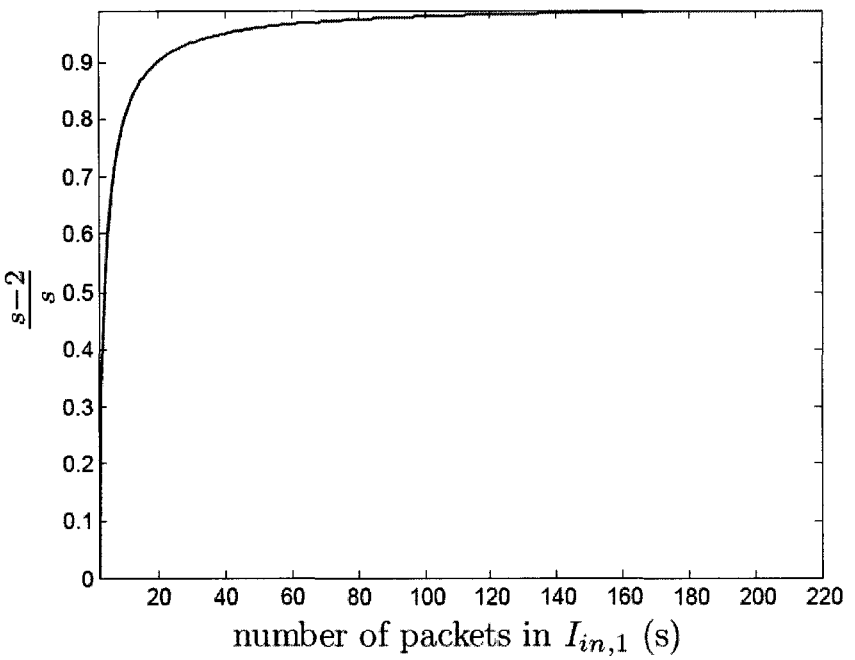

Figure 4.17: The effect of number of packets in C_T, s, on data rate for different s when spot enters the FOV only once per each spot period.

where N is the packet size in bits. Then at worst case, $s-2$ packets are received completely. Hence, the data rate would be multiplied by,

$$\frac{(s-2)}{s} = 1 - \frac{2.N}{I_{in}.R_b}. \tag{4.8}$$

For example, if $s = 3$, then $\frac{2}{3}$ of data rate can be wasted. Fig. 4.17 shows the ratio $\frac{s-2}{s}$ for different s. From (4.8), in order to keep the border effect less than 1%, packet size, N, must be chosen so that $s \geq 200$.

If spot enters the FOV more than once in one period, as shown in Fig. 4.18, then in order to achieve a good utilization of all $I_{in,i}$, the packet size must be

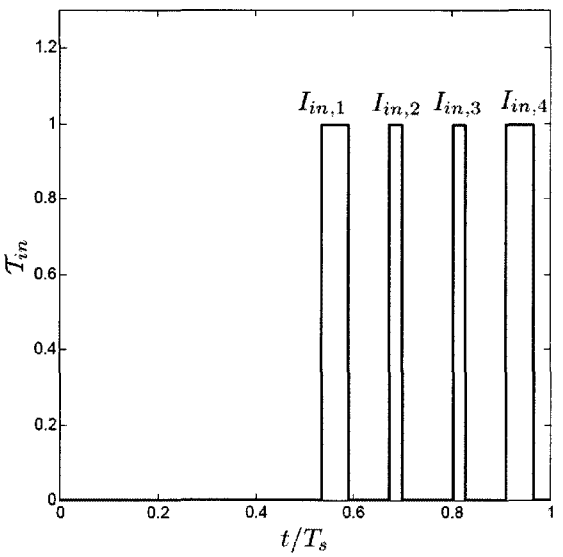

Figure 4.18: $\mathcal{T}_{in}$ for a Lissaujou path where spot enters the FOV more than once.

decreased so that,

$$\frac{2.N}{I_{in,min}.R_b} \quad \text{where} \quad I_{in,min} = \min_i(I_{in,i})$$

is negligible, and therefore, $\frac{(s-2)}{s}$ is nearly 1.

Note that it is not possible to decrease the packet size to any arbitrary amount because, as shown in Fig. 4.15, decreasing the packet size may decrease the rate. Therefore, an appropriate value for packet size must be chosen to make border effect small while still achieving a high data rate.

4.6 Conclusion

In this section erasure correcting codes are presented as a solution for random fading in DSD channel. Fixed rate codes are not appropriate for DSD channel because they are efficient only when encoder knows the probability of erasure in the channel which is not the case in DSD channel. A relatively new group of erasure correcting codes called rateless codes are introduced to combat DSD channel random fading. Rateless codes work assuming that all the received packets are received without any error. Therefore to verify the correct reception of packets, CRC check is introduced and showed to decrease the probability of error to negligible values. At the end, code design and optimization issues are presented and discussed to design these codes more efficient.

In the next chapter, a DSD channel and coding are simulated. Achievable rates are given for a given room and beam configuration.

5

Simulation Results

In this chapter, simulation assumptions and results are presented for a DSD system in $6 \times 6 \times 3$ m room similar to the one proposed in the well-known work of Kavehrad *et al.* on MSD channels [4, 33, 74]. The coded OOK on this DSD channel is simulated over an AWGN channel for three different SNRs consistent with experimentally measured spot diffusing channels and the simulated achieved rates are shown to be consistent with (4.6) in Sec. 4.5.1.

Four positions with high, moderate and low C_T in this room are chosen and the achieved rates are computed for different transmitter bitrates. The first case is a DSD system, based on a proposed spot diffusing link presented in the literature [7]. In this system, the transmitter is capable of modulating data at 100 Mbps and a raw BER of 10^{-9} using OOK modulation. The achieved rates for a DSD system using this link, for single and multiple spot cases are computed.

Next, an OOK transmitter of rate 1 Gbps is considered with the same eyesafe transmit power as in [7]. As SNR expression for OOK shows (2.12), modulating at higher rate with fixed optical power, the received SNR decreases because

SNR is proportional to $\frac{1}{R_b}$. Thus, the excess bandwidth available for the DSD channel is exploited by using power efficient L-PPM modulation techniques which require greater bandwidth. The achieved rates for this system using single and multiple spots are computed.

Finally, an OOK transmitter with rate of 10 Gbps is considered. To compensate for the decreased bit interval, the transmit optical power is increased but still remains eye safe due to the beam motion in the DSD system, as discussed in Sec. 3.5. The achieved rates for this system are also computed for single and multiple spot cases.

5.1 Assumptions and Definitions

In these simulations, we consider a $6 \times 6 \times 3$ m room used in the works of Kavehrad *et al.* [4, 33, 74]. The room reflectivities are assumed to be 0.7, 0.6 and 0.2 for ceiling, walls and floor respectively as in [38].

As shown in in Sec. 3.3, for this square room, a circular spot path has good channel characteristics while it is simple and implementable. Thus, the spot path is chosen to be a circular path with radius 2.2 m for single spot case which minimizes the blind points in the room. For the multiple spot paths, 2, 4 and 6 spots are assumed to be arranged into two circles with radii 200 cm and 300 cm, as presented in Sec. 3.4 and shown in Fig. 5.1. A spot angular speed of 10 Hz which is a practical value for a DC motor is assumed for spots which results in a spot motion period $T_s = 0.1$ s. Commercial DC motors with such speed are available [75].

The receiver FOV is assumed to be 45°, similar to the receiver proposed in [7],

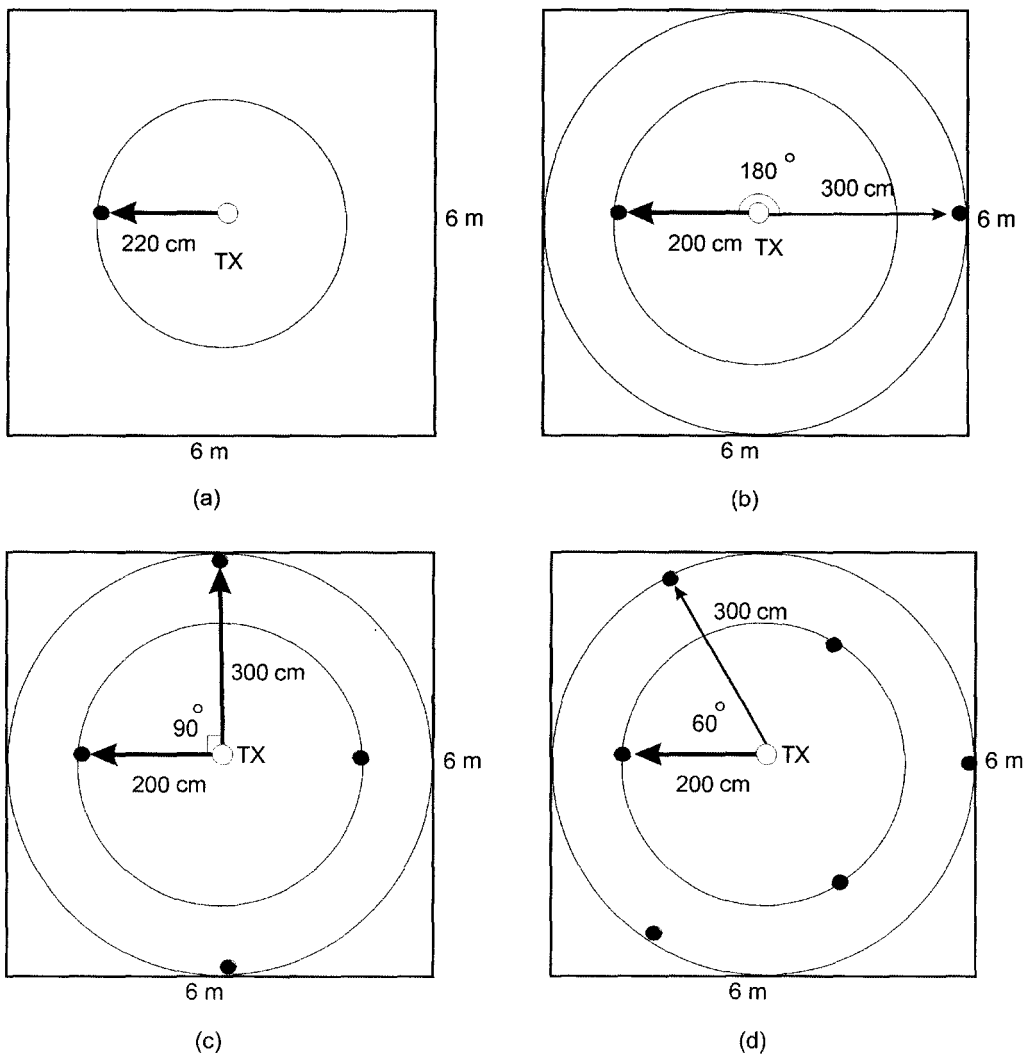

Figure 5.1: Spot configuration for circle paths with (a) 1, (b) 2, (c) 4 and (d) 6 spots, used in simulations.

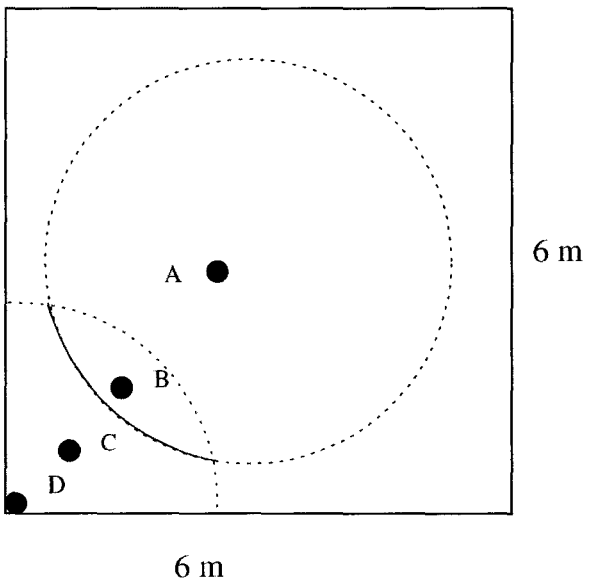

Figure 5.2: Top down view of four locations in the room A: (230 cm , 230 cm, 100 cm), B: (180 cm, 180 cm, 100 cm), C: (90 cm, 90 cm, 100 cm) and D: (5 cm, 5 cm, 100 cm). The origin is assumed to be at the bottom left corner of the room.

Number of Spots	1	2	4	6
C_T for A	0.3044	0.5606	1	1
C_T for B	0.3070	0.6026	1	1
C_T for C	0.2338	0.4567	0.9133	1
C_T for D	0.0937	0.1397	0.2791	0.4188

Table 5.1: C_T for simulated positions in the room for 1, 2, 4 and 6 spots case.

with specifications presented in Sec. 5.4. As shown in Fig. 5.2 four positions in the room are considered. These positions are chosen to have high, moderate and low C_T. Table. 5.1 shows the C_T for these positions using 1, 2, 4 and 6 spots. The set $\mathcal{T}_{in}$ defined in Sec. 3.2, is the set of times in the period that spot is in FOV in one period T_s. The $\mathcal{T}_{in}$ is shown in Fig. 5.3, Fig. 5.4, Fig. 5.5 and Fig. 5.6 for these positions.

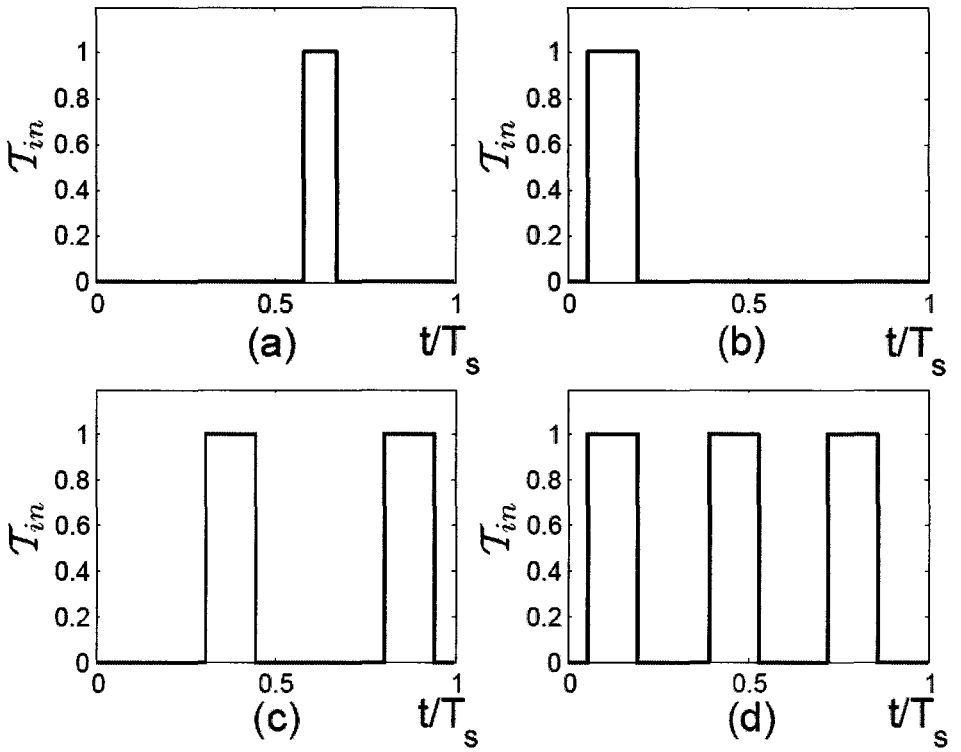

Figure 5.3: $\mathcal{T}_{in}$ for position A using (a) 1 spot (b) 2 spots (c) 4 spots and (d) 6 spots.

A previously reported LT code with $k = 1024$, $c = 0.05$ and $\delta = 0.2$ was applied to the DSD channel [8]. A high-speed IEEE 802.3 CRC-32 code from the Ethernet standard is employed to detect and drop corrupted packets [71]. It is assumed that both the transmitter and receiver have sufficient processing power to encode and decode packets for the desired rates.

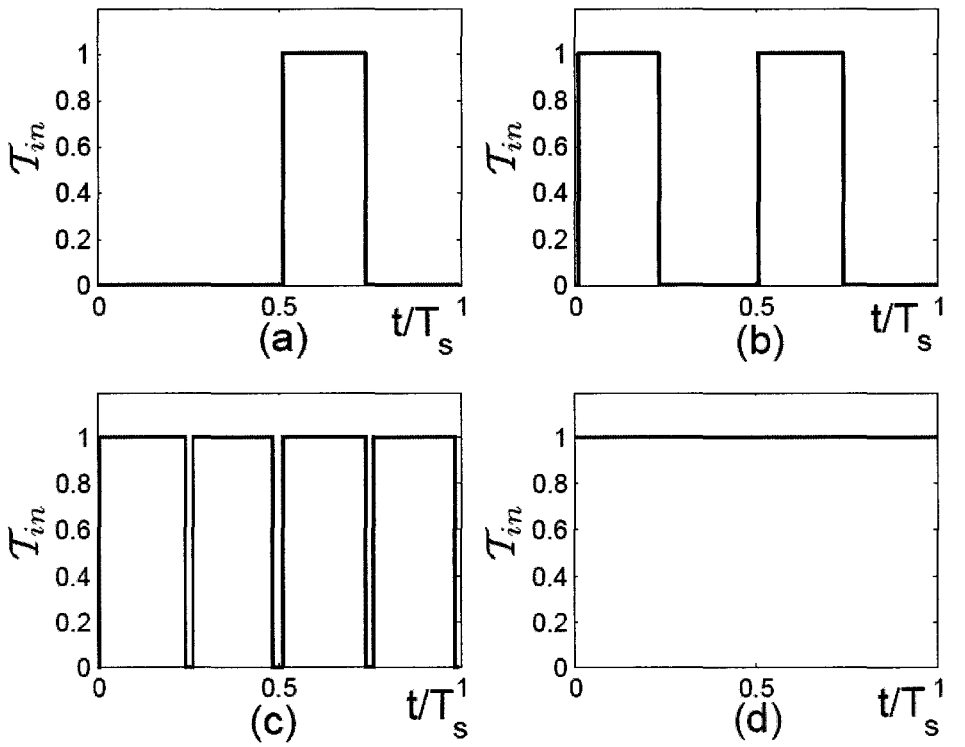

Figure 5.4: $\mathcal{T}_{in}$ for position B using (a) 1 spot (b) 2 spots (c) 4 spots and (d) 6 spots.

5.2 The DSD Link Coding Simulation

As discussed in Sec. 4.3, the LT encoder generates independent encoded packets from the message and the order of the received encoded packets is not important for decoding. Therefore, no matter which packets are received, after receiving on average $\alpha.k$ packets, the decoder is able to decode the message. The data rate using LT and CRC codes can then be predicted using (4.6). In this section, the DSD coding system presented in Sec. 4.5, is simulated over a noisy optical intensity channel to verify (4.6).

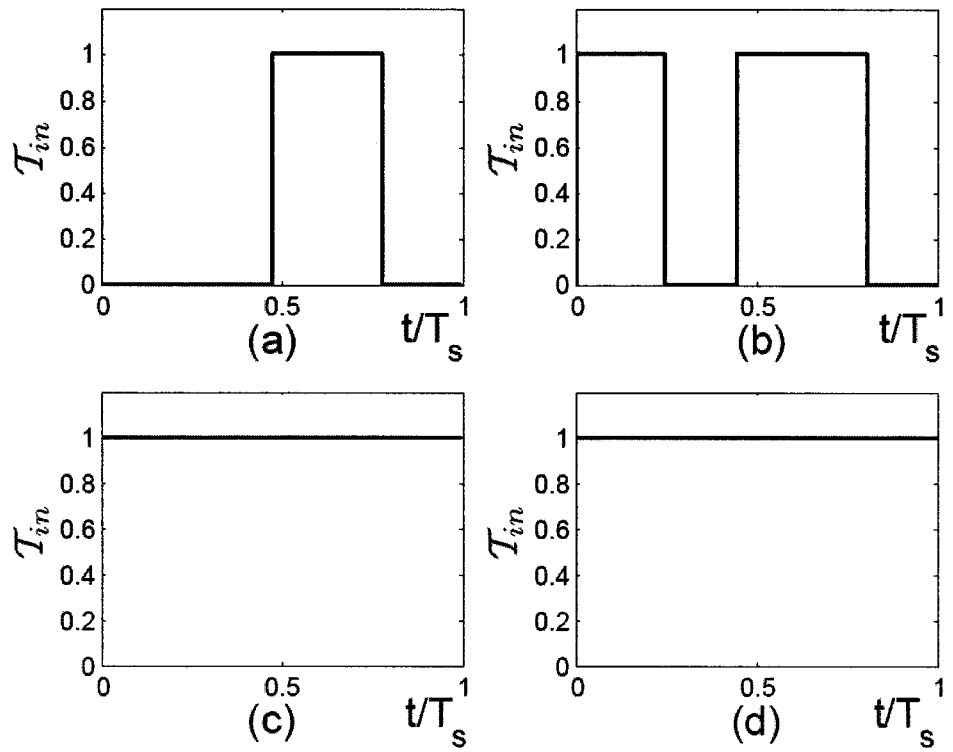

Figure 5.5: $\mathcal{T}_{in}$ for position C using (a) 1 spot (b) 2 spots (c) 4 spots and (d) 6 spots.

The coding system is simulated over an AWGN channel for several packet sizes below 1000 bytes, and at three different SNRs which will be used in simulations later in this chapter. Packets larger than 1000 bytes are not considered in this work because the complexity of the LT encoder and decoder depends linearly on packet size. At the transmitter, the LT encoder produces packets from a file and send them to the CRC-32 encoder. In this work, the C code modules provided in [76] are used for the CRC encoder. This encoder, computes the CRC code for the packets and attaches the 4-byte FCS to the packet. Then Gaussian noise inversely proportional to the channel SNR is added to

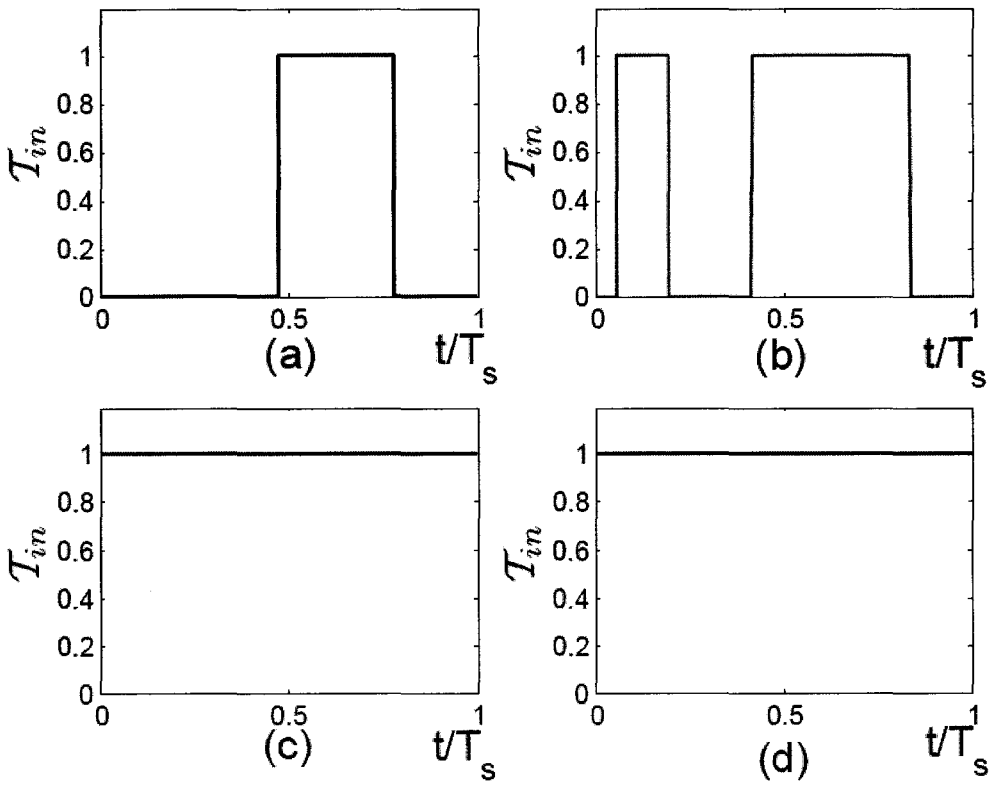

Figure 5.6: $\mathcal{T}_{in}$ for position D using (a) 1 spot (b) 2 spots (c) 4 spots and (d) 6 spots.

the packet. The receiver is assumed to employ hard decision decoding, thus, every bit is recovered by thresholding the received symbol from the channel. Next, a CRC check is recomputed for the received packet and is compared with the attached CRC check. If they are equal, the packet is sent to the LT decoder, otherwise, it is considered corrupted and dropped.

In Fig. 5.7, the simulation results are shown by '$*$' while the expected rates obtained by (4.6) are plotted within a solid line. As it can be shown from the figure, the simulation results are consistent with the rates predicted by (4.6).

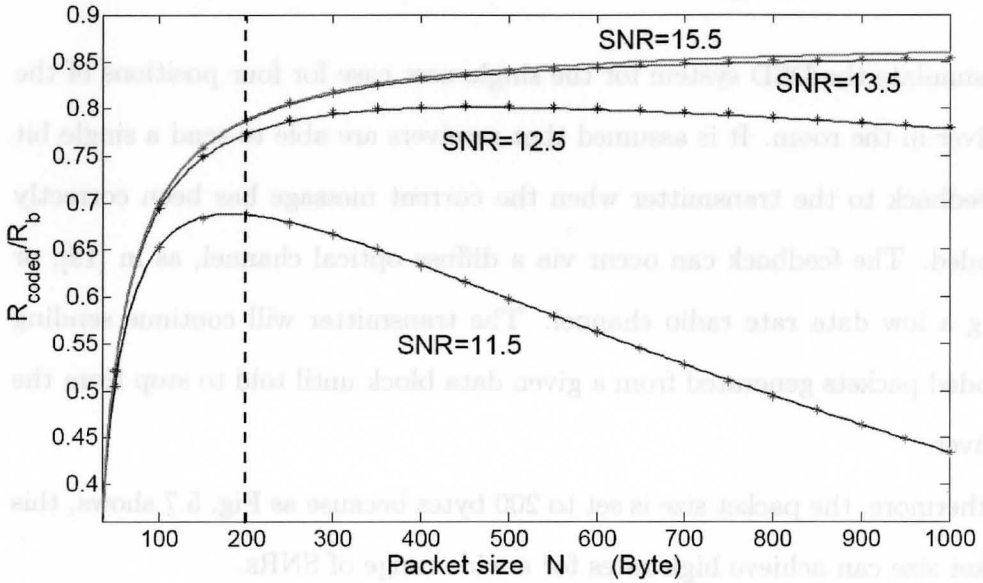

Figure 5.7: Simulated rates normalized to link rate, R_b, for three channel SNRs are shown by '$*$' while the lines show the rates predicted by (4.6).

The results show that as p increases the optimum packet size gets bigger and the R_{coded} increases. However, the difference between the plot for 15.5 dB and 13.5 dB is not significant because p is small in both cases. Therefore, for the DSD channel simulations, instead of a separate DSD channel simulation for each receiver to compute the rate, the C_T for receivers is computed by simulating the path for one period and (4.6) is applied to the C_T to compute the rate.

5.3 The Single User DSD System Simulation

We simulate the DSD system for the single user case for four positions of the receiver in the room. It is assumed that receivers are able to send a single bit of feedback to the transmitter when the current message has been correctly decoded. The feedback can occur via a diffuse optical channel, as in [19], or using a low data rate radio channel. The transmitter will continue sending encoded packets generated from a given data block until told to stop from the receiver.

Furthermore, the packet size is set to 200 bytes because as Fig. 5.7 shows, this packet size can achieve high rates for a wide range of SNRs.

5.4 The DSD Link With 100 Mbps Transmitter

In this case, the link is assumed to have the same specifications as the one proposed in [7]. The transmitter sends OOK modulated data at 100 Mbps through a low divergence eye safe beam to the spot on the ceiling. The beam has an average optical power of 75 mW and employs infrared signals at 806 nm wavelength region. The receiver is identical to the one proposed in [7] and its structure is reproduced in Fig. 5.8. The spot diameter on the ceiling is 5 cm. The receiver detector diameter is 22 mm, as shown in Fig. 5.8. It is an imaging receiver with 37 pixels and has FOV=45° which employs MRC technique for combining elements outputs. This receiver is employed in the DSD system

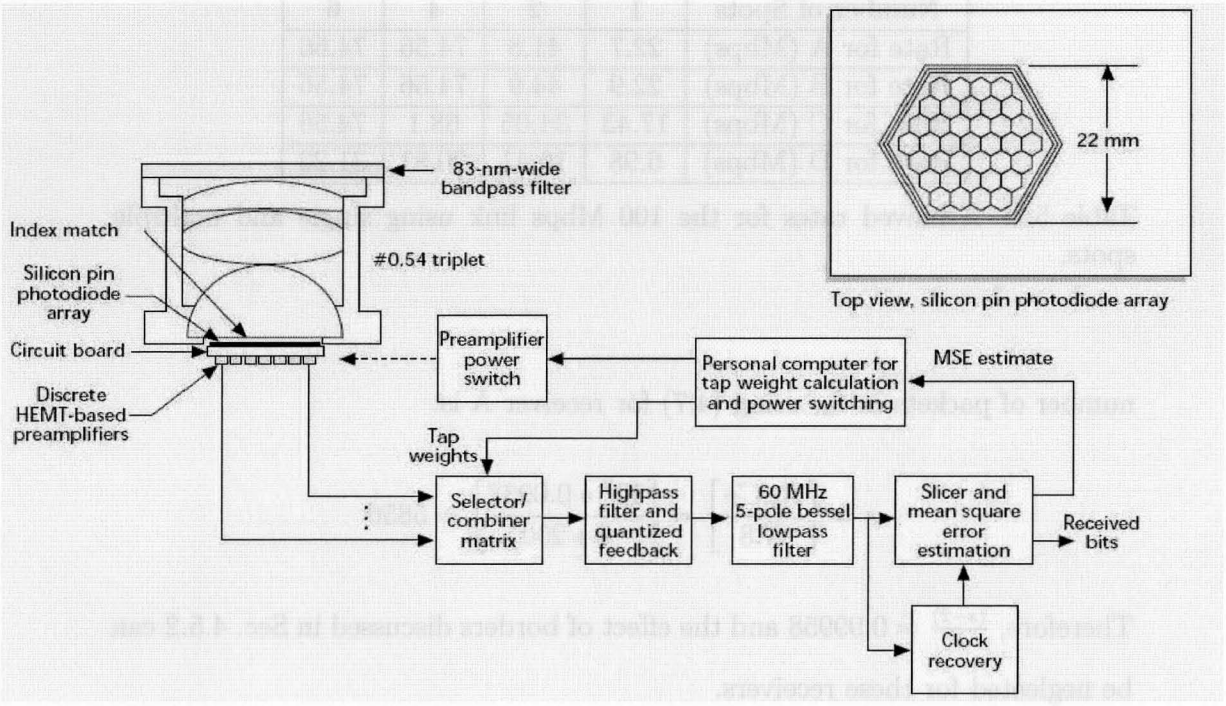

Figure 5.8: Receiver diagram for 100 Mbps link (reproduced from [7, Fig. 6]).

because it has the largest reported FOV for spot diffusing links and a large FOV imaging receiver is critical for the DSD system as discussed in Sec. 3.3. Using this setting for the transmitter and receiver, the uncoded probability of error p of the link is 10^{-9} [7] in the presence of bright sunlight and the SNR at the receiver is at least 15.5 dB.

For this link setting, the data rate for each position can be computed from (4.6). Note that if the border effect, discussed in Sec. 4.5.2, is not negligible, then (4.6) must be multiplied by (4.8) to obtain the rate. However, here we can show that border effect is negligible. The border effect is most serious for the receiver with smallest C_T, which from Table. 5.1, is receiver A. The

Number of Spots	1	2	4	6
Rate for A (Mbps)	22.7	41.8	74.56	74.56
Rate for B (Mbps)	22.9	44.9	74.56	74.56
Rate for C (Mbps)	17.43	34.05	68.1	74.56
Rate for D (Mbps)	6.98	10.41	20.81	31.22

Table 5.2: Achieved rates for the 100 Mbps link using single and multiple spots.

number of packets in I_{in} using (4.7) for receiver A is:

$$s = \left\lceil \frac{R_b.C_T}{N.8} \right\rceil = \left\lceil \frac{10^8 * 0.0937}{8 * 200} \right\rceil = 5856$$

Therefore, $\frac{(s-2)}{s} = 0.99958$ and the effect of borders discussed in Sec. 4.5.2 can be neglected for these receivers.

Table. 5.2 shows the computed rates at the proposed positions for these links. As discussed in Sec. 3.2 the DSD channel capacity is approximately equal to C_T. However, comparing Table. 5.2 and 5.1 show, the achieved rates are lower than $R_b * C_T$. This difference is due to the extra packets LT code needs to decode the message and also, dropped packets by CRC-32 code, as discussed in Sec. 4.5.1. Eqn. 4.6 shows the expression for this difference. As this equation shows, in order to get higher rates, α must decrease and l must be increased. As explained in Sec. 4.3.7, it is possible to decrease α in the expense of more complexity.

Another parameter which effects the data rate is the LT packet length l. As discussed in Sec. 4.5.1, this parameter can not be increased to any arbitrary value and the optimum value for l depends on the channel SNR and average packet header size $\overline{m}$. Ideally, l must be chosen to maximize the rate over all

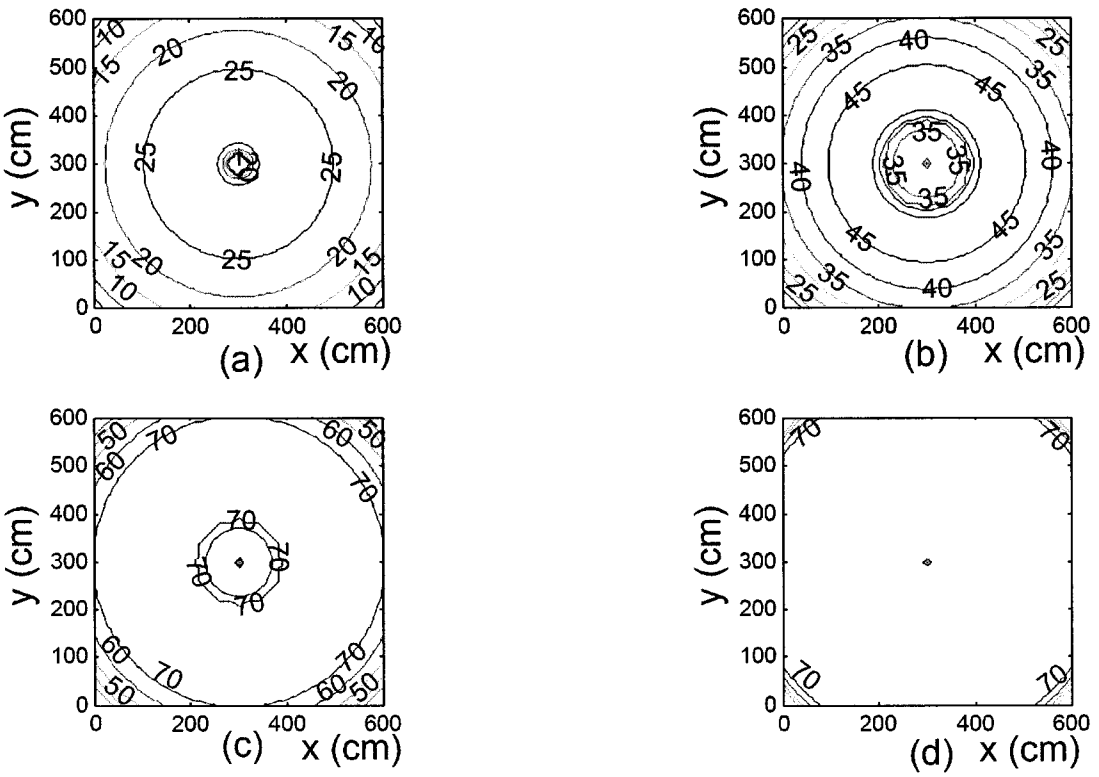

Figure 5.9: Achieved rates (Mbps) over the room for 100 Mbps link for (a) 1 spot (b) 2 spots (c) 4 spots (d) 6 spots

positions in the room. As shown in Fig. 4.6, the achieved rate is sensitive to packet size especially at lower SNRs.

Fig. 5.9 presents the achieved rates over the room for a variety of spots. As it is shown in the Fig. 5.9 (d), the rates for 6 spots case are maximum and constant for a large portion of the room. On the other hand, in the 1 spot case, shown in Fig. 5.9 (a), the rates are lower and change much more over the room. Therefore, the 6 spot is closer to the desired DSD channel which, as

discussed in Chap. 3, has a C_T distribution over the room with a high mean and low variance.

5.5 1 Gbps Link

As shown in Sec. 3.1.3, the DSD link has GHz bandwidth, in excess of 10 GHz. Therefore, it is possible to use higher rate devices with this channel.
In this section, a DSD link working at 1 Gbps is assumed, although an experimental spot diffusing channel working at this rate has not been reported yet. However, optical devices working in this rate are available and experimental LOS link working at 1 Gbps has been reported [16]. The transmitter power is assumed to be equal to the eyesafe 100 Mbps link. We assume using a receiver with similar specifications to the 100 Mbps link, except of wide bandwidth. It is assumed that noise power spectral density is the same as in the 100 Mbps link, and the SNR changes due to the increased bitrate, as in (2.12). Therefore, changing the rate from 100 Mbps to 1 Gbps without increasing the transmitted average optical power, results in 10 dB decrease in received SNR. This decrease in SNR would decrease the channel capacity dramatically. It is possible to compensate a portion of this SNR loss using more power efficient L-PPM modulation scheme. As discussed in Sec. 2.7.3.2, L-PPM modulation requires less power and more bandwidth to work at the same rate as OOK. For example, in this case of using 4-PPM modulation technique instead of OOK, as shown in Table 2.3, results in 3 dB power gain. Furthermore, 8-PPM provides 5.4 dB and 16-PPM provides 7.5 dB optical power gain over OOK. Notice that these gains come at the expense of larger required bandwidth. The wide

Number of Spots	1	2	4	6
Rate for A (Mbps)	222	409	705	705
Rate for B (Mbps)	224	440	705	705
Rate for C (Mbps)	170.6	333	666	705
Rate for D (Mbps)	68.4	102	203	305

Table 5.3: Achieved rates for the 1 Gbps link using single and multiple spots.

DSD channel bandwidth is able to support these power efficient modulations with nearly no multipath interference. Hence, we assume employing 16-PPM which requires four times bandwidth of OOK and results in the received SNR of $15.5 - 10 + 7.5 = 12.5$ dB. Table. 5.3 shows the achieved rates for this SNR and bitrate. Comparing Table. 5.3 and 5.2, we see that the rates for 1 Gbps link are not exactly 10 times of 100 Mbps link because the SNR is decreased from 15.5 dB to 12.5 dB. Consequently, p has increased which has increased and more packets are dropped by CRC.

Fig. 5.10, presents the achieved rates over the room for four cases of spots. As is shown in the figure, as the number of spots increase, the distribution of rates gets closer to a uniform distribution. The the rates for 6 spots case, shown in Fig. 5.9 (a), are maximum and constant for a large portion of the room while for the 1 spot case, shown in Fig. 5.9 (a), the rate distribution varies much more over the room and has a lower mean.

5.6 10 Gbps Link

As shown in Sec. 3.1.3, the DSD channel bandwidth is beyond 10 GHz. Thus, it is possible to a employ multi-GHz transmitter in the DSD channel. In this section, the achievable rates for a 10 Gbps transmitter are computed.

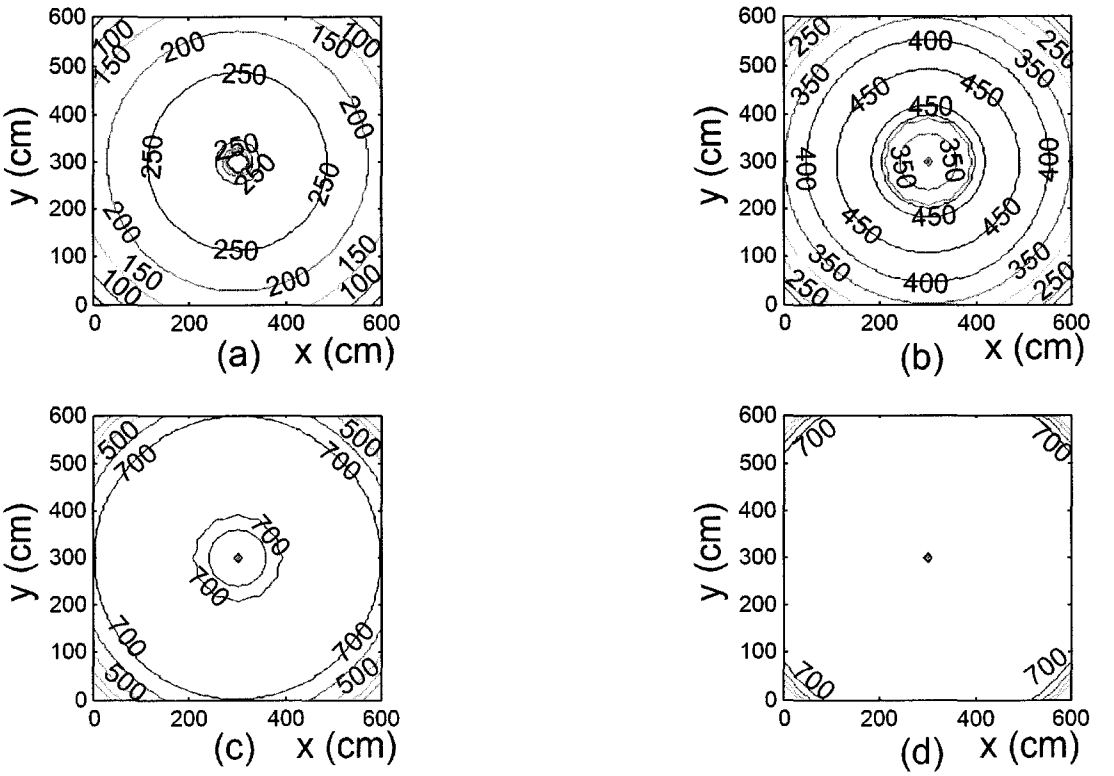

Figure 5.10: Achieved rates (Mbps) over the room for 1 Gbps link for (a) 1 spot (b) 2 spots (c) 4 spots (d) 6 spots.

Similar to the previous section, we assume using a imaging receiver working at this rate with similar specifications to the 100 Mbps case while the noise spectral density is not changed when operating at 10 Gbps. Although such a receiver working at 10 Gbps has not been reported yet, essential components for such a link are available, such as 10 Gbps commercial VCSEL and APDs [77–81]. In this case, as the SNR expression for OOK shows (2.12), sending the same average optical power, the SNR would decrease 20 dB compared

to the 100 Mbps link. Employing L-PPM to compensate this loss is not practical because compensating 20 dB power loss requires employing 1024-PPM modulation. However, as shown in Sec. 3.5, the spot motion in the DSD system, makes it possible to increase the transmitter average optical power while keep the beam eyesafe. For example, it is shown in Sec. 3.5 that for the room used in this chapter and circular path, using (3.6), it is possible to send 18 dB more average optical power in the transmitter. Thus, using OOK modulation, and increasing the transmitter power due to this gain, the achievable SNR in the room would be $15.5 - 20 + 18 = 13.5$ dB. The achieve rates for this rate and SNR are shown in Table. 5.4.

The achieved rates are not exactly 100 times of the rates in 100 Mbps link because the SNR is different and more packets are corrupted by noise and dropped by CRC in the 10 Gbps link. The rate distribution over the room for different spot numbers are plotted in Fig. 5.11. Similar to previous links, 6 spots case provides a more uniform rate distribution over the room with higher mean.

Note that in this case, the transmitter must employ safety a system to stop transmitting if the beam stops moving or does not move on the appropriate path, because in this case the beam is eyesafe only when it is moving on the determined path.

We assume that both the transmitter and the receiver have enough processing power to encode and decode the data at this rate. The CRC encoder working at 10 Gbps has been reported previously [72]. The LT encoder and decoder for the code used in this simulations, as shown in Sec. 4.5.1, require on average 12 XOR operations per bit which means they require on average 120×10^9

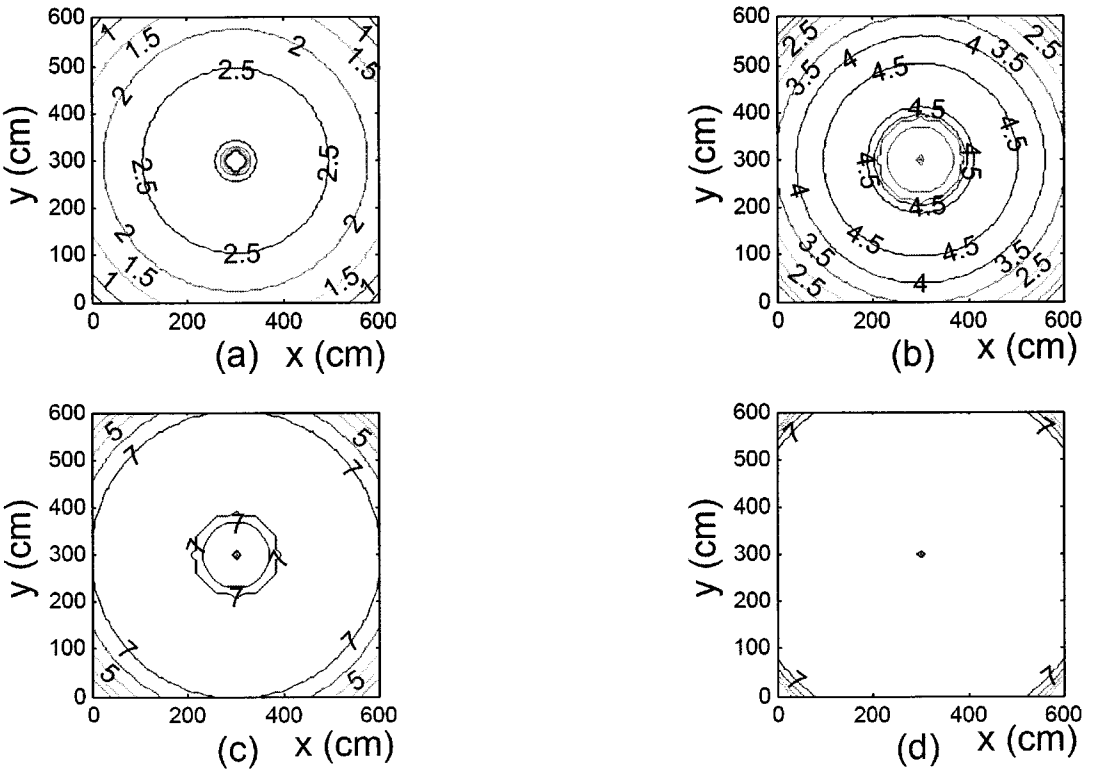

Figure 5.11: Achieved rates (Gbps) over the room for 10 Gbps link for (a) 1 spot (b) 2 spots (c) 4 spots (d) 6 spots

Number of Spots	1	2	4	6
Rate for A (Gbps)	2.26	4.17	7.44	7.44
Rate for B (Gbps)	2.28	4.48	7.44	7.44
Rate for C (Gbps)	1.74	3.4	6.8	7.44
Rate for D (Gbps)	0.7	1.04	2.07	3.12

Table 5.4: Achieved rates for the 10 Gbps link using single and multiple spots.

operations per second. However, the LT encoding/decoding process can be performed in parallel because the XOR operations are performed on the entire packets at once. For example, a 64-bit processor requires 1.875×10^9 operations per second to encode/decode this code. Commercial 64-bit processors with this and even higher speeds are available. For example, Intel Pentium Extreme edition is a 64-bit processor which works at 3.73 GHz [82]. Furthermore, the LT encoding/decoding can be implemented using parallel XOR gates. Ultimately, each bit in a packet can be processed by a separate unit, built from simple and inexpensive XOR gates. This parallel processing can reduce the system clock dramatically. For example, assuming complete parallel processing for the code with 200 bytes packets, considered in this work, each parallel coding module requires on average:

$$\frac{R_b.d_{avrg}}{N.8} = \frac{10^{10} \times 12.5}{200 \cdot 8} = 79 \times 10^6$$

operations per second.

5.7 The DSD Channel With Multiple Users

In previous simulations, we assumed there is only one receiver in the room. In this section we present initial work on extending the DSD system to multiple users in the room. Two cases are considered: (1) when receivers are able to send a single bit feedback to transmitter and (2) when there is no feedback channel between the transmitter and receiver.

5.7.1 The Multiple-user DSD Channel with Feedback

In this case, the transmitter keeps generating encoded packets from a message and sending them over the channel until all the receivers in the room send an acknowledgement, meaning that they have all decoded the message successfully. Then, the transmitter begins sending encoded packets generated from the next message. In this case, the transmitter waits for an acknowledgment from all receivers before proceeding to the next data block, therefore, the rate for all receivers is limited by the rate of the receiver present in the room with lowest capacity. For example, assuming a 100 Mbps link with six spots as Sec. 5.1, and four receivers at positions A, B, C and D, as shown in Sec. 5.4, then the rate for all receivers is 31.22 Mbps, the rate of the receiver D, which has the lowest capacity.

5.7.2 Multiple-user DSD Channel without Feedback

If the receivers are not able to transmit any feedback, it is still possible transmit data at high bit rates to any point in the room with high probability. In this case the LT code can be designed to let all receivers having C_T larger than a certain value, termed $C_T^{\min}$, be able to decode the data with the desired probability. Note that the data rate for all receivers having C_T larger or equal to $C_T^{\min}$ is constant and is equal to the achievable rate for $C_T^{\min}$. In this case, the receivers with C_T less than $C_T^{\min}$, are not able to decode all the message successfully with high probability.

One strategy to do so is dividing the entire message to portions so that receivers can decode each portion in one period of spot with desired probability P_{decode}. Therefore, as it is shown in Fig. 5.12, the packet size must be set so that

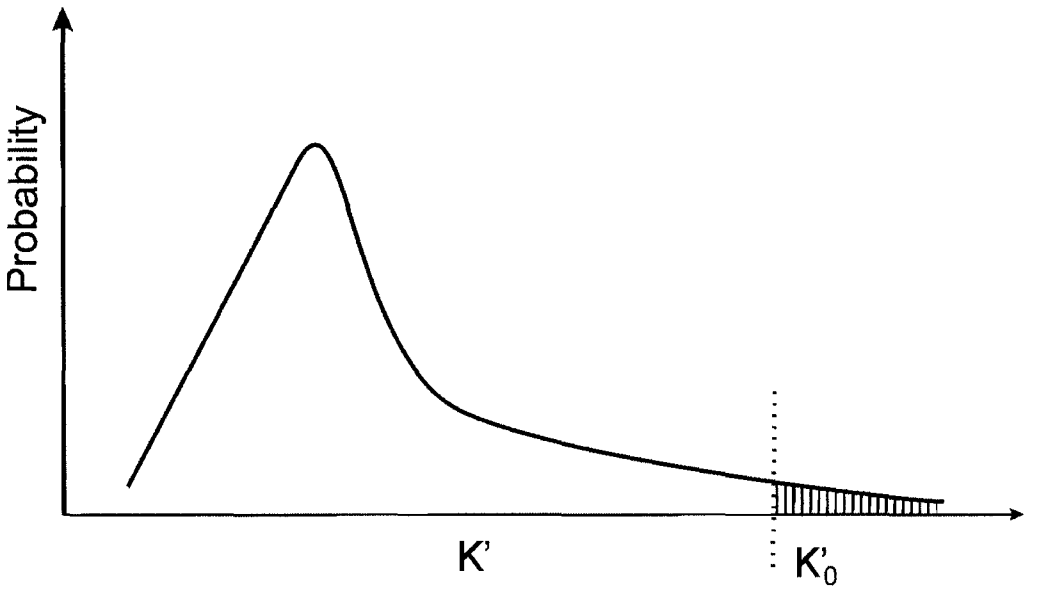

Figure 5.12: Probability of outage is the integral of $\rho_p(K')$ for $K' > K'_0$ when receivers can receive at least K'_0 packets for decoding.

receivers with $C_T = C_T^{\min}$, can receive K'_0 packets where K'_0 is selected so that:

$$P_{decode} = \int_k^{K'_0} \rho_p(K')dK'$$

and,

$$P_{outage} = 1 - P_{decode} = \int_{K'_0}^{\infty} \rho_p(K')dK'$$

Therefore, to increase the probability of successful decoding, K'_0 must be increased. In order to have K'_0 packets in $C_T^{\min}$, the packet size must be set to:

$$\text{Packet-size} = \frac{(C_T^{\min} \cdot T_s \cdot R_b \cdot (1 - P_{packet-error}))}{8(K'_0 + 2)} \tag{5.1}$$

and the data rate for all receivers which have C_T larger or equal to $C_T^{\min}$ is:

$$\frac{k \text{ Packet-size}}{T_s}$$

Note that 2 extra packets are considered to account for 2 packets received on borders of FOV. For example, for the code used in simulations setting $K_0' = \alpha\ k$, P_{outage} is 0.4. Therefore, as shown in Fig. 5.12, increasing the K_0' to $\alpha\ \beta\ k$ where $\beta > 1$ decreases the P_{outage}. For example, setting $\beta = 1.15$ results in $P_{outage} = 10^{-3}$. Therefore, in the no feedback case, there is a trade off between rate and P_{outage}.

Another trade off in the no feedback case, is between coverage and rate. Increasing $C_T^{\min}$ increases the rate but decreases the coverage. For example, consider the DSD channel with the single spot and circle path with radius 220 cm, and assume the system uses the 100 Mbps link specifications as in Sec. 5.4. As shown in Sec. 3.3, using this spot path and receiver FOV, there are some blind points in the room. Thus, it is not possible to set $C_T^{\min}$ to the minimum C_T in the room, which is zero, and provide coverage for all positions in the room. However, it is possible to set coverage by, for example, the 85-th percentile value, i.e. to provide coverage for 85% of the room positions. Hence, letting $C_T^{\min} = 0.265$, which is the 85-th percentile in this case, $\beta = 1.15$ to have $P_{outage} = 10^{-3}$ and $T_s = 0.1$ second in (5.1), the packet size is 260 bytes. The achieved rate with this value is 18.7 Mbps. Note that this rate is achievable only for receivers which have $C_T \geq C_T^{\min}$. Thus, using this settings, 85% of the room positions would achieve 18.7 Mbps data rate with the probability of outage of 10^{-3}.

Now consider using 6 spots as described in Sec. 3.4. In this case, as shown in Table. 3.5, the minimum C_T is 0.018. Therefore, by designing the code for this C_T, receivers all over the room would have the achievable rate for this C_T. Assuming similar settings, the packet size from (5.1), would be 16 bytes. The achieved rate for this packet size and $C_T^{\min} = 0.018$ is 1.3 Mbps. However, using the 95-th percentile of the C_T which is 0.9859, packet size is 781 bytes and the achievable rate becomes 64 Mbps. Therefore, decreasing the coverage from 100% to 95% in this case results in much higher rates.

Note that in this case the probability of failure is not zero, therefore, it is not suitable for applications such as data network where data loss can not be tolerated. This link can be used in applications such as audio and video broadcasting, where a small portion of data loss is acceptable for receiver.

5.7.3 Comparison

Although the no feedback link is easier to implement, the link with feedback is more flexible and provides higher average data rates. Moreover, no information about the C_T distribution is required in the feedback link while the no feedback link must be designed based on the C_T distribution over the room and the decoder dynamics. In the no feedback case, outage may happen while in feedback case, data is always decoded successfully in the receiver.

5.8 Conclusion

In this chapter, the DSD channel is simulated for different SNRs and packet size and results were consistent with rates predicted by (4.6). Therefore, the

achieved rate for any receiver in a DSD system can be computed by calculating its C_T and applying that to (4.6) as long as SNR is sufficiently large. The achieved bit rates are computed for different position in a $6 \times 6 \times 3$ m room at three different link bit rate in the presence of a feedback channel from the receiver to the transmitter in the single receiver case. Furthermore, two cases of when a feed back channel is available from receiver to transmitter and when there is no feed back available are considered for multiple receiver case. The results show that the achieved rates are close to the DSD channel capacity, C_T. Hence, they confirm that the DSD channel is well-modeled as a erasure channel with erasure probability $1 - C_T$.

6

Conclusions and Future work

Optical wireless links are attractive for indoor applications because they can achieve high bitrate and employ simple and inexpensive optoelectronic devices. However, they suffer from transmitter power limitations due to safety issues and link blockage due to incapability of optical signals to pass opaque objects. Therefore, various link configurations such as diffuse and MSD has been proposed and studied to find a configuration which can provide both high bitrate and robustness against blockage.

In this work, a new configuration for indoor optical wireless communications, called the *dynamic spot diffusing* (DSD) channel, is proposed and studied. The DSD channel is based on the spot diffusing channel which is used in MSD links. In this channel, the transmitter sends data to a small spot on the ceiling and the receiver detects the data from the reflections from the spot. This channel is a LOS channel between receiver and spot, therefore, the received multipath signals are negligible and has multi-GHz channel bandwidth. However, in the MSD configuration, fixed spots are created all over the ceiling to provide good coverage for all receivers in the room, but in the DSD configuration, one or few

spots are created and moved on the ceiling. Reducing the number of spots, reduces the DSD transmitter complexity and received multipath signal compared to the MSD configuration.

The DSD channel model is discussed and the DSD channel capacity is computed. The DSD channel is shown to be well-modeled as an *erasure* channel with erasure probability $1 - C_T$, when SNR is high enough. The DSD channel capacity depends on the DSD system parameters such as receiver FOV and spot path. In order to increase the DSD channel capacity, receivers must have the highest possible FOV. Therefore, imaging receivers are the best choice for the DSD link which provides high FOV and is able to reject much of the received ambient light and multipath signal. An appropriate spot path must provide good coverage over the entire room. Therefore, it depends on the room shape. For example, in this work it is shown that for the proposed square room, circular path shows the best characteristics among the several studied paths.

Employing multiple spots can increase the DSD channel capacity over the room significantly while the complexity of the transmitter increases moderately. For example, for the proposed room and circle path, increasing the number of spots to 2, doubles up the capacity for all the receivers. However, generally, the DSD channel capacity does not have a linear relation with number of spots. Because, after a certain number of spots, receiver have always at least one spot in their FOV and the channel capacity will not be increased by employing more spots.

Another advantage of the DSD configuration is that it makes it possible to increase the transmitter power due to the spot motion. In this configuration,

the spot is moving, thus, the human eye can not be exposed to the transmitter beam all the time. This power gain is very important because the main limitation for indoor optical wireless systems is the transmitter power limitations due to safety issues. This limitation becomes more serious especially at higher rate links because in optical wireless links, SNR is proportional to the $\frac{1}{R_b}$. Hence, increasing the bit rate with constant transmitter power results in a decrease in the SNR. Therefore, the power gain due to the DSD spot motion enables the DSD system to achieve higher rates. For example, for the proposed DSD system with circular spot path, this power gain is shown to be 18 dB which means it is possible to increase the rate 60 times while keeping the SNR at the same level.

The DSD channel is shown to be well-modeled as an erasure channel. Hence, erasure correcting codes must be employed to achieve channel capacity. In the DSD channel, the state of channel between transmitter and each receiver is unknown at transmitter but known at receiver. Thus, the spot motion adds a random fading to the DSD channel and the DSD channel is an erasure channel with unknown probability of erasure at transmitter. Previous work has shown that widely used fixed rate erasure codes such as Reed-Solomon cannot work efficiently on random fading channels, however, rateless codes have been shown to work efficiently on this channels. Thus, in order to approach the DSD channel capacity, a famous class of rateless codes termed LT codes are applied to this channel. However, LT codes are not able to detect or correct any bit errors in the received packets. Therefore, a widely used error detection code termed Cyclic-Redundancy Check (CRC) Code is used in the DSD system to detect corrupted received packets before entering the LT decoder.

	DIFFUSE	MSD	DSD
Available Bandwidth	Low	Medium	High
Achievable Bitrate	Low	Medium	High
Transmitter Complexity	Low	High	Medium
Receiver Complexity	Low	Medium	High

Table 6.1: Comparison of DSD, MSD and Diffuse Systems.

The code design issues for LT and CRC codes are discussed to optimize the DSD coding module.

Finally, the DSD system is simulated in a $6 \times 6 \times 3$ m room in Chap. 5. The achievable rates at four positions in the room are simulated employing one and multiple spots at transmitter data rates of 100 Mbps, 1 Gbps and 6 Gbps for the case where receiver is able to send one bit feedback to the transmitter. Moreover, it is shown that by appropriate code design, it is possible to achieve high bit rate when there is no feedback channel from receivers to transmitter. These simulations show that in the proposed DSD system, the achieved rates are close to the calculated channel capacity.

The DSD channel is an attractive configuration for multicast indoor optical wireless networks since it is inexpensive, flexible and has shown to be able to achieve high data rates. Table 6.1 compares DSD with MSD and DSD links. The DSD link is an attractive candidate for applications where the downlink requires higher rates than uplink, such as multimedia broadcasting, indoor wireless link which requires high security and environments where are congested by RF signals.

6.1 Future Directions

The dynamic spot diffuse configuration is a novel optical wireless link for indoor communications. It is shown to be able to achieve much higher bit rates than previous non-LOS configurations. Therefore, it is a good candidate for indoor broadcast wireless networks. Hence, one of the future directions for this work is investigating different possible multiple access techniques previously used for indoor optical wireless links and finding the most suitable one for the DSD channel among them. Building a simple prototype DSD system is another step which can help getting a deeper understanding about the DSD system and practical issues arises for implementing this system. Another fountain code termed *Raptor Code*, can be applied to the DSD channel which requires less operations compared to LT codes. In this work, a feedback channel capable of sending a single bit is considered. The operation of the DSD channel in presence of more than a single bit feedback may be investigated. Using more bits of feedback, the receiver can provide the transmitter with the channel state information which can result in better utilization of the channel. There is a strong correlation within channel states when spot enters the FOV one or a few numbers in each period. In this case, considering another type of channel model such as the Gilbert-Elliot which accounts for this correlation, may increase the capacity.

The DSD channel, unlike diffuse and MSD channels, is a dynamic system. Therefore, further investigation of path and system adaption for the DSD channel must be done.

Bibliography

[1] J. M. Kahn and J. R. Barry, "Wireless infrared communications," *Proc. IEEE*, vol. 85, pp. 265–298, Feb. 1997.

[2] D. C. O'Brien, G. E. Faulkner, K. Jim, E. B. Zyambo, D. J. Edwards, M. Whitehead, P. Stavrinou, G. Parry, J. Bellen, M. J. Sibley, V. A. Lalithambika, V. M. Joyer, R. J. Samsudin, D. M. Holburn, and R. J. Mears, "High-speed intergrated transceivers for optical wireless," *IEEE Commun. Mag.*, Mar. 2003.

[3] S. T. Jivkova and M. Kavehrad, "Multispot diffusing configuration for wireless infrared access," *IEEE Trans. Commun.*, vol. 48, no. 6, pp. 970–978, June 2000.

[4] S. Jivkova and M. Kavehrad, "Receiver designs and channel characterization for multi-spot high-bit-rate wireless infrared communications," *IEEE Trans. Commun.*, vol. 49, no. 12, pp. 2145–2153, Dec. 2001.

[5] J. R. Barry, J. M. Kahn, W. J. Krause, E. A. Lee, and D. G. Messerschmitt, "Simulation of multipath impulse response for indoor wireless optical channels," *IEEE J. Select. Areas Commun.*, vol. 11, no. 3, pp. 376–379, Apr. 1993.

[6] S. Haykin, *Communication Systems*, 4th ed. McGraw-Hill Higher Education, 2002.

[7] J. M. Kahn, R. You, P. Djahani, A. G. Weisbin, B. K. Teik, and A. Tang, "Imaging diversity receivers for high-speed infrared wireless communcation," *IEEE Commun. Mag.*, pp. 88–94, Dec. 1998.

[8] F. Uyeda, H. Xia, and A. A. Chien, "Evaluation of a high performance erasure code implemention," *Report prepared for Computer Science and Engineering Department, University of California, San Diego*, Sept. 2004.

[9] P. Koopman, "32-bit cyclic redundancy codes for Internet applications," *In Proc. Int. Conf. on Systems and Networks*, pp. 459–468, June 2002.

[10] S. Hranilovic, *Wireless Optical Communication Systems.* New York, NY: Springer, 2004.

[11] International Electrotechnical Comission, "Safety of laser products- part 1: Equipment classification, requirements and user's guide. group safety publication, reference number 825-1," 1993.

[12] Institude of Electrical and Electronics Engineers. Standards Association Website., "http://standards.ieee.org."

[13] The offical Bluetooth Web site., "http://www.bluetooth.com."

[14] UWB Forum., "http://www.uwbforum.org."

[15] Infrared Data Association. Web Site., "http://www.irda.org."

[16] D. R. Wisely, "A 1 Gbit/s optical wireless tracked architecture for atm delivery," *In Proc. IEE Coll. Opt. Free Space Commun. Links, London, U.K*, pp. 14/1–14/7, 1996.

[17] T. S. Chu and M. J. Gans, "High speed infrared local wireless communications," *IEEE Commun. Mag.*, vol. 25, no. 8, pp. 4–10, Aug. 1987.

[18] F. Parand, G. E. Faulkner and D. C. O'Brien, "Cellular tracked optical wireless demonstration link," *In IEE Proc. Optoelectron.*, vol. 150, no. 5, pp. 490–496, Oct. 2003.

[19] V. Jungnickel, A. Forck, T. Haustein, U. Kruger, V. Pohl, and C. von Helmolt, "Electronic tracking for wireless infrared communications," *IEEE Trans. Wireless Commun.*, vol. 2, no. 5, pp. 989–999, Sept. 2003.

[20] A. M. Street, K. Samaras, D. C. O'Brien, and D. J. Edwards, "High speed wireless IR-LANs using spatial addressing," *In Proc. 8th IEEE International Symposium on Mobile Radio Commun. 'Waves of the Year 2000'*, vol. 3, no. 8, pp. 969–973, Sept. 1997.

[21] J. Bellon, M. J. N. Sibley, and S. D. Greaves, "Hub architecture for infrared wireless networks in office environments," *In IEE Proc. Optoelectron.*, vol. 146, no. 2, pp. 78–82, Apr. 1999.

[22] D. C. O'Brien, G. E. Faulkner, E. B. Zyambo, K. Jim, D. J. Edwards, P. Stavrinou, G. Parry, J. Bellon, M. J. Sibley, V. A. Lalithambika, V. M. Joyner, R. J. Samsudin, D. M. Holburn, and R. J. Mears, "Integrated

transceivers for optical wireless communications," *IEEE J. Select. Topics Quantum Electron.*, vol. 11, no. 1, pp. 173–183, 2005.

[23] F. R. Gfeller and U. Bapst, "Wireless in-house communication via diffuse infrared radiation," *Proc. IEEE*, vol. 67, no. 11, pp. 1474–1486, Nov. 1979.

[24] M. D. Audeh and J. M. Kahn, "Performance evaluation of baseband OOK for wireless indoor infrared LAN's operating at 100Mb/s," *IEEE Trans. Commun.*, vol. 43, no. 6, pp. 2085–2093, June 1995.

[25] D. C. Lee and J. M. Kahn, "Experimental 25-Mb/s wireless infrared link using 4-PPM with scalar decision-feedback equalization," *In Proc. IEEE Int. Conf. Commun.*, vol. 1, no. 7-11, pp. 26–30, June 1998.

[26] G. W. Marsh and J. M. Kahn, "Performance evaluation of experimental 50-Mb/s diffuse infrared wireless link using on-off keying with decision-feedback equalization," *IEEE Trans. Commun.*, vol. 44, no. 11, pp. 1496–1504, Nov. 1996.

[27] F. Gfeller and W. Hirt, "Advanced infrared (AIr): Physical layer for reliable transmission and medium access," in *Proc. IEEE Int. Seminar Broadband Commun. Zurich*, 2000, pp. 77–84.

[28] R. R. Valadas, A. R. Tavares, A. M. de Oliveira Duarte, A. C. Moreira, and C. T. Lomba, "The infrared physical layer of the IEEE 802.11 standard for wireless local area networks," *IEEE Commun. Mag.*, vol. 36, no. 12, pp. 107–112, Dec. 1998.

[29] G. Yun and M. Kavehrad, "Spot-diffusing and fly-eye receivers for indoor infrared wireless communications," *In Proc. of IEEE Int. Conf. Sel. Top. in Wireless Commun.*, pp. 262–265, 1992.

[30] Y. A. Alqudah and M. Kavehrad, "MIMO characterization of indoor wireless optical link using a diffuse-transmission configuration," *IEEE Trans. Commun.*, vol. 51, no. 9, pp. 1554–1560, Sept. 2003.

[31] S. T. Jivkova, B. A. Hristov, and M. Kavehrad, "Power-efficient multispot-diffuse multiple-input-multiple-output approach to broad-band optical wireless communications," *IEEE Trans. Veh. Technol.*, vol. 53, no. 3, pp. 882–889, May 2004.

[32] M. R. Pakravan, E. Simova, and M. Kavehrad, "Holographic diffusers for indoor infrared communication systems," *In IEEE Proc. Global Telecommun. Conf.*, pp. 1608–1612, 1996.

[33] M. Kavehrad and S. Jivkova, "Indoor broadband optical wireless communications:optical subsystems design and their impact on channel characteristics," *IEEE Wireless Commun. Mag.*, pp. 30–35, Apr. 2003.

[34] S. Jivkova and M. Kavehrad, "Multi-spot diffusing configuration for wireless infrared access: Joint optimization of multi-beam transmitter and angle diversity receiver," *In Proc. Conf. Optical Wireless Commun. II, SPIE.*, vol. 3850, pp. 72–77, Sept. 1999.

[35] ——, "Shadowing and blockage in indoor optical wireless communications," *In IEEE Proc. Global Telecommun. Conf.*, pp. 3269–3273, 2003.

[36] A. G. Al-Ghamdi and J. M. H. Elmirghani, "Line strip spot-diffusing transmitter configuration for optical wireless systems influenced by background noise and multipath dispersion," *IEEE Trans. Commun.*, vol. 52, no. 1, pp. 37–45, Jan. 2004.

[37] ——, "Multiple spot diffusing geometries for indoor optical wireless communication systems," *Int. J. Commun. Syst.*, vol. 16, pp. 909–922, 2003.

[38] J. Carruthers and J. M. Kahn, "Angle diversity for nondirected wireless infrared communications," *In Proc. IEEE Intl. Conf. Commun. ICC*, vol. 3, pp. 1665–1670, June 1998.

[39] F. Khozeimeh and S. Hranilovic, "A dynamic spot diffusing architecture for indoor wireless optical communications," *IEEE Intl. Conf. on Commun. Istanbul,*, 2006.

[40] S. Hranilovic and F. Kschischang, "Optical intensity-modulated direct detection channels: signal space and lattice codes," *IEEE Trans. Inform. Theory*, vol. 49, no. 6, pp. 1385–1399, June 2003.

[41] J. B. Carruthers and J. M. Kahn, "Modeling of nondirected wireless infrared channels," *IEEE Trans. Commun.*, vol. 45, no. 10, pp. 1260–1268, Oct. 1997.

[42] J. B. Carruthers and S. M. Carroll, "Statistical impulse response models for indoor optical wireless channels," *Intl. J. Commun. Syst.*, vol. 18, no. 3, pp. 267–284, Mar. 2005.

[43] S. M. Carroll, "Modeling wireless infrared communications for network simulation," Ph.D. dissertation, Boston University, 2004.

[44] J. M. Kahn, W. J. Krause, and J. B. Carruthers, "Experimental characterization of non-directed indoor infrared channels," *IEEE Trans. Commun.*, vol. 43, no. 2/3/4, pp. 1613–1623, Feb/ March/ April 1995.

[45] F. Mederer, I. Ecker, J. Joos, M. Kicherer, H. J. Unold, K. J. Ebeling, M. Grabherr, R. Jger, R. King, and D. Wiedenmann, "High performance selectively oxidized VCSELs and arrays for parallel high-speed optical interconnects," *IEEE Trans. Adv. Packag.*, vol. 24, no. 4, pp. 444–449, Nov. 2001.

[46] "EMCORE Optical Devices http://www.emcore.com."

[47] "United States National Consensus Standards for laser safety. http://www.z136.org."

[48] "European Committee for Electrotechnical Standardization. http://www.cenelec.org."

[49] Y. A. Alqudah and M. Kavehrad, "Optimum order of angle diversity with equal-gain combining receivers for broad-band indoor optical wireless communications," *IEEE Trans. Veh. Technol.*, vol. 53, no. 1, pp. 94–105, Jan. 2004.

[50] F. J. Lopez-Hernandez, R. Perez-Jimenez, and A. Santamaria, "Ray-tracing algoritms for fast calculation of the channel impulse response

on diffuse IR-wireless indoor channels," *Opt. Eng.*, vol. 39, no. 10, pp. 124–130, Aug. 2000.

[51] F. J. Lopez-Hernandez and M. J. Betancor, "A novel algorithm for the calculation of the impulse response on IR wireless indoor channels," *Electron. Lett.*, vol. 33, no. 21, pp. 1804–1805, Oct. 1997.

[52] M. R. Pakravan, M. Kavehrad, and H. Hashemi, "Indoor wireless infrared channel characterization by measurements," *IEEE Trans. Veh. Technol.*, vol. 50, no. 4, pp. 1053–1073, July 2001.

[53] A. B. Carlson, *Communication systems.* New York, NY: McGraw-Hill, 1986.

[54] T. M. Cover and J. A. Thomas, *Elements of Information Theory.* Wiley, 1991.

[55] G. Ungerboeck, "Channel coding with multilevel/phase signals," *IEEE Trans. Inform. Theory*, vol. 28, no. 1, pp. 55–67, Jan. 1982.

[56] J. G. Proakis, *Digital Communications*, 4th ed. New York, NY: McGraw-Hill, 2001.

[57] P. Djahani and J. M. Kahn, "Analysis of infrared wireless links employing multibeam transmitters and imaging diversity receivers," *IEEE Trans. Commun.*, vol. 48, no. 12, pp. 2077–2088, Dec. 2000.

[58] "IS8550 HOLOTrak, Metrologic Instruments Inc. http://www.aoainc.com/press/releases2002.html."

[59] A. J. Goldsmith and P. P. Varaiya, "Fading channels: Information-thoretic and communications aspects," *IEEE Trans. Inform. Theory*, vol. 43, no. 6, pp. 2619–2692, Oct. 1997.

[60] L. Li and A. J. Goldsmith, "Capacity and optimal resource allocation for fading broadcast channels Part I Ergodic capacity," *IEEE Trans. Inform. Theory*, vol. 47, no. 3, pp. 1083–1102, Mar. 2001.

[61] I. E. Telatar, "Capacity of Multi-antenna Gaussian Channels," *European Trans. Telecommun.*, pp. 585–595, Nov. 1999.

[62] D. J. C. MacKay, *Information Theory, Inference and Learning Algorithms.* Cambridge University Press, 2004.

[63] Texas Instruments, DLP, "http://www.dlp.com/."

[64] J. Castura and Y. Mao, "Rateless coding over fading channels," *In Proc. 9th Canadian Workshop Inform. Theory*, pp. 195–197, June 2005.

[65] S. Lin and D. J. Costello, *Error Control Coding: Fundamentals and applications.* Prentice-Hall, 1983.

[66] M. Luby, "LT codes," *In Proc. Symposium Foundations of Computer Science*, pp. 271–280, 2002.

[67] J. Byers, M. Luby, and M. Mitzenmacher, "A digital fountain approach to asnychronous reliable multicast," *IEEE J. Select. Areas Commun.*, vol. 20, no. 8, pp. 1528–1540, Oct. 2005.

[68] Digital Fountain Inc, "http://www.digitalfountain.com."

[69] D. J. C. Mackay, "Fountain codes," *In IEE Proc. Commun.*, vol. 152, no. 6, pp. 1062–1068, Dec. 2005.

[70] M. T. Goodrich and R. Tamassia, *Data Structures and algorithms in JAVA*, 4th ed. John Wiley & Sons Inc, 2006.

[71] "IEEE Standard 802.3, Part 3: Carrier sense multiple access with collision detect on (CSMA/CD) access method and physical layer specifications, 2002."

[72] J. S. Lin, C. K. Lee, M. D. Shieh, and J. H. Chen, "High-speed CRC design for 10 Gbps applications," *In Proc. IEEE Intl. Symposium Circuits and Systems.*, pp. 3177–3180, May 2006.

[73] T. Fujiwara, T. Kasami, and S. Lin, "Error detecting capabilities of the shortened Hamming codes adopted for error detection in IEEE standard 802.3," *IEEE Trans. Commun.*, vol. 37, no. 9, pp. 986–989, Sept. 1989.

[74] M. K. K. Akhavan and S. T. Jivkova, "Wireless infrared in-house communications: How to achieve very high bit rates," *In IEEE Proc. Conf. Wireless Communications and Networking*, vol. 2, pp. 698–703, Sept. 2000.

[75] Hansen Corporation, "http://www.hansen-motor.com/."

[76] R. N. Williams, "A painless guide to CRC error detection algorithms. http://www.geocities.com/SiliconValley/Pines/8659/crc.htm."

[77] ZARLINK Semiconductor, "http://www.zarlink.com/."

[78] EMCORE Corporation, "http://www.emcore.com/."

[79] Mitsubishi Electric US, "http://www.mitsubishielectric.com/."

[80] Picometrix, "http://www.picometrix.com/."

[81] AVALON Photonics, "http://www.avap.ch/."

[82] "Intel Corporation. http://www.Intel.com."